UiT
THE ARCTIC
UNIVERSITY
OF NORWAY

Department of Electrical Engineering

Reliable parameter identification for synchronous machines

—

Erick Alves

Master's thesis in Electrical Engineering - June 2018

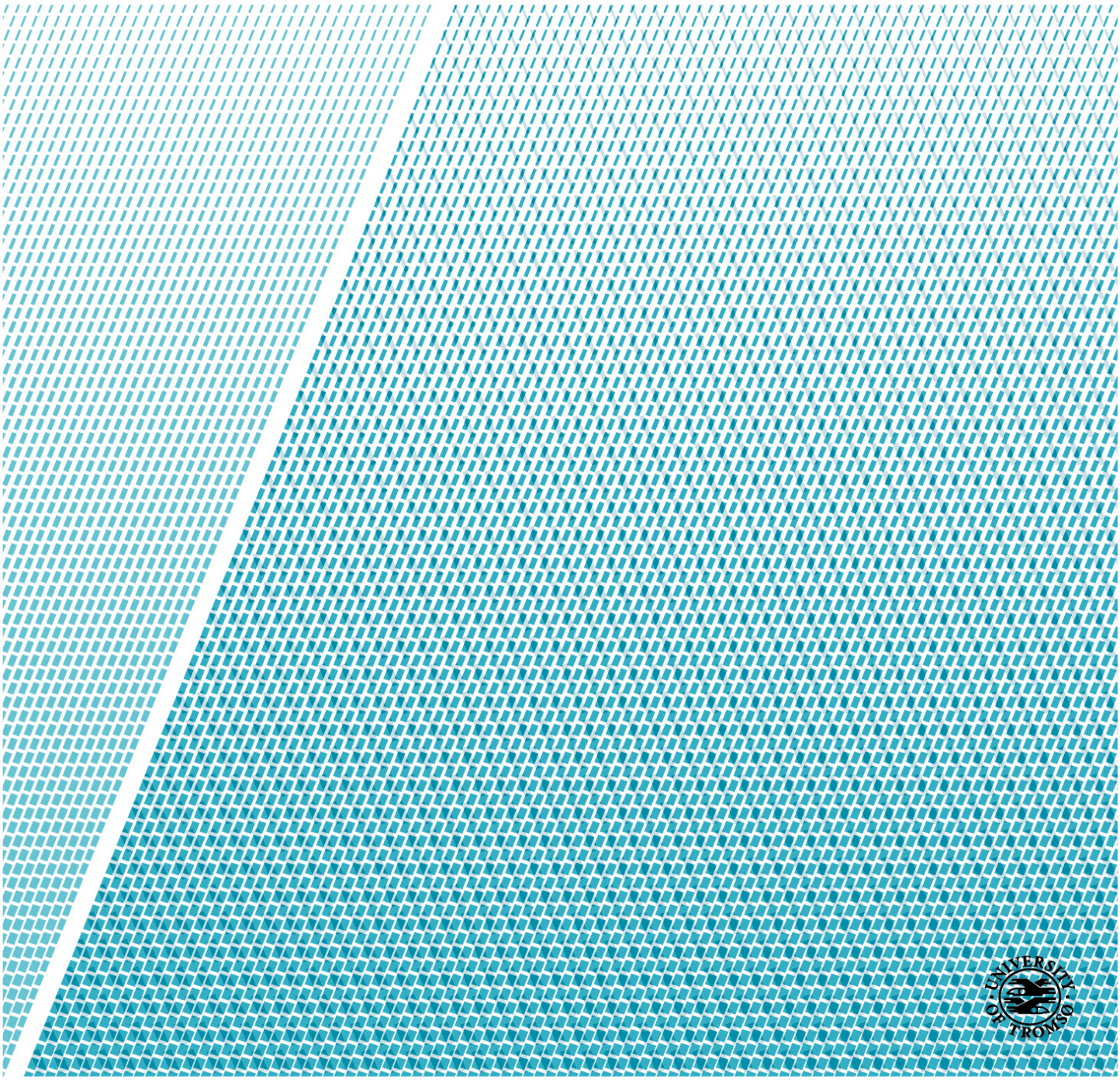

Preface

This thesis is submitted as partial fulfillment of requirements for the degree of Master of Science in Electrical Engineering at the Arctic University of Norway. It was carried out in the autumn semester of 2017 and spring semester of 2018, in cooperation with SINTEF Digital in Trondheim.

The idea of this project came out quite unexpectedly less than one year ago. At that time, the author was considering topics for his master thesis, and one of the ideas was investigating auto-tuning algorithms for controllers of synchronous machines. Then, in a summer weekend, he met his neighbor Giancarlo Marafioti at the garden of their house and told him about his idea. Giancarlo soon became interested, as he has extensive knowledge in model predictive control.

With further exploration and brainstorming in the next month, both recognized that the techniques required for auto-tuning of controllers could also be used for smart grid applications, such as condition monitoring and assessment of power grids. The author sketched some of these initial ideas in a document, and Giancarlo suggested a presentation for his employer, SINTEF Digital.

In late August these ideas were presented to Geir Mathisen, at that time, Senior Researcher at SINTEF Digital and part-time professor at NTNU. These were reviewed and streamlined during a meeting in September, at which the main points for a master project were outlined. Finally, in late September, the proposal was presented to Trond Østrem, coordinator of the Master in Electrical Engineering at UiT, and approved by the faculty.

The result of this unusual project is presented in the next pages. It is assumed the reader is familiarized with basic concepts in linear algebra, control theory, analysis of electric machines and power systems.

Trondheim, 2018-06-10

Erick Fernando Alves

Acknowledgment

There were many individuals that encouraged me in the pursuit of this project, and I would like to specially acknowledge some of them for their great contribution.

First of all, I am eternally grateful to Giancarlo Marafioti for encouraging me to pursue my ideas and for his guidance and support during the execution of this project. Also to Geir Mathisen for taking the trouble to understand the first rough ideas, to help me giving format to them, and to believe I would be able to execute all this. And, of course, to SINTEF Digital for providing me with the valuable time of their employees.

Secondly, I truly appreciate all my professors in the Master of Science in Electrical Engineering at UiT. In particular, I would like to mention Profs. Ragnhild Johanne Rensaa, Per-Ole Nyman and Lars Einar Norum, for planting the seed that made this work possible. In this realm, thanks also to Daniel do Santos Mota for introducing me to System Identification.

Not least, Christian, Leif, Lisa, Fredrik and Arwinder, I cannot thank you enough. Life in Narvik would have been unbearable without you. Also, I would never have learned how embarrassing a cat can be without Leif.

Finally, words cannot describe how grateful I am to my wife Penelope for her patience and unconditional support, even in the hardest moments.

E.F.A.

Executive Summary

This work investigates and implements algorithms for reliable parameter identification for salient pole synchronous machines that can be used for condition monitoring, on line assessment of the power grid, and adaptive control.

All these applications are steps necessary to enable a smarter power grid, in which seamless integrated digital technology provides state estimation, fault detection, and self-healing functionalities, with the ultimate goal of ensuring a reliable supply of electricity, and reducing vulnerability to natural disasters or attacks.

Considering that accurate modeling of a synchronous machine is an involved task, its model is first revised and its parameters defined. Thereafter, focus is given to develop an observer for damper winding currents, as these variables of the model are not readily available from measurement instruments in a power plant. Moreover, based on this machine model, an optimal observer for all inputs and outputs variables is developed. The goal of this observer is handling noise and correcting possible deviations in measurements caused by uncertainty of instruments or effects not included in the model. Validation of both observers shows high correlation with the reference model from Simscape Power Systems and low sensitivity to the load condition of the machine. It also shows the optimal observer maintain *goodness of fit* under a standard noise scenario.

With a model defined and inputs and outputs available, focus is given to the selection of an estimation algorithm. Recursive Least Squares is chosen based on three criteria: availability in the System Identification Toolbox of Simulink, possibility for near real-time execution, references in the literature available for comparison. With simplifications, 8 out of 13 parameters from the synchronous machine model are reliably estimated by the proposed algorithm. Estimations have very small percentage deviations from data sheet values, are in line with those reported in the literature, and are largely insensitive to noise and load conditions.

Lastly, the non linear effects of magnetic saturation is evaluated in the optimal observer and parameter estimator. When saturation is enabled in the reference model, the optimal observer is able to compensate its effects for all variables, except for one of the indirectly estimated values. This causes larger deviations in the estimation of one parameter that is directly affected by saturation. However, there is no direct correlation between the amplitude of this deviation and the saturation level, as one would expect. This leads to the conclusion that saturation effects must be included in the machine model.

Finally, it is presented a simplified model for saturation that can be easily integrated into the machine model, together with alternative methods and algorithms to estimate the remaining parameters of the synchronous machine. Despite their limitations, results presented can already be used for practical condition monitoring applications, such as detection of turn-to-turn short circuit and air-gap eccentricity.

Contents

List of Figures

List of Tables

Chapter 1

Introduction

This chapter gives an overview of the thesis topic and how the remaining part of the report is organized.

1.1 Background

"Applications of sound principles of planning, design, and operation - not revolutionary changes - are what is necessary to obtain satisfactory levels of reliability" Concordia (1968).

Synchronous generators are the bulk of power generation worldwide. In Norway, 95% of the electricity production comes from hydro power (NVE, 2017), in which the use of salient pole, synchronous generators is the norm. Therefore, the proper understanding of these devices is essential for planning, operation, and control of the power system (Kundur et al., 1994). Examples of tasks requiring adequate modeling and parametrization of synchronous machines includes load flow analysis, state estimation, stability assessment and tuning of grid controls and protection settings. These tasks are essential for a Transmission System Operator (TSO) or generation company to operate power system resources optimally and reliably.

Traditionally, synchronous generator parameters are calculated by manufacturers in the design phase using detailed information of the machine (Canay, 1969; Jackson and Winchester, 1969) or recursive methods such as Finite Element Method (FEM) analysis (Bianchi, 2005). Calculations are later validated during commissioning through acceptance or performance tests as described in IEEE and IEC Standards (IEEE, 2010; IEC, 2008). These methods for parameter identification of synchronous machines are well-proven and being used for decades to operate the power system reliably. However, they have two major shortcomings.

The first is considering that many parameter values in the system equations are constants and do not vary with time. However, several effects may impact the values of machine param-

eters over time. For example, temperature and load affects the air-gap length considerably (Dajaku and Gerling, 2012); field current level determines the saturation of the magnetic core (de Mello and Hannett, 1986); aging influences material properties. The reason for adopting this restriction is simplifying the analysis of equations, which was done manually when the theory for synchronous machines was developed. Paraphrasing Canay (1993b), the availability of powerful Information and Communication Technology (ICT) tools today makes such simplifications neither reasonable nor justifiable.

The second shortcoming is requiring the machine to be in standstill or off-line for performing the majority of tests for parameter estimation. Since this means loss of income for generation companies, tests are only executed during commissioning or planned stops. This limits greatly the amount of data and possible operational conditions that can be measured. In Norway, Statnett requires the registration of generators' parameters in SYSBAS for at least two weeks before commissioning, and an update with measured values after the machine starts commercial operation (Statnett, 2012). Yet, there is no requirement for periodical updates nor registration of distinct parameter values for different operational conditions.

An analogy for this second shortcoming is trying to forecast the weather for the next week in a certain area by taking relevant measurements once a day for 15 consecutive minutes, let's say from 08:00 to 08:15. For sure, by having this data over a decade, it is possible to forecast events such as dry or rainy season, the warmest and the coldest months of the year, the expected amount of rain or snow in a certain month. However, accuracy would be really low and one cannot expect a precise, hourly forecast of temperature or wind speed and direction based on this system. When the electric grid is operated closer to its limits, a more precise forecast of system parameters is a required feature for better state estimation and stability assessment (Bush, 2014).

1.2 Motivation

The main motivation of this master thesis is to investigate and implement algorithms for reliable parameter identification for salient pole synchronous machines. This can improve the state estimation of the electric grid with minimal disruption of the normal operation of the machine (Heydt et al., 2005) and consequently reduce uncertainties.

Moreover, storage of parameters values in a database together with the proper ICT infrastructure can enhance other applications such as:

- Condition monitoring: long-term changes in parameters indicate generator problems, such as rotor and stator windings turn-to-turn short circuit and air-gap eccentricity, and their proper monitoring can avoid catastrophic failures;

- Stability assessment: on line, accurate evaluation of power transfer limits, rotor angle and voltage stability can avoid large blackouts;
- Adaptive control: auto-tuning and gain-scheduling in the Automatic Voltage Regulator (AVR) and conditional settings in protection systems can increase stability and extend the operational range of some systems.

1.3 Problem formulation

The main goal of this master thesis is answering the following questions:

- What are the parameters of a synchronous machine?
- How non linear effects such as saturation affects them?
- How can parameters be estimated during normal operation, i.e. without taking the machine out of service?
- What are the effects of noise in the performance of the estimation procedure?
- Which of the parameters can be reliably estimated?

The actions below aims to obtain answers to these questions:

1. Review the literature: investigate and evaluate the state-of-the-art in estimation of parameters for salient pole synchronous machines based on off-line and on line measurements;
2. Model the machine: derive a mathematical model for a salient pole synchronous machine including the effects of saturation;
3. Validate the model: compare results of this derived model against the ones available in benchmark tools such as Simscape Power Systems (SPS) using data from a real machine;
4. Create an estimation procedure: implement and test algorithms in MATLAB/Simulink to estimate parameters of an advanced, non linear model in the benchmark tool;
5. Assess sensitivity: investigate the effects of noise in the estimation procedure and the sensitivity to it.

1.4 Limitations

The following limitations are taken into consideration:

- The algorithms for estimation of parameters run with the machine on line, and without taking it out of service, performing difficult and time-consuming tests or involving large perturbations;
- The required input data to the algorithms is based on common measurements available in a power plant, i.e. there is no need to install additional transducers in the machine;
- Focus is given to salient-pole, synchronous machines, since these are the bulk of power generation in Norway;
- Saturation effect is considered, since this affects considerably some parameter values;
- The data acquisition problem is separate from the parameter identification, i.e. it is assumed input data is available in a database and bad data detection and rejection was executed beforehand. However, the effect of measurement noise is considered.

1.5 Related work

Analysis, modeling and parameter estimation of synchronous generators is a century old problem in electrical engineering. However, it is still an active area of research today, due to its complexity and importance for power system planing, operation, and control.

A better understanding of electrical machines becomes necessary with the installation of the first commercial power systems at end of the 19th century. André Blondel is one of the first to study the coupling of synchronous generators to a large electric grid. His investigations led to the publication in French of "Empirical Theory of Synchronous Generator" in 1899, introducing the two-reaction theory (Capolino, 2004). This work is later expanded and translated into English (Blondel, 1913).

Due to a rapid expansion of the power industry, the interwar period is one of the most prolific in this research area. Several seminal papers are published in this period, including the abridgment of synchronous machines by Doherty and Nickle (1926, 1927, 1928, 1930), the generalized two-reaction theory by Park (1929, 1933), the methods for calculation of machine parameters by Kilgore (1931) and their determination by tests by Wright (1931), the extension of the two-reaction theory to study the machine connected to any type of balanced load by Concordia (1937) and the first state-space representation of electrical machines by Kron (1938).

In the postwar period, the exponential growth of the power system continues and efforts are focused on the documentation of the body of knowledge and its standardization using a formal mathematical approach. "AIEE 503 - Test Code for Synchronous Machines", arguably the first standard in the field, is published in 1945 (IEEE, 1983). Rankin (1945) establishes one of the most accepted per-unit bases for the rotor quantities. Also, the first editions of several influential books are printed in this period. Examples are the ones reviewing the theory and performance of electrical machines by Concordia (1951) and Adkins and Harley (1975); and the ones about power system stability by Crary (1947), Zdanov (1948) and Kimbark (1950). Finally, IEEE Std115 is published in 1965, the first international standard with test procedures for synchronous machines (IEEE, 1983).

The increased availability of computers in the 1960s allows development of more detailed and precise models by Kron (1967), Canay (1969) and Schulz et al. (1973). This leads to a better agreement between calculated and measured values of transient cases in simulations (Dandeno et al., 1973; Dineley and Morris, 1973; Dandeno et al., 1974). Hence, test methods to determine the parameters of these detailed models are soon developed by Yu and Moussa (1971), Lee and Tan (1977) and de Mello and Ribeiro (1977). Those lead to a general revision of IEEE Std115 in 1982 (IEEE, 1983).

In parallel, developments in control theory, electronics, and measurement equipment, brings the first methods of identification in the frequency domain by Manchur et al. (1972) and Shackshaft (1974). As consequence, standstill (Coultes and Watson, 1981) and on line frequency-response tests emerge (Dandeno et al., 1981). Not least, attempts to model saturation dynamically are done by Fuchs and Erdelyi (1973), Shackshaft and Henser (1979), Namba et al. (1981a), de Mello and Hannett (1986) and El-Serafi et al. (1988).

In the 1990s, several authors, such as Canay (1993b), Wang (1995), Kamwa et al. (1997) and Levi (1998), take advantage of Moore's law effects and develop very precise, high-order, non linear models including several rotor circuits and dynamic effects of saturation. Also, the increased popularity of frequency response methods culminates with their incorporation in the revision of IEEE Std115 in 1995 (IEEE Power Engineering Society, 1996). At the same time, Kamwa et al. (1990), Fairbairn and Harley (1990), Canay (1993a), Huang et al. (1994), Wang et al. (1994) and Tsai et al. (1995) make use of different approaches using system identification to develop automated procedures for parameter identification.

Later on, automated procedures for synchronous machine parameter identification are encouraged by the popularization of system identification techniques and their easy access in mathematical tools such as MATLAB© (Ljung, 2012). Methods are varied, but approaches can be summarized in analysis of transient data, such as short-circuit or load rejections; and frequency response tests, with injection of perturbations in standstill, off-line or on line operation. Successful examples of such automated procedures are extensive in the literature

and are described by Verbeeck et al. (2000), Bortoni and Jardini (2002), Karayaka et al. (2003), Kyriakides et al. (2005), Dehghani and Nikravesh (2008), among others.

1.6 Outline

- **Chapter 2** introduces the synchronous machine equations, model and parameters used in the thesis.
- **Chapter 3** present details about the implementation of an optimal observer for the inputs and outputs variables of the synchronous model described in the previous chapter, and how this observer performs in several simulation cases and noise scenarios when compared to the synchronous machine model available in Simscape Power Systems;
- **Chapter 4** describes the algorithm for parameter estimation used in this thesis, and how it performs in the same simulation cases and noise scenarios evaluated in the previous chapter;
- **Chapter 5** verify the effect of saturation in the observer and estimation algorithms, and also describes how this effect can be modeled;
- **Chapter 6** presents conclusions, discussion, and ideas for further work.
- **Appendix A** contains an automated report of the Matlab Simulink model developed for this thesis.
- **Appendices B to D** contain figures with results of the several simulations for validation of the thesis synchronous machine model and the parameter estimation algorithm. They are not included directly in the main chapters for the sake of brevity.

Chapter 2

Synchronous Machine Equations and Parameters

"There is probably more literature on synchronous machines than on any other device in electrical engineering. Unfortunately, this vast amount of material often makes the subject complex and confusing." Sauer et al. (2017)

To avoid such confusion, a review of the dynamic model of the synchronous machine is performed in this chapter. For the sake of clarity, the model is derived step by step, and effects such as the type of neutral grounding are included gradually. At the end of this chapter, the reader should be able to understand the mathematical model used in the rest of this thesis and the meaning of its parameters.

It is assumed the reader is familiarized with analysis of electric machines, therefore there is a limited description of physical concepts and a high level of abstraction. If this assumption is not correct, the author recommends referring to Mohan (2012, ch. 5) and Mohan (2014, ch. 2 and 3) before continuing further.

The notation adopted follows the IEEE convention (IEEE, 1969) and the mathematical model presented is based on the work of Machowski et al. (2008, ch. 11). Moreover, the following assumptions are made:

1. The three-phase stator winding is symmetrical, sinusoidally distributed and is wye/star connected;

2. The capacitance of all windings is neglected;

3. Each of the distributed windings is represented by a concentrated winding;

4. The change in the inductance of the stator windings due to rotor position is sinusoidal and does not contain higher harmonics;

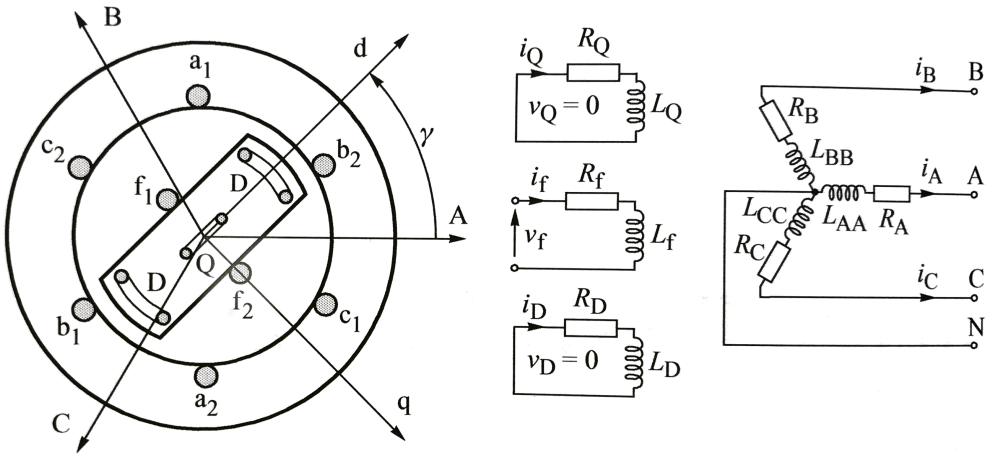

Figure 2.1: The windings in the synchronous machine and their axes (Machowski et al., 2008, p. 434)

5. Hysteresis losses are negligible but the influence of eddy currents is included in the model of the damper windings;

6. The magnetic circuits are linear (not saturated) and the inductance values do not depend on the current.[1]

2.1 Flux linkages in the (A, B, C) reference frame

Figure 2.1 shows a schematic cross-section of a synchronous machine with their windings and axes, with:

- a three-phase stator armature winding (a1, a2, b1, b2, c1, c2);
- a rotor field winding (f1, f2);
- two rotor damper windings, one in the direct axis (D) and another in the quadrature axis (Q);
- the static axes of the stator reference frame (A, B, C), where the center of phase A is used as reference;
- the rotating axes of the rotor reference frame (d, q);
- the rotor position (γ) in relation to the A-axis, where $\gamma = \gamma_0 + \omega t$.

[1] Later on, chapter 5 presents an algorithm to account for saturation effects.

The flux in each winding depends on the currents in all other windings as they are all magnetically coupled. This can be represented by the matrix equation below:

$$\begin{bmatrix} \Phi_A \\ \Phi_B \\ \Phi_C \\ \hdashline \Phi_f \\ \Phi_D \\ \Phi_Q \end{bmatrix} = \left[\begin{array}{ccc:ccc} L_{AA} & L_{AB} & L_{AC} & L_{Af} & L_{AD} & L_{AQ} \\ L_{BA} & L_{BB} & L_{BC} & L_{Bf} & L_{BD} & L_{BQ} \\ L_{CA} & L_{CB} & L_{CC} & L_{Cf} & L_{CD} & L_{CQ} \\ \hdashline L_{fA} & L_{fB} & L_{fC} & L_{ff} & L_{fD} & L_{fQ} \\ L_{DA} & L_{DB} & L_{DC} & L_{Df} & L_{DD} & L_{DQ} \\ L_{QA} & L_{QB} & L_{QC} & L_{Qf} & L_{QD} & L_{QQ} \end{array}\right] \begin{bmatrix} i_A \\ i_B \\ i_C \\ \hdashline i_f \\ i_D \\ i_Q \end{bmatrix} \tag{2.1}$$

or, in compact form:

$$\begin{bmatrix} \mathbf{\Phi}_{ABC} \\ \hdashline \mathbf{\Phi}_{fDQ} \end{bmatrix} = \left[\begin{array}{c:c} \mathbf{L_S} & \mathbf{L_{SR}} \\ \hdashline \mathbf{L}_{ST}^T & \mathbf{L}_R \end{array}\right] \begin{bmatrix} \mathbf{i}_{ABC} \\ \hdashline \mathbf{i}_{fDQ} \end{bmatrix} \tag{2.2}$$

Where:

- $\mathbf{L}_S$ submatrix of the stator self- and mutual inductances;
- $\mathbf{L}_R$ submatrix of the rotor self- and mutual inductances;
- $\mathbf{L}_{SR}$ submatrix of the rotor to stator mutual inductances.

Most of the elements forming the inductance matrix in eq. (2.1) are dependent on the rotor position. In particular, for salient pole machines, they are subject to periodic changes due to the saliency of the rotor. Considering the assumptions outlined in the introduction, these inductances are represented by a constant component and a single periodic component.

When the rotor d-axis aligns with the axis of the phase windings, the reluctance of the flux path is minimum. This is when the maximum value of the self-inductance of each stator phase winding is reached. The minimum reluctance occurs twice for each rotation, hence the stator self-inductances have the form:

$$\begin{aligned} L_{AA} &= L_S + \Delta L_S \cos 2\gamma \\ L_{BB} &= L_S + \Delta L_S \cos\left(2\gamma - \frac{2}{3}\pi\right) \\ L_{CC} &= L_S + \Delta L_S \cos\left(2\gamma - \frac{4}{3}\pi\right) \end{aligned} \tag{2.3}$$

Considering the stator windings are shifted in space by 120°, the mutual inductance between them is negative. Also, the magnitude is maximum when the rotor d-axis is halfway

between two of the stator windings axes. Thus, the stator mutual inductances have the form:

$$\begin{aligned} L_{AB} = L_{BA} &= -M_S - \Delta L_S \cos\left(2\gamma + \frac{1}{3}\pi\right) \\ L_{BC} = L_{CB} &= -M_S - \Delta L_S \cos\left(2\gamma + \pi\right) \\ L_{CA} = L_{AC} &= -M_S - \Delta L_S \cos\left(2\gamma + \frac{5}{3}\pi\right) \end{aligned} \tag{2.4}$$

The mutual inductances between stator and rotor windings have a positive maximum when the axes of a stator winding and rotor winding align and have the same positive flux direction. They have a negative minimum when the flux directions are in opposition and are zero when the axes are perpendicular. In summary, the rotor to stator mutual inductances have the form:

$$L_{Af} = L_{fA} = M_f \cos\gamma \quad L_{Bf} = L_{fB} = M_f \cos\left(\gamma - \frac{2}{3}\pi\right) \quad L_{Cf} = L_{fC} = M_f \cos\left(\gamma - \frac{4}{3}\pi\right) \tag{2.5}$$

$$L_{AD} = L_{DA} = M_D \cos\gamma \quad L_{BD} = L_{DB} = M_D \cos\left(\gamma - \frac{2}{3}\pi\right) \quad L_{CD} = L_{DC} = M_D \cos\left(\gamma - \frac{4}{3}\pi\right) \tag{2.6}$$

$$L_{AQ} = L_{QA} = M_Q \cos\gamma \quad L_{BQ} = L_{QB} = M_Q \cos\left(\gamma - \frac{2}{3}\pi\right) \quad L_{CQ} = L_{QC} = M_Q \cos\left(\gamma - \frac{4}{3}\pi\right) \tag{2.7}$$

The rotor self inductances do not depend on the rotor position and are constant. Not less, the rotor mutual inductances are zero, since the d- and q-axis are perpendicular to each other:

$$L_{fQ} = L_{Qf} = L_{DQ} = L_{QD} = 0; \quad L_{ff} = L_f; \quad L_{DD} = L_D; \quad L_{QQ} = L_Q; \quad L_{fD} = L_{Df} \tag{2.8}$$

2.2 Flux linkages in the (d, q, 0) reference frame

Each phasor (voltage, current or flux linkage) in the stator reference frame (A, B, C) can be transferred into the rotor reference frame (d, q) by a linear transformation dependent on the rotor position γ. In this case, the inverse transformation from (d, q) to (A, B, C) is not unique, i.e. an isomorphism as defined by Lay et al. (2016, ch. 4.4).

To achieve an isomorphic transformation, it is necessary to include an additional coordinate, which is usually the zero-sequence as defined by Clarke (1943) in the method of symmetrical components. This tensor is referred in the literature as the dq0-transformation

(Lipo, 1984), and is given below:

$$\begin{bmatrix} i_d \\ i_q \\ i_0 \end{bmatrix} = \begin{bmatrix} \beta_d \cos\gamma & \beta_d \cos\left(\gamma - \frac{2}{3}\pi\right) & \beta_d \cos\left(\gamma - \frac{4}{3}\pi\right) \\ \beta_q \sin\gamma & \beta_q \sin\left(\gamma - \frac{2}{3}\pi\right) & \beta_q \sin\left(\gamma - \frac{4}{3}\pi\right) \\ \beta_0 & \beta_0 & \beta_0 \end{bmatrix} \begin{bmatrix} i_A \\ i_B \\ i_C \end{bmatrix} \tag{2.9}$$

or, in compact form:

$$\mathbf{i}_{dq0} = \mathbf{W}\mathbf{i}_{ABC} \tag{2.10}$$

where $\beta_d, \beta_q, \beta_0$ are arbitrary, non-zero coefficients introduced due to the change of reference frame.

Since the dq0-transformation is an isomorphism, the inverse transformation exists according to the invertible matrix theorem (Lay et al., 2016, ch. 2.4) and is uniquely determined by:

$$\mathbf{i}_{ABC} = \mathbf{W}^{-1}\mathbf{i}_{dq0} \tag{2.11}$$

In order to make the transformation orthogonal, i.e. $\mathbf{W^{-1}} = \mathbf{W^T}$, the coefficients are chosen as $\beta_d = -\sqrt{2/3}, \beta_q = \sqrt{2/3}, \beta_0 = 1/\sqrt{3}$. This gives the following transformation matrix:

$$W = \sqrt{\frac{2}{3}} \begin{bmatrix} -\cos\gamma & -\cos\left(\gamma - \frac{2}{3}\pi\right) & -\cos\left(\gamma - \frac{4}{3}\pi\right) \\ \sin\gamma & \sin\left(\gamma - \frac{2}{3}\pi\right) & \sin\left(\gamma - \frac{4}{3}\pi\right) \\ \frac{1}{\sqrt{2}} & \frac{1}{\sqrt{2}} & \frac{1}{\sqrt{2}} \end{bmatrix} \tag{2.12}$$

This choice of coefficients also make the transformation power invariant, i.e. the power calculated in both the (A, B, C) and the (d, q) reference frames is identical. This property will be extremely useful when deriving the per-unit (pu) model in section 2.5.

The special case[2] of the dq0 transformation where the rotating speed of the (d, q) reference frame is the same as the rotor speed (ω) is usually referred to as Park transformation, in tribute to Robert H. Park. However, the original transformation proposed by Park (1929) was not orthogonal, and was later rectified by Concordia (1951).

Considering that rotor currents, voltages and flux linkages are already in the (d, q) reference frame, no transformation is necessary for them. Therefore, it is possible to write flux

[2]The (d, q) reference frame may have a rotating speed different from the rotor. This is particularly useful for analysis of asynchronous machines, although would not make any sense for a synchronous machine.

linkages and currents as:

$$\begin{bmatrix} \mathbf{\Phi}_{dq0} \\ \mathbf{\Phi}_{fDQ} \end{bmatrix} = \begin{bmatrix} \mathbf{W} & \mathbf{0} \\ \mathbf{0} & \mathbf{1} \end{bmatrix} \begin{bmatrix} \mathbf{\Phi}_{ABC} \\ \mathbf{\Phi}_{fDQ} \end{bmatrix} \qquad \begin{bmatrix} \mathbf{i}_{ABC} \\ \mathbf{i}_{fDQ} \end{bmatrix} = \begin{bmatrix} \mathbf{W}^{-1} & \mathbf{0} \\ \mathbf{0} & \mathbf{1} \end{bmatrix} \begin{bmatrix} \mathbf{i}_{dq0} \\ \mathbf{i}_{fDQ} \end{bmatrix} \tag{2.13}$$

Substituing eq. (2.2) into eq. (2.13), one obtains:

$$\begin{aligned} \begin{bmatrix} \mathbf{\Phi}_{dq0} \\ \mathbf{\Phi}_{fDQ} \end{bmatrix} &= \begin{bmatrix} \mathbf{W} & \mathbf{0} \\ \mathbf{0} & \mathbf{1} \end{bmatrix} \begin{bmatrix} \mathbf{L}_S & \mathbf{L}_{SR} \\ \mathbf{L}_{ST}^T & \mathbf{L}_R \end{bmatrix} \begin{bmatrix} \mathbf{W}^{-1} & \mathbf{0} \\ \mathbf{0} & \mathbf{1} \end{bmatrix} \begin{bmatrix} \mathbf{i}_{dq0} \\ \mathbf{i}_{fDQ} \end{bmatrix} \\ \begin{bmatrix} \mathbf{\Phi}_{dq0} \\ \mathbf{\Phi}_{fDQ} \end{bmatrix} &= \left[\begin{array}{c|c} \mathbf{W}\mathbf{L}_S\mathbf{W}^{-1} & \mathbf{W}\mathbf{L}_{SR} \\ \hline \mathbf{L}_{SR}^T\mathbf{W}^{-1} & \mathbf{L}_R \end{array}\right] \begin{bmatrix} \mathbf{i}_{dq0} \\ \mathbf{i}_{fDQ} \end{bmatrix} \end{aligned} \tag{2.14}$$

The sub-matrices from eq. (2.14) can now be calculated:

$$\mathbf{W}\mathbf{L}_S\mathbf{W}^{-1} = \mathbf{W} \begin{bmatrix} L_{AA} & L_{AB} & L_{AC} \\ L_{BA} & L_{BB} & L_{BC} \\ L_{CA} & L_{CB} & L_{CC} \end{bmatrix} \mathbf{W}^{-1} = \begin{bmatrix} L_0 & & \\ & L_d & \\ & & L_q \end{bmatrix}$$

$$\mathbf{W}\mathbf{L}_{SR} = \mathbf{W} \begin{bmatrix} L_{Af} & L_{AD} & L_{AQ} \\ L_{Bf} & L_{BD} & L_{BQ} \\ L_{Cf} & L_{CD} & L_{CQ} \end{bmatrix} \mathbf{W}^{-1} = \begin{bmatrix} kM_f & kM_D & \\ & & kM_q \\ & & \end{bmatrix}$$

$$\mathbf{L}_{SR}^T\mathbf{W}^{-1} = \mathbf{L}_{SR}^T\mathbf{W}^T = (\mathbf{W}\mathbf{L}_{SR})^T$$

Where:

- $L_0 = L_S - 2M_S$;
- $L_d = L_S + M_S + \frac{3}{2}\Delta L_S$;
- $L_q = L_S + M_S - \frac{3}{2}\Delta L_S$;
- $k = \sqrt{\frac{3}{2}}$.

With that, eq. (2.14) can be expanded into:

$$\left[\begin{array}{c} \Phi_d \\ \hline \Phi_q \\ \hline \Phi_0 \\ \hline \Phi_f \\ \hline \Phi_D \\ \hline \Phi_Q \end{array}\right] = \left[\begin{array}{c|c|c|c|c|c} L_d & & & kM_f & kM_D & \\ \hline & L_q & & & & kM_Q \\ \hline & & L_0 & & & \\ \hline kM_f & & & L_f & L_{fD} & \\ \hline kM_D & & & L_{fD} & L_D & \\ \hline & kM_Q & & & & L_Q \end{array}\right] \left[\begin{array}{c} i_d \\ \hline i_q \\ \hline i_0 \\ \hline i_f \\ \hline i_D \\ \hline i_Q \end{array}\right] \tag{2.15}$$

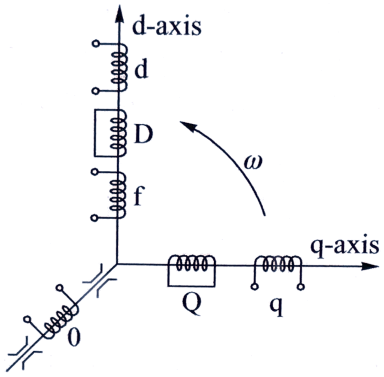

Figure 2.2: Three sets of fictitious perpendicular windings representing the synchronous machine (Machowski et al., 2008, p. 438)

From eq. (2.15), one can rewrite three independent set of equations:

$$\Phi_0 = L_0 i_0 \tag{2.16}$$

$$\begin{bmatrix} \Phi_d \\ \Phi_f \\ \Phi_D \end{bmatrix} = \begin{bmatrix} L_d & kM_f & kM_D \\ kM_f & L_f & L_{fD} \\ kM_D & L_{fD} & L_D \end{bmatrix} \begin{bmatrix} i_d \\ i_f \\ i_D \end{bmatrix} \tag{2.17}$$

$$\begin{bmatrix} \Phi_q \\ \Phi_Q \end{bmatrix} = \begin{bmatrix} L_q & kM_Q \\ kM_Q & L_Q \end{bmatrix} \begin{bmatrix} i_q \\ i_Q \end{bmatrix} \tag{2.18}$$

The dq0-transformation can be interpreted as substituting the effects of the three-phase stator armature windings shifted in space by 120° (a1, a2, b1, b2, c1, c2 in fig. 2.1), by three fictitious rotor windings all orthogonal to each other (d, q and 0 in fig. 2.2). The greatest advantage of orthogonality is the absence of magnetic coupling among the windings in different axis, reducing the number of parameters in the model and simplifying the analysis.

2.3 Voltage equations

The application of Kirchhoff's voltage law in the windings circuits of fig. 2.1 leads to:

$$\begin{bmatrix} v_A \\ v_B \\ v_C \\ -v_F \\ 0 \\ 0 \end{bmatrix} = - \begin{bmatrix} R_A & & & & & \\ & R_B & & & & \\ & & R_C & & & \\ & & & R_f & & \\ & & & & R_D & \\ & & & & & R_Q \end{bmatrix} - \frac{d}{dt} \begin{bmatrix} \Phi_d \\ \Phi_q \\ \Phi_0 \\ \Phi_f \\ \Phi_D \\ \Phi_Q \end{bmatrix} \tag{2.19}$$

Note that v_f has negative sign due to the generator convention used. Also that $v_Q = v_D = 0$, since D and Q windings are short-circuited. It is also possible to write eq. (2.19) in compact form:

$$\begin{bmatrix} \mathbf{v}_{ABC} \\ \mathbf{v}_{fDQ} \end{bmatrix} = - \begin{bmatrix} \mathbf{R}_{ABC} & \\ & \mathbf{R}_{fDQ} \end{bmatrix} \begin{bmatrix} \mathbf{i}_{ABC} \\ \mathbf{i}_{fDQ} \end{bmatrix} - \frac{d}{dt} \begin{bmatrix} \mathbf{\Phi}_{ABC} \\ \mathbf{\Phi}_{fDQ} \end{bmatrix} \tag{2.20}$$

Application of the dq0-transformation in eq. (2.20) develops into:

$$\begin{aligned}
\begin{bmatrix} \mathbf{W}^{-1} & \\ & \mathbf{1} \end{bmatrix} \begin{bmatrix} \mathbf{v}_{ABC} \\ \mathbf{v}_{fDQ} \end{bmatrix} &= - \begin{bmatrix} \mathbf{R}_{ABC} & \\ & \mathbf{R}_{fDQ} \end{bmatrix} \begin{bmatrix} \mathbf{W}^{-1} & \\ & \mathbf{1} \end{bmatrix} \begin{bmatrix} \mathbf{i}_{ABC} \\ \mathbf{i}_{fDQ} \end{bmatrix} \\
&\quad - \frac{d}{dt} \left\{ \begin{bmatrix} \mathbf{W}^{-1} & \\ & \mathbf{1} \end{bmatrix} \begin{bmatrix} \mathbf{\Phi}_{ABC} \\ \mathbf{\Phi}_{fDQ} \end{bmatrix} \right\} \\
\begin{bmatrix} \mathbf{v}_{dq0} \\ \mathbf{v}_{fDQ} \end{bmatrix} &= - \begin{bmatrix} \mathbf{W} & \\ & \mathbf{1} \end{bmatrix} \begin{bmatrix} \mathbf{R}_{ABC} & \\ & \mathbf{R}_{fDQ} \end{bmatrix} \begin{bmatrix} \mathbf{W}^{-1} & \\ & \mathbf{1} \end{bmatrix} \begin{bmatrix} \mathbf{i}_{dq0} \\ \mathbf{i}_{fDQ} \end{bmatrix} \\
&\quad - \begin{bmatrix} \mathbf{W} & \\ & \mathbf{1} \end{bmatrix} \frac{d}{dt} \left\{ \begin{bmatrix} \mathbf{W}^{-1} & \\ & \mathbf{1} \end{bmatrix} \begin{bmatrix} \mathbf{\Phi}_{dq0} \\ \mathbf{\Phi}_{fDQ} \end{bmatrix} \right\} \\
\begin{bmatrix} \mathbf{v}_{dq0} \\ \mathbf{v}_{fDQ} \end{bmatrix} &= - \begin{bmatrix} \mathbf{W}\mathbf{R}_{ABC}\mathbf{W}^{-1} & \\ & \mathbf{R}_{fDQ} \end{bmatrix} \begin{bmatrix} \mathbf{i}_{dq0} \\ \mathbf{i}_{fDQ} \end{bmatrix} \\
&\quad - \begin{bmatrix} \mathbf{W} & \\ & \mathbf{1} \end{bmatrix} \frac{d}{dt} \begin{bmatrix} \mathbf{W}^{-1}\mathbf{\Phi}_{dq0} \\ \mathbf{\Phi}_{fDQ} \end{bmatrix}
\end{aligned} \tag{2.21}$$

Now, assuming the resistance of each of the stator phases is identical, i.e. $R_A = R_B = R_C = R$, and considering $\mathbf{R}_{ABC}$ is a diagonal matrix, one finds that:

$$\mathbf{W}\mathbf{R}_{ABC}\mathbf{W}^{-1} = R\ \mathbf{W}\mathbf{W}^{-1} = R\ \mathbf{1} = \mathbf{R} \tag{2.22}$$

Also, the following equation is derived when considering that γ and consequently $\mathbf{W}$ are functions of the time:

$$\frac{d}{dt}\left(\mathbf{W}^{-1}\mathbf{\Phi}_{dq0}\right) = \frac{d}{dt}\left(\mathbf{W}^{-1}\right)\mathbf{\Phi}_{dq0} + \mathbf{W}^{-1}\frac{d}{dt}\left(\mathbf{\Phi}_{dq0}\right) \tag{2.23}$$

Multiplying eq. (2.23) by $\mathbf{W}$ on the left:

$$\mathbf{W}\frac{d}{dt}\left(\mathbf{W}^{-1}\mathbf{\Phi}_{dq0}\right) = \mathbf{W}\frac{d}{dt}\left(\mathbf{W}^{-1}\right)\mathbf{\Phi}_{dq0} + \frac{d}{dt}\left(\mathbf{\Phi}_{dq0}\right)$$

And noting that

$$\frac{d}{dt}\mathbf{W}\mathbf{W}^{-1} = \frac{d}{dt}\mathbf{1} \Rightarrow \frac{d}{dt}\left(\mathbf{W}\right)\mathbf{W}^{-1} + \mathbf{W}\frac{d}{dt}\left(\mathbf{W}^{-1}\right) = \mathbf{0} \Rightarrow \mathbf{W}\frac{d}{dt}\left(\mathbf{W}^{-1}\right) = -\frac{d}{dt}\left(\mathbf{W}\right)\mathbf{W}^{-1}$$

Equation (2.23) now becomes:

$$\mathbf{W}\frac{d}{dt}\left(\mathbf{W^{-1}}\mathbf{\Phi}_{dq0}\right) = -\frac{d}{dt}\left(\mathbf{W}\right)\mathbf{W}^{-1}\mathbf{\Phi}_{dq0} + \frac{d}{dt}\left(\mathbf{\Phi}_{dq0}\right) \tag{2.24}$$

Last but not least, it is possible to define:

$$\mathbf{\Omega} = \frac{d}{dt}\left(\mathbf{W}\right)\mathbf{W}^{-1} = \omega\begin{bmatrix}0 & 0 & -1\\ 0 & 1 & 0\\ 0 & 0 & 0\end{bmatrix} \tag{2.25}$$

which is known as the *rotation matrix* (Machowski et al., 2008, p. 441), as it introduces terms into the voltage equations which are dependent on the speed of rotation.

Finally, when substituting eqs. (2.22) to (2.25) into eq. (2.21), the voltage equations in the (d, q) reference frame are obtained:

$$\begin{bmatrix}\mathbf{v}_{dq0}\\ \mathbf{v}_{fDQ}\end{bmatrix} = -\begin{bmatrix}\mathbf{R} & \\ & \mathbf{R}_{fDQ}\end{bmatrix}\begin{bmatrix}\mathbf{i}_{dq0}\\ \mathbf{i}_{fDQ}\end{bmatrix} - \frac{d}{dt}\left\{\begin{bmatrix}\mathbf{\Phi}_{dq0}\\ \mathbf{\Phi}_{fDQ}\end{bmatrix}\right\} + \begin{bmatrix}\mathbf{\Omega} & \\ & \mathbf{0}\end{bmatrix}\begin{bmatrix}\mathbf{\Phi}_{dq0}\\ \mathbf{\Phi}_{fDQ}\end{bmatrix} \tag{2.26}$$

Which in expanded form becomes:

$$\begin{bmatrix}v_d\\ v_q\\ v_0\\ -v_f\\ 0\\ 0\end{bmatrix} = -\begin{bmatrix}R & & & & & \\ & R & & & & \\ & & R & & & \\ & & & R_f & & \\ & & & & R_D & \\ & & & & & R_Q\end{bmatrix}\begin{bmatrix}i_d\\ i_q\\ i_0\\ i_f\\ i_D\\ i_Q\end{bmatrix} - \frac{d}{dt}\left\{\begin{bmatrix}\Phi_d\\ \Phi_q\\ \Phi_0\\ \Phi_f\\ \Phi_D\\ \Phi_Q\end{bmatrix}\right\} + \omega\begin{bmatrix}-\Phi_q\\ \Phi_d\\ 0\\ 0\\ 0\\ 0\end{bmatrix} \tag{2.27}$$

Equation (2.27) expresses voltages in terms of both current and flux linkages. Considering the limitations of this thesis (refer to section 1.4), it is a huge advantage if voltages are expressed in terms of currents only, because these are easily available in a power plant, while flux linkages are not. Therefore, eq. (2.15) is used to substitute flux linkages by currents in

eq. (2.27), giving:

$$\begin{bmatrix} v_d \\ v_q \\ v_0 \\ -v_f \\ 0 \\ 0 \end{bmatrix} = -\begin{bmatrix} R & \omega L_q & & & & \omega k M_Q \\ -\omega L_d & R & & -\omega k M_f & -\omega k M_D & \\ & & R & & & \\ & & & R_f & & \\ & & & & R_D & \\ & & & & & R_Q \end{bmatrix} \begin{bmatrix} i_d \\ i_q \\ i_0 \\ i_f \\ i_D \\ i_Q \end{bmatrix} - \begin{bmatrix} L_d & & & k M_f & k M_D & \\ & L_q & & & & k M_Q \\ & & L_0 & & & \\ k M_f & & & L_f & L_{fD} & \\ k M_D & & & L_{fD} & L_D & \\ & k M_Q & & & & L_Q \end{bmatrix} \frac{d}{dt} \left\{ \begin{bmatrix} i_d \\ i_q \\ i_0 \\ i_f \\ i_D \\ i_Q \end{bmatrix} \right\} \tag{2.28}$$

Note the inductance matrix is removed from the derivative because it is not considered a function of time. This may seem a contradiction to what was stated in section 1.1. However, as presented there, changes over time of parameters are mainly due to temperature and load variations, saturation and aging. These are slow processes that will have no effect during the data acquisition period required for estimation of parameters. Therefore, it is reasonable to remove the inductance matrix of the derivative in eq. (2.28).

2.4 Effects of grounding

At this point, it is important to consider the effect of grounding in eq. (2.28), i.e. how point N in fig. 2.1 is connected to the ground. In this realm, we can have three types of connection: open, solid, or through an impedance $Z_N = R_N + j\omega L_N$. Since the first two cases can be represented by infinite or zero impedances, respectively, only the last case will be analyzed. Not least, commercial synchronous generators are mostly grounded through an impedance, in order to limit the zero-sequence current and over-voltages in unbalanced faults (Reimert, 2006, sec 5.3).

Clarke (1943, ch. VIII) shows the effect of grounding through an impedance on the zero-sequence voltage is the following: $v_0 = i_0(Z_0 + 3Z_N)$. The correction of eq. (2.28) with the grounding effect produces:

$$\begin{bmatrix} v_d \\ v_q \\ v_0 \\ -v_f \\ 0 \\ 0 \end{bmatrix} = -\begin{bmatrix} R & \omega L_q & & & & \omega k M_Q \\ -\omega L_d & R & & -\omega k M_f & -\omega k M_D & \\ & & R+3R_N & & & \\ & & & R_f & & \\ & & & & R_D & \\ & & & & & R_Q \end{bmatrix} \begin{bmatrix} i_d \\ i_q \\ i_0 \\ i_f \\ i_D \\ i_Q \end{bmatrix}$$
$$- \begin{bmatrix} L_d & & & k M_f & k M_D & \\ & L_q & & & & k M_Q \\ & & L_0+3L_N & & & \\ k M_f & & & L_f & L_{fD} & \\ k M_D & & & L_{fD} & L_D & \\ & k M_Q & & & & L_Q \end{bmatrix} \frac{d}{dt} \left\{ \begin{bmatrix} i_d \\ i_q \\ i_0 \\ i_f \\ i_D \\ i_Q \end{bmatrix} \right\} \tag{2.29}$$

2.5 Choosing a pu base

"Perhaps the one area in power systems analysis that causes more confusion than any other is that of per-unit system. This confusion is further compounded when a synchronous machine is included in the system. However, the per-unit system is well established and has a number of attractions." (Machowski et al., 2008, Appendix A.1)

Such attractions are, for example, normalizing parameters of machines with different ratings, providing an intuitive understanding of performance, and computational efficiencies. But most of all, the proper choice of a pu base for the rotor quantities can greatly reduce the number of parameters in the mathematical model.

So, in order to avoid the negative aspects of the per-unit system, the base quantities used in this thesis are reviewed in this section and defined in tables 2.1 and 2.2. The derivation of the rotor bases is explained in the remaining of this section.

At this stage, it is convenient to separate each individual winding self-inductance into its magnetizing (L_{mx}) and leakage (l_x) components, so that:

$$\begin{aligned} L_d &= L_{md} + l_l & L_D &= L_{mD} + l_D & L_f &= L_{mf} + l_f \\ L_q &= L_{mq} + l_l & L_Q &= L_{mD} + l_Q \end{aligned} \tag{2.30}$$

For the rotor base quantities, the *equal mutual flux linkages* system as defined by Anderson and Fouad (2003) is chosen. This pu system requires the mutual flux linkage in each winding

Table 2.1: Stator base quantities

Symbol	Description	Definition	Unit
V_b	Base voltage	Line to neutral Root Mean Square (RMS) terminal voltage, V_{L-N}	V
S_b	Base power	Rated apparent power per phase, $S_{1\Phi}$	V A
$S_{3\Phi}$	Base machine power	$S_{3\Phi} = 3S_{1\Phi} = 3S_b$	V A
t_b	Base time	$t_b = 1$	s
I_b	Base current	$I_b = \frac{S_b}{V_b}$	A
Z_b	Base impedance	$Z_b = \frac{V_b}{I_b} = \frac{V_b^2}{S_b}$	Ω
L_b	Base inductance	$L_b = \frac{V_b t_b}{I_b} = Z_b$	H
Φ_b	Base flux linkage	$\Phi_b = L_b I_b = V_b t_b \equiv V_b$	V s
θ_b	Base elec. angle	$\theta_b = 1$	elec. rad
ω_b	Base elec. speed	$\omega_b = \frac{\theta_b}{t_b} = 1$	elec. rad s^{-1}
θ_{mb}	Base mech. angle	$\theta_{mb} = 1$	mech. rad
ω_{mb}	Base mech. speed	$\omega_{mb} = \frac{\theta_{mb}}{t_b} = 1$	mech. rad s^{-1}

to be equal. Applying this assumption to eq. (2.15) gives:

$$\begin{aligned} d-coil: &\quad L_{md} I_b = k M_D I_{Db} = k M_f I_{fb} \\ D-coil: &\quad k M_D I_b = L_{mD} I_{Db} = L_{fD} I_{fb} \\ f-coil: &\quad k M_f I_b = L_{fD} I_{Db} = L_{mf} I_{fb} \\ q-coil: &\quad L_{mq} I_b = k M_Q I_{Qb} \\ Q-coil: &\quad k M_Q I_b = L_{mQ} I_{Qb} \end{aligned} \tag{2.31}$$

As the dq0 transformation is power invariant, the base power for each winding must be the same and equal to $Sb = V_b I_b = V_{fb} I_{fb} = V_{Db} I_{Db} = V_{Qb} I_{Qb}$. This and eq. (2.31) produce

Table 2.2: Rotor base quantities

Symbol	Description	Definition	Unit
Z_{fb}	Base impedance field winding	$Z_{fb} = \frac{V_{fb}}{I_{fb}} = k_f^2 Z_b$	Ω
Z_{Db}	Base impedance D damper winding	$Z_{Db} = \frac{V_{Db}}{I_{Db}} = k_D^2 Z_b$	Ω
Z_{Qb}	Base impedance Q damper winding	$Z_{Qb} = \frac{V_{Qb}}{I_{Qb}} = k_Q^2 Z_b$	Ω
L_{fb}	Base inductance field winding	$L_{fb} = \frac{V_{fb} t_b}{I_{fb}} = k_f^2 L_b$	H
L_{Db}	Base inductance D damper winding	$L_{Db} = \frac{V_{Db} t_b}{I_{Db}} = k_D^2 L_b$	H
L_{Qb}	Base inductance Q damper winding	$L_{Qb} = \frac{V_{Qb} t_b}{I_{Qb}} = k_Q^2 L_b$	H
M_{fb}	Base mutual inductance field winding	$M_{fb} = \frac{V_{fb} t_b}{I_b} = \frac{V_b t_b}{I_{fb}} = k_f L_b$	H
M_{Db}	Base mutual inductance D damper winding	$M_{Db} = \frac{V_{Db} t_b}{I_b} = \frac{V_b t_b}{I_{Db}} = k_D L_b$	H
M_{Qb}	Base mutual inductance Q damper winding	$M_{Qb} = \frac{V_{Qb} t_b}{I_b} = \frac{V_b t_b}{I_{Qb}} = k_Q L_b$	H
L_{fDb}	Base mutual inductance f and D windings coupling	$L_{fDb} = \frac{V_{fb} t_b}{I_{Db}} = \frac{V_{Db} t_b}{I_{fb}} = k_f k_D L_b$	H

the *rotor scaling factors*:

$$\begin{aligned}
\frac{V_{fb}}{V_b} &= \frac{I_b}{I_{fb}} = \sqrt{\frac{L_{mf}}{L_{md}}} = \frac{kM_f}{L_{md}} = \frac{L_{mf}}{kM_f} = \frac{L_{fD}}{kM_D} \equiv k_f \\
\frac{V_{Db}}{V_b} &= \frac{I_b}{I_{Db}} = \sqrt{\frac{L_{mD}}{L_{md}}} = \frac{kM_D}{L_{md}} = \frac{L_{mD}}{kM_D} = \frac{L_{fD}}{kM_f} \equiv k_D \\
\frac{V_{Qb}}{V_b} &= \frac{I_b}{I_{Qb}} = \sqrt{\frac{L_{mQ}}{L_{mq}}} = \frac{kM_Q}{L_{mq}} = \frac{L_{mQ}}{kM_Q} \equiv k_Q
\end{aligned} \tag{2.32}$$

The definitions from table 2.1 together with eq. (2.32) produce the pu system described in table 2.2. Now, calculating all the mutual inductances in pu and using again the relationships

in eq. (2.32), one obtains:

$$\begin{aligned}
L_{mdpu} &= \frac{L_{md}}{L_b} \\
kM_{fpu} &= \frac{kM_f}{M_{fb}} = \frac{kM_f}{k_f L_b} = \frac{k_f L_{md}}{k_f L_b} = L_{mdpu} \\
L_{mfpu} &= \frac{L_{mf}}{L_{fb}} = \frac{L_{mf}}{k_f^2 L_b} = \frac{k_f k M_f}{k_f^2 L_b} = L_{mdpu} \\
kM_{Dpu} &= \frac{kM_D}{M_{Db}} = \frac{kM_D}{k_D L_b} = \frac{k_D L_{md}}{k_D L_b} = L_{mdpu} \\
L_{fDpu} &= \frac{L_{fD}}{L_{fDb}} = \frac{L_{fD}}{k_f k_D L_b} = \frac{k_f k M_D}{k_f k_D L_b} = L_{mdpu}
\end{aligned} \tag{2.33}$$

$$\begin{aligned}
L_{mqpu} &= \frac{L_{mq}}{L_b} \\
kM_{Qpu} &= \frac{kM_Q}{M_{Qb}} = \frac{kM_Q}{k_Q L_b} = \frac{k_Q L_{mq}}{k_Q L_b} = L_{mqpu} \\
L_{mQpu} &= \frac{L_{mQ}}{L_{Qb}} = \frac{L_{mQ}}{k_Q^2 L_b} = \frac{k_Q k M_Q}{k_Q^2 L_b} = L_{mqpu}
\end{aligned} \tag{2.34}$$

Equations (2.33) and (2.34) demonstrate a very interesting feature of the chosen pu system: the per-unit values of all mutual inductances on one axis are equal. That is:

$$L_{md} = L_{mf} = kM_f = kM_D \equiv L_{ad} \tag{2.35}$$

$$L_{mq} = L_{mQ} = kM_Q \equiv L_{aq} \tag{2.36}$$

Substituting eqs. (2.35) and (2.36) into eq. (2.30) and then into eq. (2.29), one obtains

the pu model of the synchronous machine used in this thesis:

$$\begin{bmatrix} v_d \\ v_q \\ v_0 \\ -v_f \\ 0 \\ 0 \end{bmatrix} = -\overbrace{\begin{bmatrix} R & \omega(L_{aq}+l_l) & & & & \omega L_{aq} \\ -\omega(L_{ad}+l_l) & R & & -\omega L_{ad} & -\omega L_{ad} & \\ & & R+3R_N & & & \\ & & & R_f & & \\ & & & & R_D & \\ & & & & & R_Q \end{bmatrix}}^{\mathbf{R_{sm}}} \begin{bmatrix} i_d \\ i_q \\ i_0 \\ i_f \\ i_D \\ i_Q \end{bmatrix}$$
$$- \underbrace{\begin{bmatrix} L_{ad}+l_l & & & L_{ad} & L_{ad} & \\ & L_{aq}+l_l & & & & L_{aq} \\ & & L_0+3L_N & & & \\ L_{ad} & & & L_{ad}+l_f & L_{ad} & \\ L_{ad} & & & L_{ad} & L_{ad}+l_D & \\ & L_{aq} & & & & L_{aq}+l_Q \end{bmatrix}}_{\mathbf{L_{sm}}} \frac{d}{dt} \left\{ \begin{bmatrix} i_d \\ i_q \\ i_0 \\ i_f \\ i_D \\ i_Q \end{bmatrix} \right\} \tag{2.37}$$

Or in compact form:

$$\mathbf{v_{dq0fDQ}} = -\mathbf{R_{sm}}\mathbf{i_{dq0fDQ}} - \mathbf{L_{sm}}\frac{d}{dt}\mathbf{i_{dq0fDQ}} \tag{2.38}$$

Equation (2.38) shows that, in matricial form, a synchronous machine can be reduced to an impedance with a resistive part $\mathbf{R_{sm}}$ and an inductive part $\mathbf{L_{sm}}$.

2.5.1 Choosing the rotor scaling factors

Assigning values to the rotor scaling factors is the last step to uniquely define a pu base. If one inspects eq. (2.29) and consider

- steady-state, i.e. $\frac{d}{dt}\mathbf{i_{dq0fDQ}} = \mathbf{0}$;
- stator resistances are negligible, i.e. $R = 0$;
- no-load operation, i.e. $i_d = i_q = 0$;

the following relationships are written:

$$v_d = -\omega k M_Q i_Q \tag{2.39}$$
$$v_q = \omega k M_f i_f + \omega k M_D i_D \tag{2.40}$$

Now, lets assume that

- rated stator current $\sqrt{\frac{3}{2}}I_b$ at the Q-damper winding should induce rated stator voltage $\sqrt{\frac{3}{2}}V_b$ at the d-axis;
- rated no-load field current I_{fn} with no current flowing in the D-damper winding should induce rated stator voltage $\sqrt{\frac{3}{2}}V_b$ at the q-axis;
- rated stator current $\sqrt{\frac{3}{2}}I_b$ at the D-damper winding with no field current flowing should induce rated stator voltage $\sqrt{\frac{3}{2}}V_b$ at the q-axis.

With these assumptions and the relationships from eq. (2.32) substituted into eqs. (2.39) and (2.40), deductions of the rotor scaling factors follow:

$$\begin{aligned}\sqrt{\frac{3}{2}}V_b &= \omega k M_f I_{fn} \\ \sqrt{\frac{3}{2}}\frac{V_b}{I_b} &= \omega k M_f \frac{I_{fn}}{I_b} = \omega k_f \frac{L_{md}}{Z_b}\frac{I_{fn}}{I_b} = \omega k_f L_{ad}\frac{I_{fn}}{I_b} \\ k_f &= \sqrt{\frac{3}{2}}\frac{1}{\omega L_{ad}}\frac{I_{fn}}{I_b}\end{aligned} \tag{2.41}$$

$$\begin{aligned}\sqrt{\frac{3}{2}}V_b &= \omega k M_D \sqrt{\frac{3}{2}}I_b \\ 1 &= \omega\frac{kM_D}{Z_b} = \omega k_D \frac{L_{md}}{Z_b} = \omega k_D L_{ad} \\ k_D &= \frac{1}{\omega L_{ad}}\end{aligned} \tag{2.42}$$

$$\begin{aligned}\sqrt{\frac{3}{2}}V_b &= -\omega k M_Q \sqrt{\frac{3}{2}}I_b \\ -1 &= \omega\frac{kM_Q}{Z_b} = \omega k_Q \frac{L_{mq}}{Z_b} = \omega k_Q L_{aq} \\ k_Q &= -\frac{1}{\omega L_{aq}}\end{aligned} \tag{2.43}$$

Notice that eq. (2.12) scales values from the (A, B, C) reference frame by $\sqrt{\frac{3}{2}}$. Worth to mention is that a number of authors, such as Adkins and Harley (1975) and Kundur et al.

(1994, section 3.3), favors the choice of $\beta_d = \beta_q = 2/3, \beta_0 = 1/3$ in eq. (2.12). With this, there is no scaling between the (A, B, C) and the (d, q, 0) reference frames. However, the transformation is not orthogonal and consequently not power invariant, so scaling factors are required in the machine inductances instead.

2.6 The parameters of a synchronous machine

The matrices $\mathbf{R_{sm}}$ and $\mathbf{L_{sm}}$ in eq. (2.37) contains all relevant parameters for the dynamic analysis of a salient-pole synchronous machine. From them, the *standard parameters* as presented in table 2.3 can be defined. These are used in reduced-order models for planning, operation, and control of the power system, while the matrices elements are interesting for verification of the machine design and condition monitoring.

The standard parameters are not explicitly estimated in this thesis, but can be easily calculated using the definitions in table 2.3 when matrices $\mathbf{R_{sm}}$ and $\mathbf{L_{sm}}$ are given.

Table 2.3: Standard parameters of a salient-pole synchronous machine as defined by Kundur et al. (1994, section 4.2)

Symbol	Description	Definition
X_d	d-axis synchronous reactance	$\omega(L_{ad}+l_l)$
T'_{d0}	d-axis transient open circuit time constant	$\frac{L_{ad}+l_f}{R_f}+\frac{L_{ad}+l_D}{R_D}$
T'_d	d-axis transient short circuit time constant	$\frac{1}{R_f}(l_f+\frac{L_{ad}l_l}{L_{ad}+l_l})+\frac{1}{R_D}(l_D+\frac{L_{ad}l_l}{L_{ad}+l_l})$
T''_{d0}	d-axis sub-transient open circuit time constant	$\frac{1}{T'_{d0}R_fR_D}(l_D+\frac{L_{ad}l_f}{L_{ad}+l_f})(L_{ad}+l_f)$
T''_d	d-axis sub-transient short circuit time constant	$\frac{1}{T'_dR_fR_D}(l_D+\frac{L_{ad}l_ll_f}{L_{ad}l_l+L_{ad}l_f+l_ll_f})(l_f+\frac{L_{ad}l_l}{L_{ad}+l_l})$
X'_d	d-axis transient reactance	$X_d\frac{T'_d}{T'_{d0}}$
X''_d	d-axis sub-transient reactance	$X'_d\frac{T''_d}{T''_{d0}}$
X_q	q-axis synchronous reactance	$\omega(L_{aq}+l_l)$
T''_{q0}	q-axis sub-transient open circuit time constant	$\frac{(L_{aq}+l_Q)}{R_Q}$
X''_q	q-axis sub-transient reactance	$\omega(l_l+\frac{L_{aq}l_Q}{L_{aq}+l_Q})$

Chapter 3

Optimal observer with Kalman filter

This chapter presents details about the practical implementation of an optimal observer in MATLAB/Simulink using the model described in chapter 2, and how it performs compared to the synchronous machine model available in SPS.

It is assumed the reader is familiarized with basic concepts of modeling and validation in control theory, in particular linear state-space representation. If this is not the case, it is recommended referring first to Ljung and Glad (2016, ch. 3 and 15) and Glad and Ljung (2000, ch. 1 and 2) before proceeding.

3.1 Kalman filters

For good parameter estimation of synchronous machines, it is necessary to accurately and precisely measure inputs and outputs of eq. (2.37). However, there are some practical challenges when trying to perform that:

- Damper winding currents cannot be measured directly;
- Measurements are extremely affected by noise due to the high level of electromagnetic interference in a power plant;
- Voltage and current measurements may come from several independent sources, such as potential and current transformers for measurement or protection, each of them having different precision and accuracy values.

Kalman filters are used to optimally estimate variables of interest when these cannot be measured directly, but both indirect measurements and prior knowledge about the system model are available. They are also used to find the best estimate of states from a state-space model by combining measurements from various sensors in the presence of noise (Ulusoy, 2018b). Hence, they are a good choice to tackle the practical challenges above.

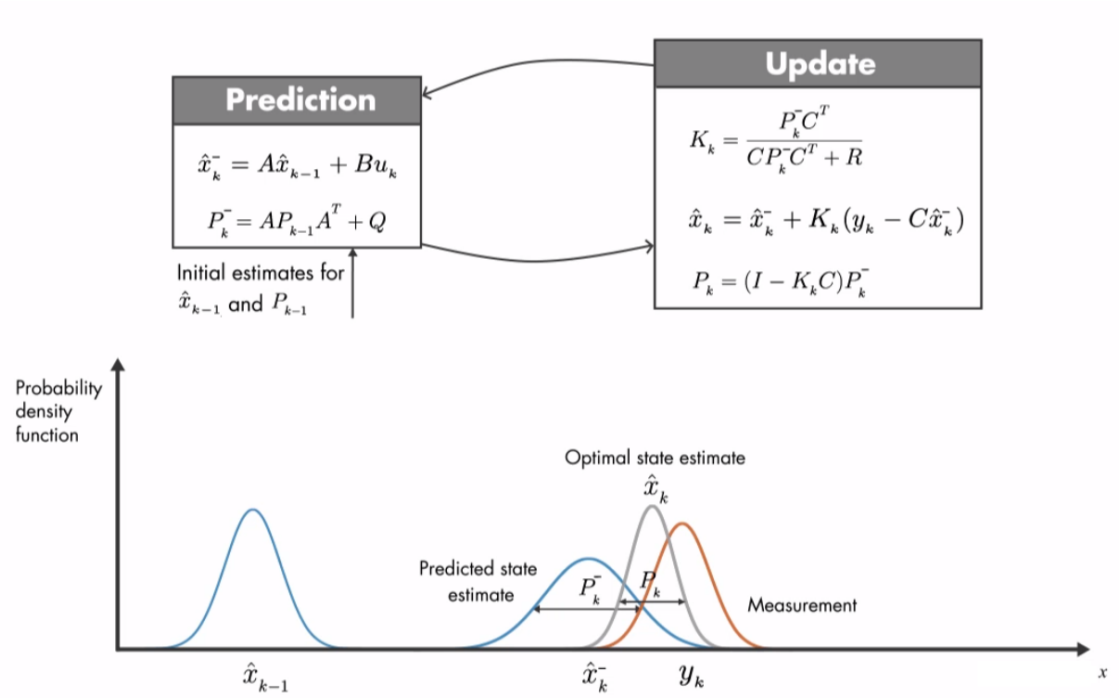

Figure 3.1: Kalman filter algorithm, adapted from (Ulusoy, 2018a)

By definition, a Kalman Filter (KF) is an optimal state observer designed for stochastic systems (Glad and Ljung, 2000, ch. 5.7). It is implemented in a two-step process, called *a priori* estimate and *a posteriori* estimate. The first step is the prediction part, where the system model is used to calculate the *a priori* state estimate $\hat{x}_k^-$ and the error covariance P_k^-, which is a measure of uncertainty in the estimated state $\hat{x}_k$. This variance comes from the process noise Q and propagation of the uncertain $\hat{x}_{k-1}$, i.e. the state estimate from the previous time step. At the very start of the algorithm, the k-1 values for $\hat{x}$ and P come from their initial estimates.

The second step of the algorithm uses $\hat{x}_k^-$ calculated in the prediction step and updates it to find the *a posteriori* state estimate $\hat{x}$ and the error covariance P_k. The Kalman gain K_k is calculated such that it minimizes P_k. By weighting the correction term $(y_k - C\hat{x}_k^-)$, K_k determines how heavily the measurement y_k and the *a priori* estimate $\hat{x}_k^-$ contributes to the calculation of $\hat{x}_k$. If the measurement noise R is small, y_k is trusted more and contributes to the calculation of $\hat{x}_k$ more than $\hat{x}_k^-$ does. In the opposite case, where the error in the *a priori* estimate P_k^- is small, $\hat{x}_k^-$ is trusted more and the computation of $\hat{x}_k$ mostly comes from this estimate.

Once calculated the update equations, $\hat{x}_k$ is used in the next time step to predict the new $\hat{x}_k^-$ and the algorithm repeats itself. Notice that to estimate $\hat{x}_k$, the algorithm does not need all the past information, only $\hat{x}_{k-1}$, P_{k-1}, and y_k. This is what makes the KF recursive. The algorithm is better visualized and understood in fig. 3.1.

In this thesis, the KF is used as an optimal observer, with the main purpose of filtering and correcting measurements using prior knowledge about the synchronous machine model and its parameters. In addition to the state-space definition, three additional matrices are required for specification of a KF:

- **Q**, a SxS matrix (S=number of states) in which the diagonal elements represents the noise covariance of the states, also called process noise covariance matrix;
- **R**, a YxY matrix (Y=number of outputs) in which the diagonal elements represents the noise covariance of the outputs, also called measurement noise covariance matrix;
- **N**, a SxY matrix in which the elements represents the noise cross-covariance between states and outputs, also called process and measurement noise cross-covariance matrix.

For a more formal definition of disturbance models refer to Glad and Ljung (2000, chap. 5), in particular measurement and system disturbances, optimal observers and Kalman filters.

It is assumed $\mathbf{N} = \mathbf{0}$, i.e. there is no cross-correlation between the noise of states and outputs. The other matrices are defined as:

$$\mathbf{Q} = \begin{bmatrix} 0.05 & & & & & & \\ & 0.05 & & & & & \\ & & 0.05 & & & & \\ & & & 0.05 & & & \\ & & & & 0.03 & & \\ & & & & & 0.03 \end{bmatrix} \quad \mathbf{R} = \begin{bmatrix} 0.05 & & & & & \\ & 0.05 & & & & \\ & & 0.05 & & & \\ & & & 0.05 & & \\ & & & & 0.05 & \\ & & & & & 0.05 \end{bmatrix} \tag{3.1}$$

Notice that the choice of diagonal **Q** and **R** matrices represents a naive assumption that state and output changes are uncorrelated. These values produce robust results in several load conditions with and without noise or saturation, as seen in sections 3.5, 4.4 and 5.1. However, they might need fine tuning in the field for better performance, according to the level of noise, measurement accuracy and precision of each power plant. In practice, these values are also affected by the variance of elements of $\mathbf{A}, \mathbf{B}, \mathbf{C}, \mathbf{D}$.

3.2 State space representation

A linear system in state space form (Ljung and Glad, 2016, appendix A) can be described by:

$$\begin{aligned} \frac{d}{dt}\mathbf{x} &= \mathbf{A}\mathbf{x} + \mathbf{B}\mathbf{u} \\ \mathbf{y} &= \mathbf{C}\mathbf{x} + \mathbf{D}\mathbf{u} \end{aligned} \tag{3.2}$$

Where:

- $\mathbf{u}$ is the input vector;
- $\mathbf{x}$ is the state vector;
- $\mathbf{y}$ is the output vector.

By inspection of eq. (2.37), it would be natural to assume $\mathbf{u} = \begin{bmatrix} v_d & v_q & v_0 & v_f & v_D & v_Q \end{bmatrix}^T$, $\mathbf{y} = \mathbf{x} = \begin{bmatrix} i_d & i_q & i_0 & i_f & i_D & i_Q \end{bmatrix}^T$, $\mathbf{A} = -\mathbf{L_{sm}}^{-1}\mathbf{R_{sm}}$, $\mathbf{B} = -\mathbf{L_{sm}}^{-1}$, $\mathbf{C} = \mathbf{I}$, $\mathbf{D} = \mathbf{0}$, and consider the modeling done.

Nonetheless, for control purposes of a synchronous machine, it is more natural to assume $\mathbf{u} = \begin{bmatrix} i_d & i_q & i_0 & v_f & v_D & v_Q \end{bmatrix}^T$, since stator currents are defined by loads, field voltage is delivered by the excitation system and $v_D = v_Q = 0$. Thus, $\mathbf{y} = \begin{bmatrix} v_d & v_q & v_0 & i_f & i_D & i_Q \end{bmatrix}^T$ and matrices $\mathbf{A}, \mathbf{B}, \mathbf{C}, \mathbf{D}$ must be redefined for a proper state space representation.

Assuming the second choice of input variables, the definition of matrices $\mathbf{A}, \mathbf{B}, \mathbf{C}, \mathbf{D}$ is easily achieved without major changes to the structure of eq. (2.37) by extending the model presented in fig. 2.1. Let suppose a balanced, star-connected load with resistance $R_{dl} = 10^4 Z_b$ is inserted at the ABC terminals of the machine, as shown in fig. 3.2. With that extension, the stator voltages in the (d, q, 0) reference frame can be expressed as:

$$v_d = R_{dl}(i_d - i_{dt}) \qquad v_q = R_{dl}(i_q - i_{qt}) \qquad v_0 = R_{dl}(i_0 - i_{0t}) \tag{3.3}$$

Notice that the dummy load R_{dl} is considerably larger than the real load of the machine, therefore the difference between the terminal currents i_{at}, i_{bt}, i_{ct} and stator currents i_a, i_b, i_c

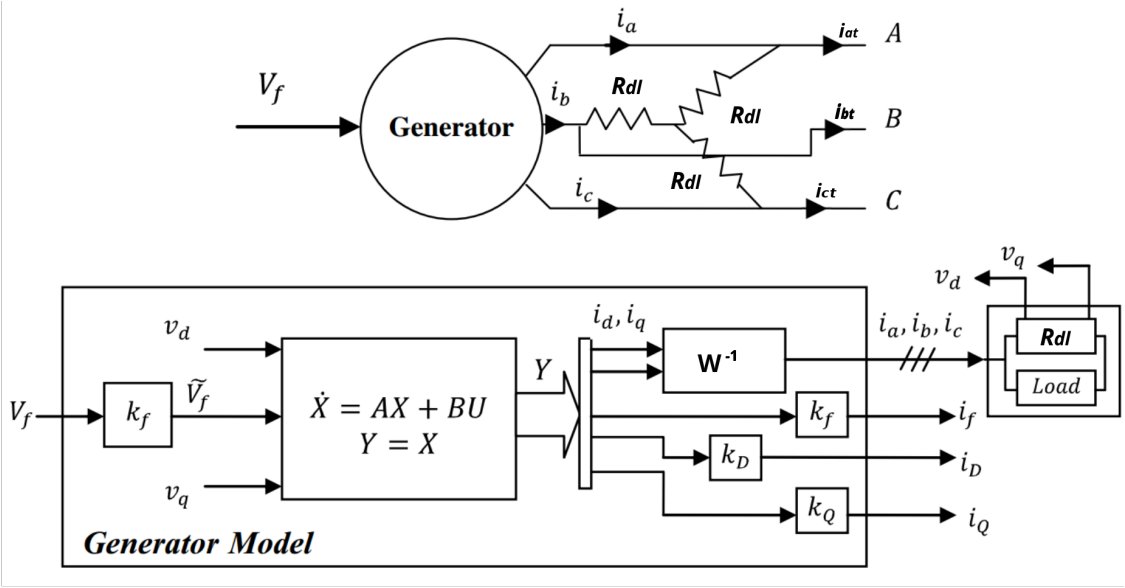

Figure 3.2: Generator model with a dummy load, adapted from Barakat et al. (2010)

is negligible. Substituting eq. (3.3) into eq. (2.37), one obtains:

$$\begin{bmatrix} R_{dl}i_{dt} \\ R_{dl}i_{qt} \\ R_{dl}i_{0t} \\ v_f \\ 0 \\ 0 \end{bmatrix} = \overbrace{\begin{bmatrix} R+R_{dl} & \omega(L_{aq}+l_l) & & & & \omega L_{aq} \\ -\omega(L_{ad}+l_l) & R+R_{dl} & & & -\omega L_{ad} & -\omega L_{ad} \\ & & R+3R_N+R_{dl} & & & \\ & & & R_f & & \\ & & & & R_D & \\ & & & & & R_Q \end{bmatrix}}^{\mathbf{R_{smdl}}} \begin{bmatrix} i_d \\ i_q \\ i_0 \\ i_f \\ i_D \\ i_Q \end{bmatrix}$$

$$\underbrace{\begin{bmatrix} L_{ad}+l_l & & & L_{ad} & L_{ad} & \\ & L_{aq}+l_l & & & & L_{aq} \\ & & L_0+3L_N & & & \\ L_{ad} & & & L_{ad}+l_f & L_{ad} & \\ L_{ad} & & & L_{ad} & L_{ad}+l_D & \\ & L_{aq} & & & & L_{aq}+l_Q \end{bmatrix}}_{\mathbf{L_{sm}}} \frac{d}{dt} \left\{ \begin{bmatrix} i_d \\ i_q \\ i_0 \\ i_f \\ i_D \\ i_Q \end{bmatrix} \right\} \quad (3.4)$$

The following state space is defined based on eqs. (3.3) and (3.4):

$$
\begin{aligned}
\mathbf{u} &= \begin{bmatrix} R_{dl}i_{dt} & R_{dl}i_{qt} & R_{dl}i_{0t} & v_f & 0 & 0 \end{bmatrix}^T \\
\mathbf{x} &= \begin{bmatrix} i_d & i_q & i_0 & i_f & i_D & i_Q \end{bmatrix}^T & \mathbf{y} &= \begin{bmatrix} v_d & v_q & v_0 & i_f & i_D & i_Q \end{bmatrix}^T \\
\mathbf{A} &= -\mathbf{L_{sm}}^{-1}\mathbf{R_{smdl}} & \mathbf{B} &= \mathbf{L_{sm}}^{-1} \\
\mathbf{C} &= \begin{bmatrix} R_{dl} & & & & & \\ & R_{dl} & & & & \\ & & R_{dl} & & & \\ & & & 1 & & \\ & & & & 1 & \\ & & & & & 1 \end{bmatrix} & \mathbf{D} &= \begin{bmatrix} -1 & & & & & \\ & -1 & & & & \\ & & -1 & & & \\ & & & 0 & & \\ & & & & 0 & \\ & & & & & 0 \end{bmatrix}
\end{aligned}
\tag{3.5}
$$

3.3 Observer for damper winding currents

For optimal state estimation, output measurements must be fed into the KF algorithm. As the damper winding currents i_D, i_Q cannot be measured directly, an observer must be implemented for this purpose.

The transfer function for the observer of i_D and i_Q is derived by applying the Laplace transform to rows 5 and 6 of eq. (3.4), and manipulating the expressions further to obtain:

$$
\begin{aligned}
i_D &= -\frac{sL_{ad}}{s(L_{ad} + l_D) + R_D}(i_d + i_f) \\
i_Q &= -\frac{sL_{aq}}{s(L_{aq} + l_Q) + R_Q} i_q
\end{aligned}
\tag{3.6}
$$

3.4 Implementation in MATLAB/Simulink

To validate the KF and the Observer for Damper Windings (ODW), a simulation file in MATLAB/Simulink is implemented. A brief review of this file is given in this section. For more details, refer to appendix A, which presents a report of every component and its parameters.

The main section of the Simulink file (fig. 3.3) contains a synchronous machine model in pu from the SPS library connected to an RL load and the dummy load. Parameters of a real synchronous machine are taken from examples 3.1, 3.2 and 8.1 of Kundur et al. (1994, p. 91,102,345). The rotor speed ω is assumed constant, i.e. the prime mover and its turbine governor are not modeled because the mechanical dynamics are much slower than the electrical and have little impact in the results.

The field voltage is provided by an excitation system block from Simscape Power System,

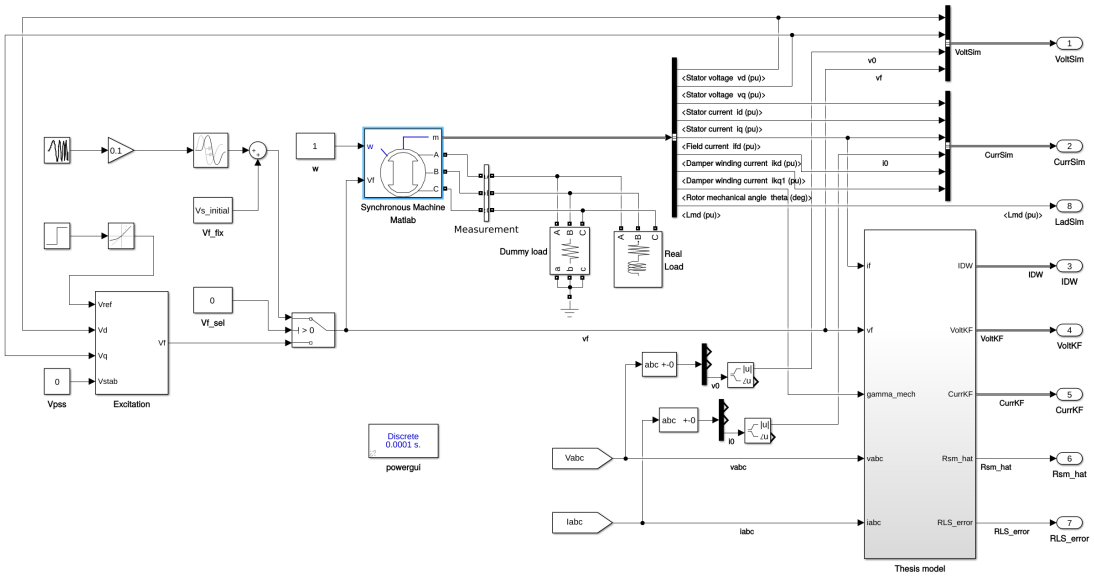

Figure 3.3: Main section of the Simulink model

which implements a DC1C type excitation as described in IEEE (2016). The choice of parameters for the AVR gives a fast and stable response, without overshoot in the terminal voltage. However, they are not optimized and a power system stabilizer is not included, as detailed modeling and optimization of the excitation system are out of the scope of this thesis.

The outputs of the synchronous machine model, i.e. stator and field measurements $v_a, v_b, v_c, v_f, i_a, i_b, i_c, i_f$ together with the rotor mechanical angle γ, are fed into the *Thesis model* subsystem. There, the first step is scaling measurements to their RMS values and convert them from International System of Units (SI) to the thesis pu base, according to tables 2.1 and 2.2.

The next step is adding band-limited white noise and re-sampling measurements into a

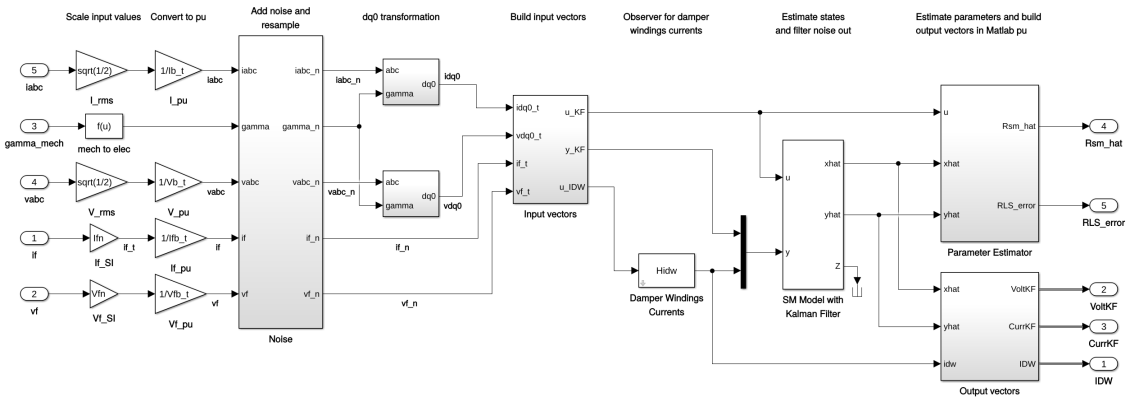

Figure 3.4: *Thesis model* subsystem of the Simulink model

lower sample frequency f_s, in order to make them more realistic. In the simulations, f_s is assumed as 400 Hz. According to the author experience, this is a typical minimum value for data logging in measurement units available in most Norwegian power plants, such as digital protection relays.

This is followed by the dq0 transformation, which is performed according to eqs. (2.11) and (2.12). Then, the next subsystem organizes the measurements into vectors to feed the ODW and the KF, which are implemented using eqs. (3.1), (3.5) and (3.6).

Finally, estimated states and outputs are fed into the *Parameter Estimator* subsystem, which is detailed later in chapter 4. They are also re-converted to Matlab pu for comparison and validation of results. This is necessary because the synchronous machine model from SPS uses the dq0 transformation and pu system defined by Kundur et al. (1994, sections 3.3, 3.4). Thus stator variables are divided by $\sqrt{\frac{3}{2}}$, as discussed in section 2.5.1, and field variables use as base their no-load rated values.

3.5 Validation of the thesis model

For validation of ODW and KF, the simulation file runs with the following load conditions, where P represent the active power and Q the reactive power:

- Case 1: P = 0 pu, Q = 0 pu (no load);
- Case 2: P = 0.25 pu, Q = 0 pu;
- Case 3: P = 0.5 pu, Q = 0.5 pu;
- Case 4: P = 0.5 pu, Q = -0.5 pu;
- Case 5: P = 0.9 pu, Q = 0.4359 pu (rated load).

In all cases, the simulation starts at rated stator voltage. In order to observe transient behavior, a step of +5% is applied to the reference of the AVR at time $t = 9$ seconds. At this moment, saturation in the SPS model is disabled. Validation for the latter is addressed in section 5.1.

The initial states of SPS are calculated using the Machine Initialization tool from powergui block in order to avoid loss of synchronism. However, initial states of ODW and KF are all zero, so it is necessary some seconds of simulation to achieve steady state. This also shows KF is stable even when wrong initial conditions are given and with large transients.

In addition, for each simulation case, the following noise scenarios are explored:

- No noise scenario: noise power density $N_p = 0$;

- Standard noise scenario: noise power density $N_p = 10^{-10}\frac{\text{W}}{\text{Hz}}$;
- High noise scenario: noise power density $N_p = 10^{-9}\frac{\text{W}}{\text{Hz}}$.

Results are shown in appendix B and compared measuring the *goodness of fit* between the synchronous machine models of the thesis (x) and SPS (x_{ref}). The cost function used is the Normalized Mean Square Error (NMSE), defined as:

$$NMSE = 1 - \frac{\|x_{ref} - x\|^2}{\|x_{ref} - mean(x_{ref})\|^2} \tag{3.7}$$

where $\|$ indicates the Euclidean or L^2 norm of a vector. NMSE costs vary between $-\infty$ (bad fit) to 1 (perfect fit). If the cost function is equal to zero, then x is no better than a straight line at matching x_{ref}.

A summary of these results is presented in table 3.1 and below follow some remarks about them:

- The mean correlation between KF and SPS for all variables is close to unity in the no noise scenario. This shows the two models are nearly equivalent;
- The low standard deviation between all cases indicates the correlation is not sensitive to the load connected to the machine;
- Also in the standard noise scenario, correlation between KF and SPS is relatively close to unity and with small standard deviation;
- As expected, the performance of ODW in the noise scenarios is degraded, but it is considerably improved by KF;
- The performance of KF gets better in the high noise scenario when the load increases, because the Signal-to-Noise Ratio (SNR) also improves;
- NMSE of v_d and i_Q are very low in case 1 (no load) because their values tend to zero and, since the noise power is constant, the SNR is extremely low. This makes NMSE measurement not relevant for these cases, so they are excluded from the standard deviation (Std dev) calculation.

Table 3.1: NMSE values for all simulation cases and noise scenarios

Variable	**Case 1**	**Case 2**	**Case 3**	**Case 4**	**Case 5**	**Mean**	**Std dev**
			No noise scenario				
v_d KF	1.0000	1.0000	1.0000	1.0000	1.0000	1.0000	8.082e-10
v_q KF	1.0000	1.0000	1.0000	1.0000	1.0000	1.0000	1.638e-09
i_f KF	1.0000	1.0000	1.0000	1.0000	1.0000	1.0000	6.681e-06
i_D ODW	0.9999	0.9999	0.9999	0.9999	0.9999	0.9999	7.582e-07
i_D KF	0.9998	0.9988	0.9980	0.9969	0.9954	0.9978	1.689e-03
i_Q ODW	1.0000	1.0000	1.0000	1.0000	1.0000	1.0000	7.213e-08
i_Q KF	-393.5	0.9931	0.9950	0.9999	0.9987	0.9967	3.191e-03
			Standard noise scenario				
v_d KF	-392.9	0.9527	0.9544	0.9963	0.9846	0.9720	2.185e-02
v_q KF	0.9962	0.9942	0.9938	0.9882	0.9877	0.9920	3.835e-03
i_f KF	0.9962	0.9968	0.9992	0.9954	0.9994	0.9974	1.773e-03
i_D ODW	0.8653	0.8559	0.8180	0.8997	0.7772	0.8432	4.697e-02
i_D KF	0.9538	0.9498	0.9362	0.9629	0.9199	0.9446	1.679e-02
i_Q ODW	-4902	0.8971	0.8684	0.9908	0.9327	0.9223	5.269e-02
i_Q KF	-2134	0.9568	0.9488	0.9967	0.9751	0.9693	2.131e-02
			High noise scenario				
v_d KF	-3939	0.5270	0.5437	0.9632	0.8459	0.7199	2.186e-01
v_q KF	0.9619	0.9423	0.9385	0.8817	0.8773	0.9204	3.835e-02
i_f KF	0.9621	0.9684	0.9916	0.9546	0.9937	0.9741	1.763e-02
i_D ODW	-0.3465	-0.4406	-0.8192	-0.0025	-1.2272	-0.5672	4.698e-01
i_D KF	0.5408	0.5101	0.3811	0.6580	0.2415	0.4663	1.597e-01
i_Q ODW	-49021	-0.0285	-0.3153	0.9078	0.3269	0.2227	5.269e-01
i_Q KF	-17806	0.6288	0.5307	0.9675	0.7609	0.7220	1.889e-01

Chapter 4

Algorithms for Parameter Estimation

Parameter estimation is one application of the wider discipline of *system identification*. The overall problem of system identification is, given

- a set of process signal values over time;
- a model structure with a set of constraints to satisfy;
- an approximation or error criterion;

determine a model that satisfies the set of constraints and results in the least approximation error according to the stated criterion (Mukhopadhyay, 2004).

For the scope of this thesis, the set of process signal values over time $\mathbf{u}, \mathbf{y}$ and the model structure with a set of constraints to satisfy are given by eq. (2.37), where the final goal is estimating the elements of matrices $\mathbf{Rsm}, \mathbf{Lsm}$. So, the only piece left is defining an approximation or error criterion.

The literature has some accounts of approximation or error criteria for parameter identification of synchronous machines, such as Extended Kalman Filter (EKF) (Namba et al., 1981b), Levenberg–Marquardt algorithm (Bortoni and Jardini, 2002), RLS (Karayaka et al., 2003; Kyriakides et al., 2005), Prony method (Dehghani and Nikravesh, 2008), among others.

In this thesis, the approximation or error criteria used is the RLS. The main reasons for this choice are:

- RLS is readily available in the System Identification Toolbox of Simulink, which is a huge advantage considering the limited time for preparation of the thesis;
- Near real-time execution is possible with RLS due to its recursive nature and low computational effort compared to other methods. If implemented directly in an Intelligent Electronic Device (IED) or a fog computing solution, this is an essential consideration;
- Benchmarks are available in the literature for comparison of results.

4.1 Recursive Least Squares Estimation

The RLS estimation involves the recursive application of the well-known least squares regression algorithm, so that each new data point is used to modify or correct a previous estimate of the parameters based on a linear correlation of the system model.

To understand this concept, a simple example is given. Let say the average $\bar{x}(n)$ of a data set $x(n) = \{x_1, x_2, \cdots, x_n\}$ should be calculated, that is:

$$\bar{x}(n) = \frac{1}{n}\sum_{i=1}^{n} x_i = \frac{x_1 + \cdots + x_n}{n} \tag{4.1}$$

Now, suppose a new value is added to the dataset, so $x(n+1) = \{x_1, x_2, \cdots, x_n, x_{n+1}\}$. How can the average $\bar{x}(n+1)$ be calculated recursively, i.e. using only the new sample value x_{n+1}, the previous average $\bar{x}(n)$ and the number of samples n?

By rearranging the equation for $\bar{x}(n+1)$, one gets:

$$\begin{aligned}
\bar{x}(n+1) &= \frac{1}{n+1}\sum_{i=1}^{n+1} x_i = \frac{x_1 + \cdots + x_n + x_{n+1}}{n+1} \\
(n+1)\bar{x}(n+1) &= (x_1 + x_2 + \cdots + x_n) + x_{n+1} = n\bar{x}(n) + x_{n+1} \\
\bar{x}(n+1) &= n(\bar{x}(n) - \bar{x}(n+1)) + x_{n+1} \\
&= n(\frac{x_1 + \cdots + x_n}{n} - \frac{x_1 + \cdots + x_n + x_{n+1}}{n+1}) + x_{n+1} \\
&= \frac{n(n+1)(x_1 + \cdots + x_n) - n^2(x_1 + \cdots + x_n + x_{n+1}) + n(n+1)(x_{n+1})}{n(n+1)} \\
&= \frac{n(x_1 + \cdots + x_n) + n(x_{n+1})}{n(n+1)} \\
&= \frac{(n+1)(x_1 + \cdots + x_n) + n(x_{n+1}) - (x_1 + \cdots + x_n)}{n(n+1)} \\
&= \frac{(x_1 + \cdots + x_n)}{n} + \frac{1}{n+1}(x_{n+1} - \frac{(x_1 + \cdots + x_n)}{n}) \\
&= \bar{x}(n) + \frac{1}{n+1}(x_{n+1} - \bar{x}(n)) \\
&= \bar{x}(n) + K(x_{n+1} - \bar{x}(n))
\end{aligned} \tag{4.2}$$

which is the answer to the problem. Note two important elements in eq. (4.2):

1. The gain K, dependent on how many samples were processed
2. The term $(x_{n+1} - \bar{x}(n))$, called *innovation* which is the difference between the new value x_{n+1} and the a priori estimation $\bar{x}(n)$

In a general linear regression algorithm, the fitting model is given by:

$$\mathbf{y_t} = \theta_t^T \mathbf{x_t} + \mathbf{e_t}, t = 1, 2, \ldots, n \tag{4.3}$$

where

- $\mathbf{y_t}$ is the output vector;
- $\mathbf{x_t}$ is the input vector;
- θ_t is the parameter matrix;
- $\mathbf{e_t}$ is the prediction error and represents effects of measurement errors in $\mathbf{y_t}$, $\mathbf{x_t}$ or dynamics not modeled.

Notice that the input vector may be non linearly related to the output vector, and only parameters must be linearly related to the input vector. To apply the least squares regression, it is necessary first to define a cost function. This is given by

$$\mathbf{C_t}(\theta_t) = \sum_{i=1}^{t} \lambda^{t-i} (\mathbf{y_t} - \theta_t^T \mathbf{x_t})^T (\mathbf{y_t} - \theta_t^T \mathbf{x_t}) \tag{4.4}$$

where $0 < \lambda \leq 1$ is the *forgetting factor*, which gives exponentially less weight to older error samples.

When minimizing eq. (4.4), i.e. derivating it and making it equal to zero, one finds the following least square solution

$$\left(\sum_{i=1}^{t} \lambda^{t-i} \mathbf{x_i} \mathbf{x_i}^T \right) \hat{\theta}_t = \left(\sum_{i=1}^{t} \lambda^{t-i} \mathbf{y_i} \mathbf{x_i} \right) \tag{4.5}$$

assuming the matrix $\mathbf{R_t} = \left(\sum_{i=1}^{t} \lambda^{t-i} \mathbf{x_i} \mathbf{x_i}^T \right)$ can be inverted.

Now, using the same principle from the first simple example, i.e making the algorithm recursive, and considering that $\mathbf{R}_{t-1} = \mathbf{R_t} - \mathbf{x_t} \mathbf{x_t}^T$, follows that:

$$\begin{aligned}
\hat{\theta}_t &= \mathbf{R}_t^{-1} \left(\sum_{i=1}^{t-1} \lambda^{t-i} \mathbf{y_i} \mathbf{x_i} + \mathbf{y_t} \mathbf{x_t} \right) \\
&= \mathbf{R}_t^{-1} \left(\mathbf{R}_{t-1}^{-1} \hat{\theta}_{t-1} + \mathbf{y_t} \mathbf{x_t} \right) \\
&= \hat{\theta}_{t-1} + \mathbf{R}_t^{-1} \left(\mathbf{y_t} \mathbf{x_t} - (\mathbf{x_t} \mathbf{x_t}^T) \hat{\theta}_{t-1} \right) \\
&= \hat{\theta}_{t-1} + \mathbf{R}_t^{-1} \mathbf{x_t} \left(\mathbf{y_t} - (\mathbf{x_t}^T) \hat{\theta}_{t-1} \right)
\end{aligned} \tag{4.6}$$

Finally, to obtain the final recursive algorithm, the matrix inversion lemma (Strang, 2005) is applied to $\mathbf{R}_t^{-1}$:

$$\mathbf{R}_t^{-1} = \frac{1}{\lambda}\left(\mathbf{R}_{t-1}^{-1} - \frac{\mathbf{R}_{t-1}^{-1}(\mathbf{x_t}\mathbf{x_t}^T)\mathbf{R}_{t-1}^{-1}}{\lambda + \mathbf{x_t}^T\mathbf{R}_{t-1}^{-1}\mathbf{x_t}}\right) \tag{4.7}$$

As so, the following recursive equations are used for the RLS algorithm:

$$\begin{aligned}
\epsilon_t &= \mathbf{y_t} - (\mathbf{x_t}^T)\hat{\theta}_{t-1} \\
\mathbf{P}_t = \mathbf{R}_t^{-1} &= \frac{1}{\lambda}\left(\mathbf{P}_{t-1} - \frac{\mathbf{P}_{t-1}(\mathbf{x_t}\mathbf{x_t}^T)\mathbf{P}_{t-1}}{\lambda + \mathbf{x_t}^T\mathbf{P}_{t-1}\mathbf{x_t}}\right) \\
\mathbf{K}_t = \mathbf{P}_t\mathbf{x_t} &= \left(\frac{1}{\lambda + \mathbf{x_t}^T\mathbf{P}_{t-1}\mathbf{x_t}}\right)\mathbf{P}_{t-1}\mathbf{x_t}\mathbf{P}_t \\
\hat{\theta}_t &= \hat{\theta}_{t-1} + \mathbf{K}_t\epsilon_t
\end{aligned} \tag{4.8}$$

where

- ϵ_t is the absolute error of the approximation;
- $\mathbf{P}_t$ is the parameter covariance matrix;
- $\mathbf{K}_t$ is the RLS gain;
- $\hat{\theta}_t$ is the estimated parameter matrix.

In its first iteration ($t = 1$), initial values $\mathbf{P}_0$ and $\hat{\theta}_0$ must be provided. More details and formal approaches are given by Ljung (1999, chap 11) and Pelckmans (2013, chap. 8).

The attentive reader may have noticed the RLS algorithm is very similar to the KF explained in section 3.1. Indeed, RLS and KF are closely related and the former can be considered a special case of the latter (Borodachev, 2016).

4.2 Simplification of the synchronous machine equation

Considering simultaneous estimation of the 14 parameters of the synchronous machine with RLS estimation generates poor results (Kyriakides et al., 2005), simplifications are required. Thus, steady-state is assumed, i.e. $\frac{d}{dt}\mathbf{i_{dq0fDQ}} = \mathbf{0}$, and eq. (2.38) is reduced to:

$$\mathbf{v_{dq0fDQ}} = -\mathbf{R}\mathbf{i_{dq0fDQ}} \tag{4.9}$$

With this simplification, eq. (4.9) has the same form of eq. (4.3). Therefore, parameters from matrix $\mathbf{R_{sm}}$ can be estimated using a recursive algorithm, but not $\mathbf{L_{sm}}$. But notice that 4 out of 8 parameters from $\mathbf{L_{sm}}$ are also present in $\mathbf{R_{sm}}$.

Another practical assumption is the stator resistance R should not be estimated in rows 1 and 2 of matrix $\mathbf{R_{sm}}$. The arguments for this assumption are:

- R is not used for the calculation of any standard parameter, as defined in table 2.3;
- R in pu is usually two to three orders of magnitude smaller than other parameters in these rows ($\omega L_d, \omega L_{ad}, \omega L_q, \omega L_{aq}$);
- Variations of up to 200% of the datasheet values of R were obtained when using RLS estimation with the cases and noise scenarios described in section 3.5. So, it is assumed proper identification with this estimation method would be challenging.

Using these assumptions, eq. (2.37) can be re-arranged to:

$$\begin{bmatrix} v_d - Ri_d \\ v_q - Ri_q \\ v_0 \\ -v_f \\ 0 \\ 0 \end{bmatrix} = - \begin{bmatrix} & \omega L_q & & & & \omega L_{aq} \\ -\omega L_d & & & -\omega L_{ad} & -\omega L_{ad} & \\ & & R + 3R_N & & & \\ & & & R_f & & \\ & & & & R_D & \\ & & & & & R_Q \end{bmatrix} \begin{bmatrix} i_d \\ i_q \\ i_0 \\ i_f \\ i_D \\ i_Q \end{bmatrix} \tag{4.10}$$

Notice that in eq. (4.10), the stator voltages v_d, v_q are compensated with the voltage drops in the stator resistance Ri_d, Ri_q. Also $R + 3R_N$ is estimated in the third row. In summary, eq. (2.37) is only re-arranged to avoid the estimation of R individually, as this parameter is not useful for planning, operation, and control of the power system. Moreover, its use for condition monitoring is compromised because it cannot be estimated reliably. Not least, if the value of R is unknown, it can be set to zero without major consequences.

Last but not least, the steady-state condition is detected in run-time by monitoring that the damper windings currents are below a certain level, since current flows in these windings only in transient conditions. This approach produces good results, as shown in section 4.4.

4.3 Parameter Estimator Subsystem

In the *Parameter Estimator* subsystem (fig. 4.1), the first step is to detect steady-state, which is done following the procedure below:

1. Filter the damper winding currents with moving average to remove noise and calculate their absolute value

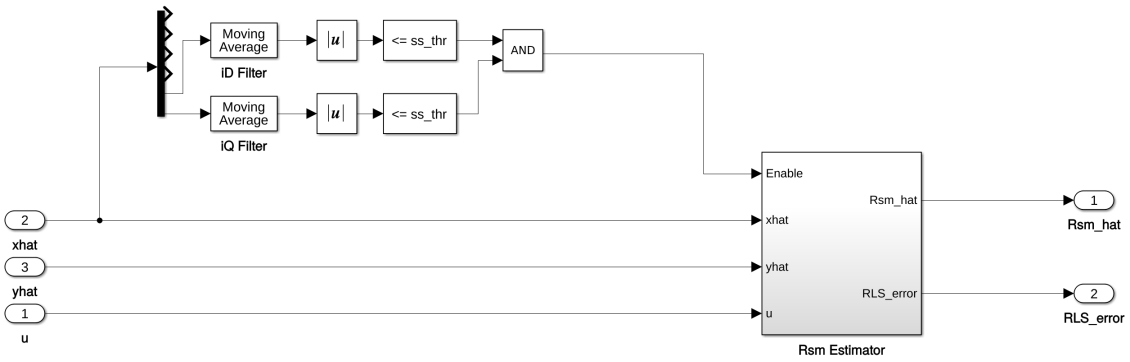

Figure 4.1: *Parameter estimator* subsystem of the Simulink model

2. Compare this result to the configurable threshold level *ss_thr*. This variable is an input value in the accompanying Matlab script and is set at 0.005 pu.

3. If both i_D and i_Q are below the threshold, then it is assumed the synchronous machine is in steady-state.

The threshold level for the steady-state condition is defined after simulations in several load conditions, with and without noise. However, it might require fine tuning in the field for better performance, according to the noise level, measurement accuracy and precision of each power plant.

The steady-state condition, together with vectors u, *xhat* and *yhat* of the KF are fed into the *Rsm Estimator* subsystem (fig. 4.2). There, these vectors are broken into their individual components and manipulated according to eq. (4.10) for feeding six RLS estimators from the System Identification Toolbox of Simulink.

The latter implements the recursive algorithm described by eq. (4.8), where the equivalence between Simulink nomenclature and the equations presented are:

- $Regressors = \mathbf{x_t}$;
- $Output = \mathbf{y_t}$;
- $Parameters = \theta_t$;
- $Error = \epsilon_t$.

On top of that, $\mathbf{P}_0, \lambda, \hat{\theta}_0$ are block parameters. The value for $\mathbf{P}_0$ is chosen as 0.05. The forgetting factor λ is related to the RLS memory time T_m by $\lambda = 1 - \dfrac{1}{f_s T_m}$, which is chosen as 10 seconds. Both values are user inputs in the accompanying Matlab script and empirically defined, so they might have to be adjusted for each machine. The initial parameter values comes from user inputs, the same used to define the state-space matrices from the KF.

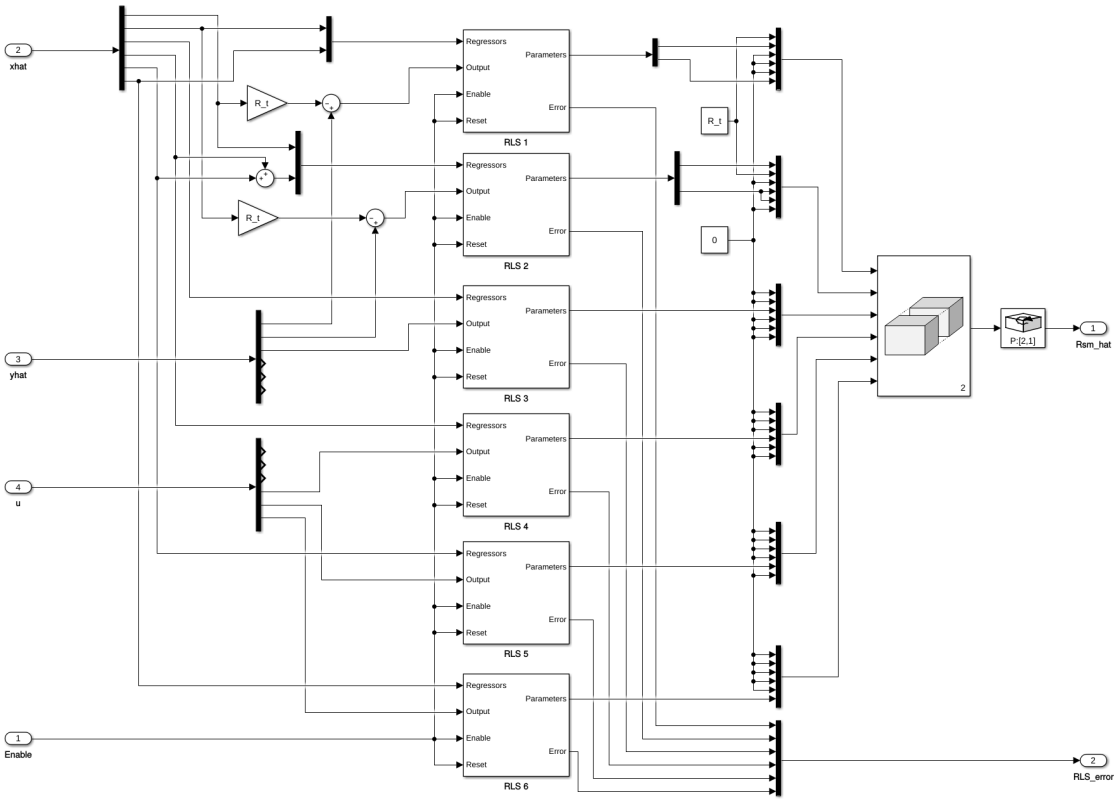

Figure 4.2: *Rsm estimator* subsystem of the Simulink model

Not least, *Enable* and *Reset* inputs are connected to the steady-state condition. When the latter is false, the *Enable* input stops the processing of the RLS algorithm and holds the last valid estimation in the outputs. When steady-state is back to true, the *Reset* input forces the process to restart from the scratch, i.e. adopting the initial conditions $\mathbf{P}_0$ and $\hat{\theta}_0$. This step is necessary because the value of $\mathbf{P}_t$ may become very small after a long steady-state period, and a large transient could cause instability of the RLS algorithm. If estimated parameters are used in adaptive control, this instability may lead to bursting phenomena (Marafioti et al., 2014).

Lastly, the outputs of the six RLS blocks are aggregated and connected to the outputs *Rsm_hat* and *RLS_error*, which are respectively the estimated value of the matrix $\mathbf{R_{sm}}$ and the vector ϵ_t.

4.4 Validation of the Parameter Estimator

For validation of the parameter estimator, the simulation file runs at exactly the same conditions as described in section 3.5. The exception is the +5% step is applied to the reference of the AVR at time $t = 17$ seconds, in order to allow the RLS algorithm to run during at

least one period of the memory time T_m. At this moment, saturation in the SPS model is disabled. Parameter estimation with the latter is addressed in section 5.1.

Results are shown in appendix C. They are evaluated measuring both the error in percentage from the data sheet values informed for the SPS model and the RLS absolute error, i.e. ϵ_t in eq. (4.8). Summaries of these evaluations are presented in tables 4.1 to 4.4.

Below follow some remarks about them:

- The RLS algorithm estimates parameters of the SPS machine with very small percentage deviations, whose values are in line with those reported by Kyriakides et al. (2005);
- The low standard deviation between all cases indicates the estimation is not sensitive to the load connected to the machine;
- Noise power has small influence in the quality of the parameter estimation for both evaluation methods, i.e. percentage error and absolute RLS error;
- The strategy to disable and reset the RLS algorithm during transients is successful, since its mean absolute error decreases to very small values and no instability is observed in the estimated parameters for all cases and noise scenarios. Also for long time simulations of 300 seconds in all noise scenarios (not included in the results for sake of brevity), instabilities are not detected.

Table 4.1: Percentage errors in the last 5 seconds of estimation using data sheet values as baseline - Before step

Parameter	**Case 1**		**Case 2**		**Case 3**		**Case 4**		**Case 5**		**Absolute**	
	mean	std dev	mean	std dev	mean	std dev	mean	std dev	mean	std dev	mean	std dev
No noise scenario												
ωL_d	0.000	0.000	0.015	0.000	0.022	0.000	0.142	0.000	0.034	0.000	0.043	0.057
ωL_q	0.379	0.004	-0.078	0.034	-0.877	0.031	-0.217	0.011	-0.791	0.017	-0.317	0.522
$R + 3R_N$	0.000	0.000	0.000	0.000	0.000	0.000	0.000	0.000	0.000	0.000	0.000	0.000
ωL_{ad}	0.002	0.000	-0.105	0.000	-0.047	0.000	-0.199	0.000	-0.058	0.000	-0.082	0.076
R_f	0.815	0.161	0.051	0.011	0.001	0.000	0.002	0.000	-0.001	0.000	0.173	0.359
R_D	-0.013	0.000	0.000	0.000	0.000	0.000	-0.001	0.000	0.000	0.000	-0.003	0.005
ωL_{aq}	0.026	0.000	-0.035	0.001	-0.022	0.001	-0.022	0.001	-0.021	0.001	-0.015	0.024
R_Q	-0.001	0.000	-0.026	0.000	-0.024	0.000	-0.025	0.000	-0.024	0.000	-0.020	0.011
Standard noise scenario												
ωL_d	-0.020	0.004	0.003	0.002	0.014	0.002	0.135	0.001	0.027	0.001	0.032	0.060
ωL_q	0.360	0.009	-0.081	0.035	-0.880	0.031	-0.218	0.011	-0.794	0.018	-0.322	0.517
$R + 3R_N$	-0.083	0.058	-0.044	0.044	-0.023	0.042	-0.023	0.042	-0.023	0.042	-0.039	0.026
ωL_{ad}	0.006	0.001	-0.102	0.001	-0.049	0.001	-0.199	0.002	-0.061	0.001	-0.081	0.077
R_f	0.740	0.148	-0.011	0.013	-0.033	0.010	-0.075	0.022	-0.030	0.009	0.118	0.348
R_D	-0.031	0.003	-0.012	0.003	-0.012	0.002	-0.015	0.003	-0.012	0.003	-0.016	0.008
ωL_{aq}	0.038	0.001	-0.028	0.000	-0.010	0.002	-0.015	0.001	-0.005	0.003	-0.004	0.025
R_Q	-0.007	0.001	-0.030	0.001	-0.032	0.002	-0.030	0.001	-0.033	0.002	-0.026	0.011
High noise scenario												
ωL_d	-0.198	0.037	-0.102	0.024	-0.054	0.016	0.091	0.008	-0.027	0.013	-0.058	0.106
ωL_q	0.133	0.047	-0.090	0.037	-0.907	0.031	-0.224	0.011	-0.816	0.016	-0.381	0.458
$R + 3R_N$	-0.841	0.579	-0.441	0.435	-0.161	0.414	-0.161	0.414	-0.231	0.407	-0.367	0.289
ωL_{ad}	0.016	0.003	-0.108	0.006	-0.082	0.010	-0.223	0.010	-0.093	0.010	-0.098	0.085
R_f	0.517	0.112	-0.144	0.049	-0.108	0.031	-0.250	0.072	-0.084	0.026	-0.014	0.303
R_D	-0.186	0.032	-0.120	0.025	-0.111	0.024	-0.134	0.029	-0.115	0.025	-0.133	0.031
ωL_{aq}	0.118	0.015	0.029	0.012	0.110	0.027	0.050	0.014	0.148	0.035	0.091	0.049
R_Q	-0.063	0.012	-0.067	0.009	-0.082	0.014	-0.069	0.010	-0.099	0.018	-0.076	0.015

Table 4.2: Percentage errors in the last 5 seconds of estimation using data sheet values as baseline - After step

Parameter	**Case 1**		**Case 2**		**Case 3**		**Case 4**		**Case 5**		**Absolute**	
	mean	std dev	mean	std dev	mean	std dev	mean	std dev	mean	std dev	mean	std dev
No noise scenario												
ωL_d	-0.001	0.000	-0.572	0.000	-1.629	0.000	-4.036	0.004	-3.258	0.001	-1.899	1.721
ωL_q	0.256	0.004	-0.074	0.035	-0.874	0.031	-0.216	0.011	-0.788	0.018	-0.339	0.481
$R + 3RN$	0.000	0.000	0.000	0.000	0.000	0.000	0.000	0.000	0.000	0.000	0.000	0.000
ωLad	-0.079	0.005	3.931	0.003	3.256	0.001	5.172	0.006	5.199	0.001	3.496	2.164
R_f	0.518	0.104	0.062	0.014	0.002	0.000	0.002	0.000	0.000	0.000	0.117	0.226
R_D	-0.012	0.000	0.000	0.000	0.000	0.000	-0.001	0.000	0.000	0.000	-0.003	0.005
ωLaq	0.022	0.000	-0.036	0.001	-0.023	0.001	-0.022	0.001	-0.022	0.001	-0.016	0.022
R_Q	-0.001	0.000	-0.026	0.000	-0.024	0.000	-0.025	0.000	-0.024	0.000	-0.020	0.011
Standard noise scenario												
ωL_d	-0.019	0.004	-0.584	0.003	-1.637	0.002	-4.042	0.005	-3.264	0.002	-1.909	1.717
ωL_q	0.222	0.008	-0.079	0.035	-0.878	0.031	-0.217	0.011	-0.791	0.018	-0.349	0.472
$R + 3RN$	-0.065	0.056	-0.042	0.044	-0.022	0.042	-0.023	0.042	-0.023	0.042	-0.035	0.019
ωLad	-0.076	0.005	3.934	0.003	3.254	0.001	5.173	0.005	5.196	0.000	3.496	2.163
R_f	0.410	0.084	-0.004	0.013	-0.033	0.010	-0.081	0.024	-0.031	0.009	0.052	0.202
R_D	-0.027	0.003	-0.012	0.003	-0.012	0.002	-0.015	0.003	-0.012	0.003	-0.016	0.007
ωLaq	0.032	0.001	-0.028	0.000	-0.010	0.002	-0.015	0.001	-0.005	0.003	-0.005	0.022
R_Q	-0.007	0.001	-0.029	0.001	-0.031	0.002	-0.030	0.001	-0.033	0.002	-0.026	0.011
High noise scenario												
ωL_d	-0.109	0.026	-0.082	0.024	-0.057	0.019	0.093	0.011	-0.028	0.016	-0.037	0.079
ωL_q	-0.136	0.032	-0.214	0.002	-0.968	0.006	-0.255	0.001	-0.848	0.003	-0.484	0.392
$R + 3RN$	-0.398	0.352	-0.268	0.337	-0.314	0.331	-0.342	0.326	-0.334	0.321	-0.331	0.047
$\omega L_{ad}(i_f)$	0.012	0.001	-0.110	0.003	-0.086	0.011	-0.226	0.009	-0.096	0.010	-0.101	0.085
R_f	0.263	0.057	0.126	0.065	0.102	0.030	-0.065	0.122	0.064	0.030	0.098	0.118
$\omega L_{ad}(i_D)$	0.053	0.013	0.045	0.011	0.043	0.011	0.022	0.005	0.034	0.009	0.040	0.012
R_D	-0.096	0.023	-0.092	0.024	-0.090	0.023	-0.113	0.029	-0.092	0.024	-0.097	0.009
ωL_{aq}	0.042	0.010	0.047	0.011	0.107	0.026	0.054	0.013	0.132	0.034	0.076	0.041
R_Q	-0.034	0.008	-0.053	0.008	-0.065	0.013	-0.042	0.010	-0.078	0.017	-0.054	0.018

Table 4.3: RLS absolute errors in the last 5 seconds of estimation - Before step

Block	**Case 1**		**Case 2**		**Case 3**		**Case 4**		**Case 5**		**Absolute**	
	mean	std dev	mean	std dev	mean	std dev	mean	std dev	mean	std dev	mean	std dev
No noise scenario												
RLS 1	4.6e-04	1.1e-06	7.8e-04	1.7e-04	7.1e-04	1.6e-04	5.5e-04	1.3e-04	6.3e-04	1.4e-04	6.3e-04	1.3e-04
RLS 2	3.2e-04	6.3e-05	-1.9e-04	4.4e-05	-1.1e-04	2.5e-05	-4.3e-04	9.9e-05	-1.6e-04	3.7e-05	-1.1e-04	2.7e-04
RLS 3	-9.6e-19	7.0e-16	-3.3e-17	2.1e-13	1.4e-16	2.4e-13	-4.2e-19	8.5e-17	-7.0e-16	1.0e-12	-1.2e-16	3.3e-16
RLS 4	-4.6e-06	9.2e-07	-5.7e-07	1.3e-07	-2.7e-08	6.3e-09	1.4e-10	3.2e-11	1.4e-08	3.2e-09	-1.0e-06	2.0e-06
RLS 5	1.1e-08	3.5e-11	2.0e-06	2.4e-10	2.2e-06	1.0e-12	5.0e-06	1.1e-11	3.4e-06	2.4e-12	2.5e-06	1.9e-06
RLS 6	9.2e-07	2.5e-12	8.2e-07	4.0e-09	7.9e-07	4.5e-09	8.8e-08	4.5e-09	6.1e-07	4.5e-09	6.5e-07	3.3e-07
Standard noise scenario												
RLS 1	4.7e-04	1.6e-03	7.6e-04	1.6e-03	6.8e-04	2.1e-03	5.6e-04	1.4e-03	5.9e-04	2.2e-03	6.1e-04	1.1e-04
RLS 2	3.1e-04	1.2e-03	-1.7e-04	1.2e-03	-7.8e-05	1.2e-03	-4.0e-04	1.3e-03	-1.3e-04	1.2e-03	-9.2e-05	2.6e-04
RLS 3	6.1e-06	8.2e-04	6.1e-06	8.2e-04	6.1e-06	8.2e-04	6.1e-06	8.2e-04	6.1e-06	8.2e-04	6.1e-06	2.3e-12
RLS 4	-3.7e-06	2.4e-05	2.0e-08	2.4e-05	5.7e-07	2.4e-05	5.9e-07	2.4e-05	6.1e-07	2.4e-05	-3.7e-07	1.9e-06
RLS 5	1.5e-07	1.6e-05	2.2e-06	1.6e-05	2.3e-06	1.6e-05	5.1e-06	1.7e-05	3.5e-06	1.6e-05	2.7e-06	1.8e-06
RLS 6	9.2e-07	2.0e-06	8.2e-07	2.0e-06	8.3e-07	2.6e-06	1.1e-07	2.3e-06	6.6e-07	3.0e-06	6.7e-07	3.3e-07
High noise scenario												
RLS 1	4.8e-04	4.9e-03	7.3e-04	5.0e-03	5.2e-04	6.5e-03	5.2e-04	4.4e-03	3.7e-04	6.9e-03	5.2e-04	1.3e-04
RLS 2	3.4e-04	3.8e-03	-1.1e-04	3.8e-03	-1.4e-05	3.8e-03	-3.3e-04	4.0e-03	-6.2e-05	3.8e-03	-3.5e-05	2.4e-04
RLS 3	1.9e-05	2.6e-03	1.9e-05	2.6e-03	1.9e-05	2.6e-03	1.9e-05	2.6e-03	1.9e-05	2.6e-03	1.9e-05	8.6e-11
RLS 4	-2.2e-06	7.6e-05	1.3e-06	7.6e-05	1.9e-06	7.6e-05	1.9e-06	7.6e-05	1.7e-06	7.6e-05	9.3e-07	1.8e-06
RLS 5	4.6e-07	4.9e-05	2.4e-06	5.0e-05	2.5e-06	5.0e-05	5.3e-06	5.5e-05	3.8e-06	5.2e-05	2.9e-06	1.8e-06
RLS 6	9.1e-07	6.4e-06	8.3e-07	6.4e-06	9.1e-07	8.1e-06	1.6e-07	7.1e-06	7.8e-07	9.5e-06	7.2e-07	3.2e-07

Table 4.4: RLS absolute errors in the last 5 seconds of estimation - After step

Block	**Case 1**		**Case 2**		**Case 3**		**Case 4**		**Case 5**		**Absolute**	
	mean	std dev	mean	std dev	mean	std dev	mean	std dev	mean	std dev	mean	std dev
No noise scenario												
RLS 1	4.8e-04	7.7e-08	5.2e-05	1.3e-05	2.2e-04	5.4e-05	2.5e-05	6.5e-06	1.3e-04	3.3e-05	1.8e-04	1.8e-04
RLS 2	3.5e-04	8.6e-05	-3.2e-04	8.0e-05	-1.9e-04	4.9e-05	-5.4e-04	1.4e-04	-2.5e-04	6.6e-05	-1.9e-04	3.3e-04
RLS 3	1.0e-18	7.5e-16	-3.6e-17	2.2e-13	2.3e-16	2.5e-13	1.8e-18	8.8e-17	-7.3e-16	1.1e-12	-1.1e-16	3.7e-16
RLS 4	-1.9e-07	4.8e-08	1.7e-06	4.2e-07	7.5e-07	1.9e-07	2.6e-06	6.7e-07	1.4e-06	3.7e-07	1.2e-06	1.0e-06
RLS 5	1.1e-08	7.3e-13	2.1e-06	3.9e-09	2.3e-06	3.5e-10	5.3e-06	1.2e-11	3.6e-06	8.1e-11	2.7e-06	1.9e-06
RLS 6	9.9e-07	7.6e-11	8.7e-07	7.2e-09	8.5e-07	4.9e-10	9.6e-08	3.1e-14	6.5e-07	1.2e-10	6.9e-07	3.5e-07
Standard noise scenario												
RLS 1	4.4e-04	1.6e-03	3.4e-05	1.6e-03	1.9e-04	2.1e-03	5.3e-06	1.4e-03	1.0e-04	2.3e-03	1.6e-04	1.8e-04
RLS 2	3.1e-04	1.2e-03	-3.5e-04	1.2e-03	-2.2e-04	1.2e-03	-5.7e-04	1.3e-03	-2.8e-04	1.3e-03	-2.2e-04	3.3e-04
RLS 3	-1.7e-05	8.0e-04	-1.7e-05	8.0e-04	-1.7e-05	8.0e-04	-1.7e-05	8.0e-04	-1.7e-05	8.0e-04	-1.7e-05	2.8e-13
RLS 4	-3.2e-07	2.4e-05	1.6e-06	2.4e-05	6.7e-07	2.4e-05	2.5e-06	2.4e-05	1.3e-06	2.4e-05	1.2e-06	1.1e-06
RLS 5	2.1e-07	1.6e-05	2.3e-06	1.6e-05	2.5e-06	1.6e-05	5.5e-06	1.8e-05	3.8e-06	1.7e-05	2.9e-06	2.0e-06
RLS 6	9.9e-07	2.0e-06	8.7e-07	2.1e-06	8.4e-07	2.7e-06	9.0e-08	2.3e-06	6.2e-07	3.2e-06	6.8e-07	3.6e-07
High noise scenario												
RLS 1	3.5e-04	5.1e-03	-2.4e-05	5.2e-03	1.0e-04	6.8e-03	-4.7e-05	4.5e-03	1.7e-05	7.2e-03	8.0e-05	1.6e-04
RLS 2	2.5e-04	3.9e-03	-4.1e-04	3.9e-03	-2.8e-04	3.9e-03	-6.3e-04	4.1e-03	-3.4e-04	3.9e-03	-2.8e-04	3.3e-04
RLS 3	-5.4e-05	2.5e-03	-5.4e-05	2.5e-03	-5.4e-05	2.5e-03	-5.4e-05	2.5e-03	-5.4e-05	2.5e-03	-5.4e-05	1.1e-11
RLS 4	-5.9e-07	7.5e-05	1.5e-06	7.5e-05	4.8e-07	7.5e-05	2.3e-06	7.5e-05	1.2e-06	7.5e-05	9.7e-07	1.1e-06
RLS 5	6.4e-07	5.0e-05	2.8e-06	5.2e-05	2.9e-06	5.2e-05	5.9e-06	5.8e-05	4.2e-06	5.4e-05	3.3e-06	1.9e-06
RLS 6	1.0e-06	6.5e-06	8.8e-07	6.5e-06	8.1e-07	8.5e-06	7.6e-08	7.4e-06	5.8e-07	1.0e-05	6.7e-07	3.7e-07

Chapter 5

The Effects of Saturation

5.1 Validation with Saturation

For validation of ODW, KF and RLS with saturation, the simulation file runs at exactly the same conditions as described in sections 3.5 and 4.4, but with saturation enabled in the SPS synchronous machine model using the curve in fig. 5.1.

Results are presented in appendix D and their summary is available in tables 5.1 to 5.5. Below follow some remarks about them:

- The KF effectively compensates saturation effects for v_q, i_f. When comparing NMSE values with table 3.1, there are only marginal deviations.

- The KF does not compensate saturation effects for i_D. Saturation changes the value of L_{ad}, which is the main component of the zero and pole of i_D transfer function in the ODW, as shown in eq. (3.6). The variation of L_{ad} makes the state transition function non linear, and improper for a KF to handle. An alternative would be using an Extended or Unscented KF, which can handle non linear state transition functions, and compensate the value of L_{ad} dynamically using the algorithm presented in section 5.2. This possibility was briefly explored, but meaningful results could not be presented in this report due to time limitation.

- The error for ωL_{ad} estimation increases considerably and this is expected due to the saturation effect. However, there is no direct correlation between the amplitude of this deviation and the saturation level, as one would expect. This fact is clearly seen in case 4, which has the largest error for $\omega L_d, \omega L_{ad}$, but the lowest level of saturation, i.e. the smallest field current of all cases. Hence, it is necessary to model this effect to have a proper estimation of parameters.

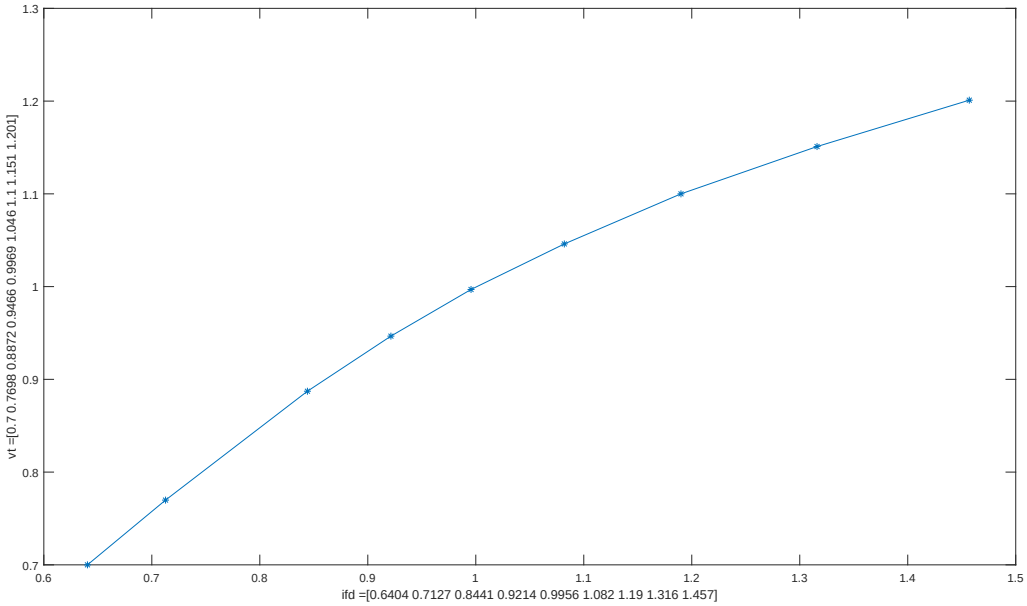

Figure 5.1: Saturation curve used for validation, values in Matlab pu base

- Noise power continues to have small influence on the quality of the parameter estimation even with errors in the model caused by saturation. This seems to be an advantage of the KF over other filtering techniques reported in the literature by Karayaka et al. (2003); Kyriakides et al. (2005), which still have to be corroborated with practical results.

5.2 Saturation Model

"Saturation effects are highly nonlinear and depend on the generator loading conditions so trying to account for them accurately in the generator model is nigh on impossible." (Machowski et al., 2008, Section 11.1.8)

Due to this, magnetic saturation in the stator and rotor iron has been ignored in the modeling of previous sections. However, it is introduced here a simple saturation model that: produces acceptable results; is linked to the physical process; and uses easily obtainable data (Machowski et al., 2008; Anderson and Fouad, 2003; Kundur et al., 1994).

The magnetic circuit of a synchronous machine comprises an iron path (rotor and stator cores) and an air path (air-gap). The relationship between mmf and flux in such a circuit is represented by the general curve shown in fig. 5.2.a. When the iron path is unsaturated, the relationship between mmf and flux is linear and represented by the *air-gap line*, segment

Table 5.1: NMSE values for all simulation cases and noise scenarios with saturation

Variable	**Case 1**	**Case 2**	**Case 3**	**Case 4**	**Case 5**	**Mean**	**Std dev**
			No noise scenario				
v_d KF	1.0000	1.0000	1.0000	1.0000	1.0000	1.0000	4.671e-10
v_q KF	1.0000	1.0000	1.0000	1.0000	1.0000	1.0000	1.778e-09
i_f KF	1.0000	1.0000	1.0000	1.0000	1.0000	1.0000	6.962e-06
i_D ODW	0.5904	0.8797	0.6168	0.9968	0.9744	0.8116	1.951e-01
i_D KF	0.5943	0.8742	0.5997	0.9968	0.9649	0.8060	1.960e-01
i_Q ODW	-0.6178	0.9998	0.9999	1.0000	0.9999	0.9999	8.425e-05
i_Q KF	-37.03	0.9967	0.9978	0.9999	0.9996	0.9985	1.509e-03
			Standard noise scenario				
v_d KF	-167.5	0.9752	0.9775	0.9983	0.9926	0.9859	1.131e-02
v_q KF	0.9981	0.9973	0.9970	0.9947	0.9944	0.9963	1.650e-03
i_f KF	0.9994	0.9992	0.9998	0.9974	0.9997	0.9991	9.706e-04
i_D ODW	0.5123	0.8070	0.5186	0.9582	0.8726	0.7337	2.064e-01
i_D KF	0.5663	0.8483	0.5652	0.9836	0.9298	0.7786	2.002e-01
i_Q ODW	-579	0.9363	0.9234	0.9956	0.9651	0.9551	3.211e-02
i_Q KF	-249.3	0.9736	0.9702	0.9984	0.9871	0.9823	1.295e-02
			High noise scenario				
v_d KF	-1684	0.7521	0.7750	0.9833	0.9259	0.8591	1.132e-01
v_q KF	0.9811	0.9729	0.9703	0.9472	0.9440	0.9631	1.650e-02
i_f KF	0.9941	0.9916	0.9977	0.9743	0.9972	0.9910	9.664e-03
i_D ODW	-0.1771	0.1639	-0.3546	0.6110	-0.0378	0.0411	3.709e-01
i_D KF	0.3265	0.6255	0.2638	0.8651	0.6175	0.5397	2.454e-01
i_Q ODW	-5774	0.3659	0.2363	0.9558	0.6520	0.5525	3.201e-01
i_Q KF	-2157	0.7647	0.7220	0.9840	0.8747	0.8363	1.176e-01

Table 5.2: Percentage errors in the last 5 seconds of estimation using data sheet values as baseline - Before step with saturation

Parameter	**Case 1**		**Case 2**		**Case 3**		**Case 4**		**Case 5**		**Absolute**	
	mean	std dev	mean	std dev	mean	std dev	mean	std dev	mean	std dev	mean	std dev
No noise scenario												
ωL_d	-0.001	0.000	-0.572	0.000	-1.629	0.000	-4.036	0.004	-3.258	0.001	-1.899	1.721
ωL_q	0.256	0.004	-0.074	0.035	-0.874	0.031	-0.216	0.011	-0.788	0.018	-0.339	0.481
$R + 3R_N$	0.000	0.000	0.000	0.000	0.000	0.000	0.000	0.000	0.000	0.000	0.000	0.000
ωL_{ad}	-0.079	0.005	3.931	0.003	3.256	0.001	5.172	0.006	5.199	0.001	3.496	2.164
R_f	0.518	0.104	0.062	0.014	0.002	0.000	0.002	0.000	-0.000	0.000	0.117	0.226
R_D	-0.012	0.000	-0.000	0.000	-0.000	0.000	-0.001	0.000	-0.000	0.000	-0.003	0.005
ωL_{aq}	0.022	0.000	-0.036	0.001	-0.023	0.001	-0.022	0.001	-0.022	0.001	-0.016	0.022
R_Q	-0.001	0.000	-0.026	0.000	-0.024	0.000	-0.025	0.000	-0.024	0.000	-0.020	0.011
Standard noise scenario												
ωL_d	-0.019	0.004	-0.584	0.003	-1.637	0.002	-4.042	0.005	-3.264	0.002	-1.909	1.717
ωL_q	0.222	0.008	-0.079	0.035	-0.878	0.031	-0.217	0.011	-0.791	0.018	-0.349	0.472
$R + 3R_N$	-0.065	0.056	-0.042	0.044	-0.022	0.042	-0.023	0.042	-0.023	0.042	-0.035	0.019
ωL_{ad}	-0.076	0.005	3.934	0.003	3.254	0.001	5.173	0.005	5.196	0.000	3.496	2.163
R_f	0.410	0.084	-0.004	0.013	-0.033	0.010	-0.081	0.024	-0.031	0.009	0.052	0.202
R_D	-0.027	0.003	-0.012	0.003	-0.012	0.002	-0.015	0.003	-0.012	0.003	-0.016	0.007
ωL_{aq}	0.032	0.001	-0.028	0.000	-0.010	0.002	-0.015	0.001	-0.005	0.003	-0.005	0.022
R_Q	-0.007	0.001	-0.029	0.001	-0.031	0.002	-0.030	0.001	-0.033	0.002	-0.026	0.011
High noise scenario												
ωL_d	-0.187	0.036	-0.683	0.024	-1.700	0.015	-4.078	0.011	-3.310	0.011	-1.992	1.669
ωL_q	0.009	0.046	-0.088	0.037	-0.905	0.031	-0.223	0.011	-0.814	0.016	-0.404	0.425
$R + 3R_N$	-0.616	0.557	-0.439	0.435	-0.161	0.414	-0.161	0.414	-0.230	0.407	-0.321	0.200
ωL_{ad}	-0.066	0.006	3.929	0.004	3.222	0.009	5.154	0.004	5.168	0.008	3.481	2.150
R_f	0.238	0.064	-0.144	0.050	-0.112	0.033	-0.272	0.078	-0.088	0.027	-0.076	0.189
R_D	-0.176	0.030	-0.120	0.025	-0.111	0.024	-0.134	0.029	-0.116	0.025	-0.131	0.027
ωL_{aq}	0.110	0.014	0.030	0.012	0.111	0.027	0.050	0.014	0.148	0.035	0.090	0.049
R_Q	-0.059	0.011	-0.066	0.009	-0.082	0.014	-0.069	0.010	-0.099	0.018	-0.075	0.016

Table 5.3: Percentage errors in the last 5 seconds of estimation using data sheet values as baseline - After step with saturation

Parameter	**Case 1**		**Case 2**		**Case 3**		**Case 4**		**Case 5**		**Absolute**	
	mean	std dev	mean	std dev	mean	std dev	mean	std dev	mean	std dev	mean	std dev
No noise scenario												
ωL_d	0.000	0.000	-0.299	0.001	-0.905	0.001	-4.032	0.006	-2.964	0.001	-1.640	1.768
ωL_q	-0.012	0.003	-0.223	0.002	-0.972	0.010	-0.260	0.001	-0.850	0.004	-0.463	0.421
$R + 3R_N$	0.000	0.000	0.000	0.000	0.000	0.000	0.000	0.000	0.000	0.000	0.000	0.000
ωL_{ad}	-3.510	0.006	2.085	0.006	1.840	0.001	5.167	0.008	4.758	0.002	2.068	3.464
R_f	0.020	0.005	-0.169	0.043	-0.039	0.010	-0.329	0.086	-0.066	0.018	-0.117	0.137
R_D	-0.003	0.000	-0.000	0.000	-0.000	0.000	-0.004	0.000	-0.000	0.000	-0.002	0.002
ωL_{aq}	-0.001	0.000	0.000	0.000	0.000	0.000	0.000	0.000	0.000	0.000	-0.000	0.001
R_Q	-0.001	0.000	-0.021	0.000	-0.016	0.000	-0.004	0.000	-0.012	0.000	-0.011	0.008
Standard noise scenario												
ωL_d	-0.011	0.003	-0.308	0.003	-0.912	0.002	-4.037	0.007	-2.969	0.002	-1.647	1.765
ωL_q	-0.023	0.006	-0.219	0.001	-0.968	0.008	-0.258	0.000	-0.847	0.003	-0.463	0.418
$R + 3R_N$	-0.039	0.035	-0.029	0.034	-0.031	0.033	-0.034	0.033	-0.035	0.032	-0.034	0.004
ωL_{ad}	-3.506	0.006	2.087	0.006	1.839	0.001	5.167	0.007	4.757	0.001	2.069	3.462
R_f	0.116	0.018	-0.083	0.047	0.007	0.014	-0.220	0.090	-0.025	0.020	-0.041	0.123
R_D	-0.013	0.002	-0.009	0.002	-0.009	0.002	-0.015	0.003	-0.010	0.003	-0.011	0.003
ωL_{aq}	0.003	0.001	0.005	0.001	0.011	0.002	0.005	0.001	0.014	0.003	0.007	0.005
R_Q	-0.004	0.001	-0.024	0.001	-0.020	0.001	-0.007	0.001	-0.019	0.002	-0.015	0.009
High noise scenario												
ωL_d	-0.108	0.027	-0.388	0.023	-0.965	0.015	-4.064	0.013	-3.005	0.011	-1.706	1.738
ωL_q	-0.130	0.031	-0.213	0.002	-0.967	0.006	-0.255	0.001	-0.845	0.003	-0.482	0.392
$R + 3R_N$	-0.386	0.344	-0.268	0.337	-0.311	0.330	-0.341	0.326	-0.334	0.321	-0.328	0.043
ωL_{ad}	-3.498	0.006	2.082	0.003	1.811	0.007	5.153	0.003	4.733	0.006	2.056	3.452
R_f	0.321	0.055	0.104	0.070	0.106	0.031	0.025	0.112	0.064	0.033	0.124	0.115
R_D	-0.095	0.023	-0.092	0.024	-0.090	0.023	-0.113	0.029	-0.092	0.024	-0.096	0.009
ωL_{aq}	0.041	0.010	0.047	0.011	0.107	0.026	0.054	0.013	0.133	0.034	0.076	0.041
R_Q	-0.032	0.008	-0.053	0.008	-0.066	0.013	-0.041	0.010	-0.078	0.018	-0.054	0.018

Table 5.4: RLS absolute errors in the last 5 seconds of estimation - Before step with saturation

Block	**Case 1**		**Case 2**		**Case 3**		**Case 4**		**Case 5**		**Absolute**	
	mean	std dev	mean	std dev	mean	std dev	mean	std dev	mean	std dev	mean	std dev
No noise scenario												
RLS 1	4.6e-04	1.1e-06	7.8e-04	1.7e-04	7.1e-04	1.6e-04	5.5e-04	1.3e-04	6.3e-04	1.4e-04	6.3e-04	1.3e-04
RLS 2	3.2e-04	6.3e-05	-1.9e-04	4.4e-05	-1.1e-04	2.5e-05	-4.3e-04	9.9e-05	-1.6e-04	3.7e-05	-1.1e-04	2.7e-04
RLS 3	-9.6e-19	7.0e-16	-3.3e-17	2.1e-13	1.4e-16	2.4e-13	-4.2e-19	8.5e-17	-7.0e-16	1.0e-12	-1.2e-16	3.3e-16
RLS 4	-4.6e-06	9.2e-07	-5.7e-07	1.3e-07	-2.7e-08	6.3e-09	1.4e-10	3.2e-11	1.4e-08	3.2e-09	-1.0e-06	2.0e-06
RLS 5	1.1e-08	3.5e-11	2.0e-06	2.4e-10	2.2e-06	1.0e-12	5.0e-06	1.1e-11	3.4e-06	2.4e-12	2.5e-06	1.9e-06
RLS 6	9.2e-07	2.5e-12	8.2e-07	4.0e-09	7.9e-07	4.5e-09	8.8e-08	4.5e-09	6.1e-07	4.5e-09	6.5e-07	3.3e-07
Standard noise scenario												
RLS 1	4.7e-04	1.6e-03	7.6e-04	1.6e-03	6.8e-04	2.1e-03	5.6e-04	1.4e-03	5.9e-04	2.2e-03	6.1e-04	1.1e-04
RLS 2	3.1e-04	1.2e-03	-1.7e-04	1.2e-03	-7.8e-05	1.2e-03	-4.0e-04	1.3e-03	-1.3e-04	1.2e-03	-9.2e-05	2.6e-04
RLS 3	6.1e-06	8.2e-04	6.1e-06	8.2e-04	6.1e-06	8.2e-04	6.1e-06	8.2e-04	6.1e-06	8.2e-04	6.1e-06	2.3e-12
RLS 4	-3.7e-06	2.4e-05	2.0e-08	2.4e-05	5.7e-07	2.4e-05	5.9e-07	2.4e-05	6.1e-07	2.4e-05	-3.7e-07	1.9e-06
RLS 5	1.5e-07	1.6e-05	2.2e-06	1.6e-05	2.3e-06	1.6e-05	5.1e-06	1.7e-05	3.5e-06	1.6e-05	2.7e-06	1.8e-06
RLS 6	9.2e-07	2.0e-06	8.2e-07	2.0e-06	8.3e-07	2.6e-06	1.1e-07	2.3e-06	6.6e-07	3.0e-06	6.7e-07	3.3e-07
High noise scenario												
RLS 1	4.8e-04	4.9e-03	7.3e-04	5.0e-03	5.2e-04	6.5e-03	5.2e-04	4.4e-03	3.7e-04	6.9e-03	5.2e-04	1.3e-04
RLS 2	3.4e-04	3.8e-03	-1.1e-04	3.8e-03	-1.4e-05	3.8e-03	-3.3e-04	4.0e-03	-6.2e-05	3.8e-03	-3.5e-05	2.4e-04
RLS 3	1.9e-05	2.6e-03	1.9e-05	2.6e-03	1.9e-05	2.6e-03	1.9e-05	2.6e-03	1.9e-05	2.6e-03	1.9e-05	8.6e-11
RLS 4	-2.2e-06	7.6e-05	1.3e-06	7.6e-05	1.9e-06	7.6e-05	1.9e-06	7.6e-05	1.7e-06	7.6e-05	9.3e-07	1.8e-06
RLS 5	4.6e-07	4.9e-05	2.4e-06	5.0e-05	2.5e-06	5.0e-05	5.3e-06	5.5e-05	3.8e-06	5.2e-05	2.9e-06	1.8e-06
RLS 6	9.1e-07	6.4e-06	8.3e-07	6.4e-06	9.1e-07	8.1e-06	1.6e-07	7.1e-06	7.8e-07	9.5e-06	7.2e-07	3.2e-07

Table 5.5: RLS absolute errors in the last 5 seconds of estimation - After step with saturation

Block	**Case 1**		**Case 2**		**Case 3**		**Case 4**		**Case 5**		**Absolute**	
	mean	std dev	mean	std dev	mean	std dev	mean	std dev	mean	std dev	mean	std dev
No noise scenario												
RLS 1	4.8e-04	7.7e-08	5.2e-05	1.3e-05	2.2e-04	5.4e-05	2.5e-05	6.5e-06	1.3e-04	3.3e-05	1.8e-04	1.8e-04
RLS 2	3.5e-04	8.6e-05	-3.2e-04	8.0e-05	-1.9e-04	4.9e-05	-5.4e-04	1.4e-04	-2.5e-04	6.6e-05	-1.9e-04	3.3e-04
RLS 3	1.0e-18	7.5e-16	-3.6e-17	2.2e-13	2.3e-16	2.5e-13	1.8e-18	8.8e-17	-7.3e-16	1.1e-12	-1.1e-16	3.7e-16
RLS 4	-1.9e-07	4.8e-08	1.7e-06	4.2e-07	7.5e-07	1.9e-07	2.6e-06	6.7e-07	1.4e-06	3.7e-07	1.2e-06	1.0e-06
RLS 5	1.1e-08	7.3e-13	2.1e-06	3.9e-09	2.3e-06	3.5e-10	5.3e-06	1.2e-11	3.6e-06	8.1e-11	2.7e-06	1.9e-06
RLS 6	9.9e-07	7.6e-11	8.7e-07	7.2e-09	8.5e-07	4.9e-10	9.6e-08	3.1e-14	6.5e-07	1.2e-10	6.9e-07	3.5e-07
Standard noise scenario												
RLS 1	4.4e-04	1.6e-03	3.4e-05	1.6e-03	1.9e-04	2.1e-03	5.3e-06	1.4e-03	1.0e-04	2.3e-03	1.6e-04	1.8e-04
RLS 2	3.1e-04	1.2e-03	-3.5e-04	1.2e-03	-2.2e-04	1.2e-03	-5.7e-04	1.3e-03	-2.8e-04	1.3e-03	-2.2e-04	3.3e-04
RLS 3	-1.7e-05	8.0e-04	-1.7e-05	8.0e-04	-1.7e-05	8.0e-04	-1.7e-05	8.0e-04	-1.7e-05	8.0e-04	-1.7e-05	2.8e-13
RLS 4	-3.2e-07	2.4e-05	1.6e-06	2.4e-05	6.7e-07	2.4e-05	2.5e-06	2.4e-05	1.3e-06	2.4e-05	1.2e-06	1.1e-06
RLS 5	2.1e-07	1.6e-05	2.3e-06	1.6e-05	2.5e-06	1.6e-05	5.5e-06	1.8e-05	3.8e-06	1.7e-05	2.9e-06	2.0e-06
RLS 6	9.9e-07	2.0e-06	8.7e-07	2.1e-06	8.4e-07	2.7e-06	9.0e-08	2.3e-06	6.2e-07	3.2e-06	6.8e-07	3.6e-07
High noise scenario												
RLS 1	3.5e-04	5.1e-03	-2.4e-05	5.2e-03	1.0e-04	6.8e-03	-4.7e-05	4.5e-03	1.7e-05	7.2e-03	8.0e-05	1.6e-04
RLS 2	2.5e-04	3.9e-03	-4.1e-04	3.9e-03	-2.8e-04	3.9e-03	-6.3e-04	4.1e-03	-3.4e-04	3.9e-03	-2.8e-04	3.3e-04
RLS 3	-5.4e-05	2.5e-03	-5.4e-05	2.5e-03	-5.4e-05	2.5e-03	-5.4e-05	2.5e-03	-5.4e-05	2.5e-03	-5.4e-05	1.1e-11
RLS 4	-5.9e-07	7.5e-05	1.5e-06	7.5e-05	4.8e-07	7.5e-05	2.3e-06	7.5e-05	1.2e-06	7.5e-05	9.7e-07	1.1e-06
RLS 5	6.4e-07	5.0e-05	2.8e-06	5.2e-05	2.9e-06	5.2e-05	5.9e-06	5.8e-05	4.2e-06	5.4e-05	3.3e-06	1.9e-06
RLS 6	1.0e-06	6.5e-06	8.8e-07	6.5e-06	8.1e-07	8.5e-06	7.6e-08	7.4e-06	5.8e-07	1.0e-05	6.7e-07	3.7e-07

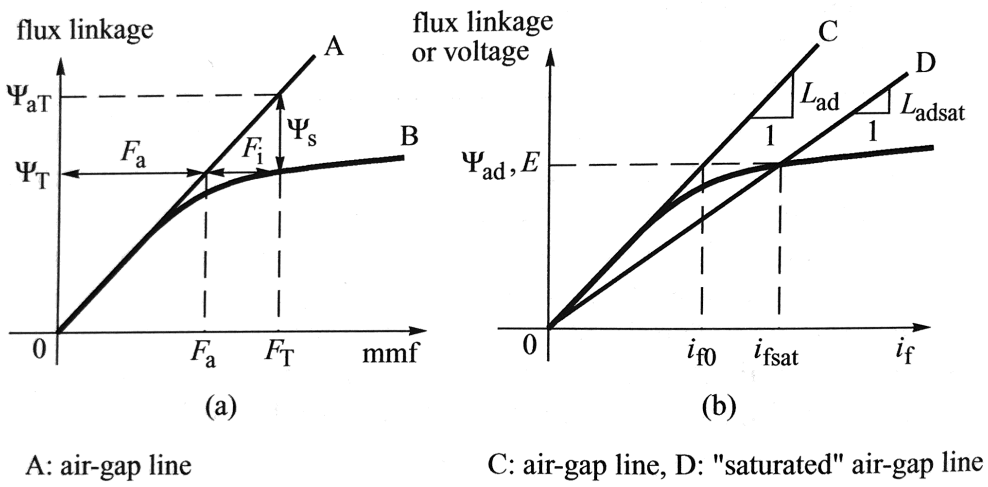

Figure 5.2: Saturation characteristics: (a) curve for a magnetic circuit with flux path in iron and air; (b) synchronous machine open-circuit saturation characteristic (Machowski et al., 2008, p. 458)

0A. In this situation, the reluctance of the magnetic circuit is dominated by the reluctance of the air-gap.

When the iron saturates, the relationship is not linear and follows the *saturation curve*, segment 0B. Therefore, for a given total flux linkage Ψ_T, there are two components in the total mmf F_T: the air-gap mmf F_a and the iron mmf F_i, such that $F_T = F_a + F_i$.

Moreover, the total flux linkage Ψ_T can be interpreted as the air-gap flux linkage Ψ_{aT}, a theoretical flux linkage in the air-gap without saturation effects, subtracted from the saturation flux linkage Ψ_s, such that: $\Psi_{aT} = \Psi_T + \Psi_s$.

Using triangle similarity in fig. 5.2.a, the *saturation factor* K_{sd} is defined as:

$$K_{sd} = \frac{F_a}{F_a + F_i} = \frac{\Psi_T}{\Psi_T + \Psi_s} = \frac{\Psi_T}{\Psi_{aT}} \tag{5.1}$$

Having defined a saturation factor, it is necessary to provide a simple method of calculating its value for any load condition using data readily available. For that, the following assumptions are made:

1. The open-circuit saturation curve can be used under load conditions;

2. As the leakage flux path is mainly in the air, the leakage inductances are independent of saturation. This implies that only the mutual inductances L_{ad}, L_{aq} are affected by saturation,

3. Saturation on the d-axis and q-axis are independent of each other;

4. For salient pole machines, since the q-axis reluctance is dominated by air paths, saturation effects are ignored.

In steady-state $i_D = i_Q = 0$ and the derivative of all currents are zero. Hence, it is possible to obtain the following expressions from eq. (2.37):

$$\begin{aligned} v_d &= -Ri_d - \omega(L_{aq} + l_l)i_q \\ v_d + Ri_d + \omega l_l i_q &= -\omega L_{aq} i_q \\ -\frac{v_d + Ri_d + \omega l_l i_q}{\omega} &= \Psi_{aq} \end{aligned} \tag{5.2}$$

$$\begin{aligned} v_q &= \omega(L_{ad} + l_l)i_d - Ri_q + \omega L_{ad} i_f \\ v_q + Ri_d - \omega l_l i_d &= \omega L_{ad}(i_d + i_f) \\ \frac{v_q + Ri_q - \omega l_l i_d}{\omega} &= \Psi_{ad} \end{aligned} \tag{5.3}$$

$$\begin{aligned} v_0 &= 0 \\ \Psi_0 &= 0 \end{aligned} \tag{5.4}$$

$$\Psi_T = \sqrt{\Psi_{ad}^2 + \Psi_{aq}^2 + \Psi_0^2} = \sqrt{\Psi_{ad}^2 + \Psi_{aq}^2} \tag{5.5}$$

When the synchronous machine is in no-load operation (i.e. open circuit), $i_d = i_q = 0$. Substituting these values in eqs. (5.2) to (5.5), one easily deduces that:

$$\begin{aligned} v_d &= \Psi_{aq} = 0 \\ v_q &= \Psi_{ad} = \omega L_{ad} i_f = \Psi_{ad} \\ \Psi_T &= \Psi_{ad} = v_q \end{aligned} \tag{5.6}$$

and the open-circuit saturation curve in fig. 5.2.b can be directly related to the magnetic saturation of the d-axis. In other words, the vertical axis in fig. 5.2.b when plotted in pu is interpreted as either voltage or flux linkage, and the horizontal axis is interpreted as either current or mmf

Finally, if at some open-circuit voltage E the required flux linkage is Ψ_{ad}, then the required field current will be i_{f0} if there is no saturation of the iron. However, if saturation is present,

the required current will be i_{fsat}. Taking this into consideration and using eqs. (5.1) and (5.6):

$$i_{fsat} = \frac{i_{f0}}{K_{sd}} \tag{5.7}$$

$$L_{ad} = \frac{\Psi_{ad}}{i_{f0}} \tag{5.8}$$

$$L_{adsat} = \frac{\Psi_T}{i_{fsat}} = \frac{\Psi_{ad}}{i_{fsat}} \tag{5.9}$$

$$L_{adsat} = K_{sd} L_{ad} \tag{5.10}$$

Note that L_{ad} is the slope of the air-gap line (segment 0C), while L_{adsat} is the slope of the "saturated" air-gap line (segment 0D). In load operation, L_{ad} is calculated considering Ψ_T as given in eq. (5.5) and assuming eq. (5.10) is still valid. (Kundur et al., 1994, Section 3.8.2)

Last but not least, it is necessary to fit the open-circuit saturation characteristic by a well defined function in order to calculate K_{sd} and consequently the saturation flux linkage Ψ_s at any operation point. This is done using the following conditional function in pu:

$$\Psi_s = \begin{cases} 0, \Psi_T \leq \Psi_{T0} \\ A_{sat} e^{B_{sat}(\Psi_T - \Psi_{T0})}, \Psi_T > \Psi_{T0} \end{cases} \tag{5.11}$$

where:

- Ψ_{T0} is the flux linkage level where the saturation effect starts
- A_{sat}, B_{sat} are constants easily calculated by performing a least-square approximation in the known saturation curve starting at Ψ_{T0}

In summary, the procedure for calculating K_{sd} is:

1. With the saturation curve in hands, determine Ψ_{T0} and the air-gap line.
2. Interpolate the difference between the air-gap line and the saturation curve with an exponential function of type Ae^{Bx} to obtain A_{sat}, B_{sat}
3. Knowing $v_d, v_q, i_d, i_q, i_f, \omega, R, l_l$, calculate $\Psi_{aq}, \Psi_{ad}, \Psi_T$ using eqs. (5.2), (5.3) and (5.5)
4. Calculate Ψ_s using eq. (5.11)
5. Calculate K_{sd} using eq. (5.1)

Chapter 6

Conclusions, Discussion, and Further Work

This final chapter summarizes the work done and results achieved. It also discusses the major findings and put them "in the big picture", together with recommendations for next steps.

6.1 Summary and Conclusions

The focus of this thesis has been investigating and implementing algorithms for reliable parameter identification for salient pole synchronous machines that can be used for condition monitoring, on line assessment of the power grid, and adaptive control.

Naturally, the first step to achieve this goal is defining the parameters of a synchronous machine. It may seem obvious, but the derivation of an accurate model for a three-phase synchronous machine is an involved task that occupied many bright minds for over a century, as described in section 1.5. This was not different in this thesis, where good part of the effort was put to model the machine and understand the vast and sometimes confusing literature about the subject. Therefore, chapter 2 is dedicated to revise the basic equations of the synchronous machine. Based on them and the pu system defined by table 2.1, the model and parameters in pu are defined by eq. (2.37). Last but not least, section 2.6 defines how to convert the parameters from eq. (2.37) to the *standard parameters* used in reduced-order models for planning, operation, and control of the power system.

The next step is designing an optimal observer to measure inputs and outputs of the model obtained in the previous chapter. This step is necessary because inputs and outputs should be based on common measurements available in a power plant, as defined in section 1.4. Measurement of damper winding currents is usually not possible, so an observer for them is necessary. On top of that, other practical issues include handling noise and measurements from several sources, each of them having different precision and accuracy values. To handle

these challenges, a Kalman Filter (KF) is implemented using a state-space representation derived from an extended model of the synchronous machine, given by eqs. (3.4) and (3.5).

Results of the validation of this KF without saturation effects is presented in section 3.5 and shows almost perfect correlation with the synchronous machine model available in Simscape Power Systems (SPS) when using Normalized Mean Square Error (NMSE). The results also show the correlation is not sensitive to the load connected to the machine, and that *goodness of fit* is maintained under a "standard" noise scenario. As one would expect, performance degrades in the "high" noise scenario, specially when the Signal-to-Noise Ratio (SNR) is extremely low.

After the foundation is laid, i.e. a model is defined and inputs and outputs are available, focus is given to the selection of an algorithm and error criterion for parameter estimation. Recursive Least Squares (RLS) is chosen based on three criteria: availability in the System Identification Toolbox of Simulink, possibility for near real-time execution, references in the literature available for comparison.

Next, considering that simultaneous estimation of the 14 parameters of the synchronous mrachine with RLS produces poor results (Kyriakides et al., 2005), some simplifications of the model are assumed as described in section 4.2. In summary, these simplifications are: steady-state is assumed (i.e. $\frac{d}{dt}\mathbf{i_{dq0fDQ}} = \mathbf{0}$), and the parameter R is not estimated. The steady state condition is detected in run-time by monitoring that damper winding currents are below a configurable threshold level. The RLS estimator is disabled when a transient state is detected, and reset once the steady state is back to avoid instability and bursting phenomena if parameter estimation is used in adaptive control. See considerations and additional comments in section 6.2.3.

With simplifications, 8 out of 13 parameters from the synchronous machine model are reliably estimated by the proposed algorithm: $R + 3R_N, R_f, R_D, R_Q, \omega L_d, \omega L_{ad}, \omega L_q, \omega L_{aq}$. The ones not being estimated are: $R, L_0 + 3L_N, L_f, L_D, L_Q$, in which R is not relevant for planning, operation, and control of the power system.

The RLS estimation algorithm is then tested without saturation effects using the same cases and noise scenarios used for validation of the KF. Results of these simulations show very small percentage deviations from the data sheet values, and are in line with those reported by Kyriakides et al. (2005). However, the estimator developed in this thesis is largely insensitive to noise and load conditions, contrary to the former, which may be considered a valuable contribution if corroborated with practical results. Also, the strategy for detection of steady state and disabling/resetting the RLS estimator seems successful, as no instability was observed in the estimated parameters, even during long time simulations of 300 seconds.

Last but not least, the non linear effects of saturation are evaluated in section 5.1 by repeating previous tests with saturation enabled in the synchronous machine model from

SPS. Results show the KF effectively compensates saturation effects for v_q, i_f and correlation with SPS is very high. However, this is not true for i_D because its measurement is provided by the Observer for Damper Windings (ODW), whose zeros and poles are directly affected by the saturation of L_{ad}. This effect reduces considerably the *goodness of fit* of i_D compared to SPS. Moreover, the error for ωL_{ad} estimation increases considerably and this is expected due to the saturation effect. However, there is no direct correlation between the amplitude of this deviation and the saturation level, as one would expect. A fact that is clearly seen in case 4, which has the largest error for ωL_{ad}, but the lowest saturation level.

This leads to the conclusion that saturation effects must be considered and included in the model. Taking this into account, a simplified model for saturation is introduced in section 5.2, based on a recursive algorithm and previous knowledge of the open-circuit characteristic of the synchronous machine. Initial investigations for inclusion of this non linear model in an Extended Kalman Filter (EKF) have started, but time for delivery of this report came before meaningful results could be achieved. On top of that, an Extended Kalman Filter (EKF) can be used for estimating the values of $L_0 + 3L_N, L_f, L_D, L_Q$, by assuming these parameters are states with derivatives equal to zero.

6.2 Discussion

It is important to keep in mind that the goal of this project was never to produce the ultimate, state-of-the-art parameter estimator for a synchronous machine, but rather a minimum viable product that could be executed in the short time available for a master thesis and used to test some initial hypothesis.

Despite the fact that saturation effects are not properly handled yet, this thesis fairly answers the main questions of the problem formulation, i.e.:

- What are the parameters of a synchronous machine?
- How non linear effects such as saturation affects them?
- How can parameters be estimated during normal operation, i.e. without taking the machine out of service?
- What are the effects of noise in the performance of the estimation procedure?
- Which of the parameters can be reliably estimated?

So the reader should aim to see the big picture of this work, some of the intermediary results achieved and what can be developed further if proper human and financial resources are applied. All applications mentioned here are steps necessary to enable a smarter power

grid, in which seamless integrated digital technology provides state estimation, fault detection and self-healing functionalities, with the ultimate goal of ensuring a reliable supply of electricity, and reducing vulnerability to natural disasters or attacks.

6.2.1 Condition Monitoring

Useful condition monitoring applications for salient-pole synchronous machine can be developed today, using only some of the parameters reliably estimated with saturation effects in this thesis, namely: $R_f, R_D, R_Q, \omega L_{aq}$. Some examples follow below:

- An indirect measurement of the air-gap and stator turns can be obtained from L_{aq}, since the magnetizing reactance is inversely proportional to the air-gap and squarely proportional to the number of stator turns (Mohan, 2014, sec 2-3-3).
- Turn-to-turn short circuits in the rotor winding can be detected by proper long-term analysis of R_f, as this type of defect would naturally reduce its value. Moreover, this monitoring can be further enhanced if a proper method to estimate l_f is implemented.
- Broken damper winding can be detected by proper long-term analysis of R_D, R_Q, as this type of defect would naturally increase their values.

If these methods are proven precise and accurate in practice, they can be used to equip virtually all salient-pole synchronous machine on a very low price tag, as no additional sensors in the machine are required and measurements of the input and output signals of the algorithm are already available in IEDs dedicated for protection.

6.2.2 On-line Assessment of the Power Grid

For on line assessment of the power grid, the *standard parameters* as defined in table 2.3 can be transferred in near-real time to control centers using existing Supervisory Control And Data Acquisition (SCADA) infrastructure. Control centers will then transfer these further to dispatch centers of the Transmission System Operator (TSO), who might use more precise and accurate values for load flow analysis, state estimation and stability assessment when necessary.

The advantage of this method is the computation effort can be distributed, i.e. the complex synchronous machine models are handled locally in each power plant, by the parameter estimator proposed in this thesis. Then dispatch centers could continue to use simplified models and bulk methods whenever necessary, such for fast decoupled load flow in their wide-area analysis. But they can also use more accurate and precise values for state estimation and stability assessment of critical corridors with near-real time information of each relevant machine in the grid.

All this can be done in the near future with minor intervention in existing platforms. In general, Information and Communication Technology (ICT) infrastructure between all actors is already in place today. So, the main effort would be interfacing this information with databases of dispatch centers.

For this to happen, the parameter estimator must handle properly saturation effects and estimate reliably values for $L_d, L_{ad}, L_f, L_D, L_Q$.

6.2.3 Adaptive Control

For adaptive control, the *standard parameters* as defined in table 2.3 can be transferred in near-real time to control and protection equipment using existing or future ICT infrastructure, such as IEC 61850 protocols (International Electrotechnical Commission et al., 2011). Alternatively, they can also be embedded in these equipment.

With this information available in near real-time, control and protection equipment such as AVRs and protection IEDs can implement adaptive control techniques such as self-tuning, gain scheduling and model predictive control.

For this to happen, the parameter estimator must handle properly saturation effects and estimate reliably values for $L_d, L_{ad}, L_f, L_D, L_Q$. On top of that, stability and robustness of the parameter estimation must be deeply investigated to avoid problems such as lack of persistent excitation and bursting phenomena. These investigations are not in the scope of this thesis, however the interested reader can refer to Moore (1983); Anderson (1985, 2005); Marafioti et al. (2014) and included references in these articles.

6.3 Recommendations for Further Work

As one should have noticed by now, this thesis only scratches the surface of main applications envisioned for reliable parameter identification for salient pole synchronous machines. And it also left a couple of open points that must be solved before any application can be put into practice. Many of these challenges were already mentioned through out the text and are summarized below.

6.3.1 Modeling of saturation

As shown in section 5.1, the machine model without saturation effects is not good enough. Therefore, the next natural step is incorporating the saturation factor presented in section 5.2 in the KF. This will make the system non linear, so the optimal observer must be updated to an Extended or Unscented KF.

Alternatively, a more advanced non linear model of the machine including saturation in its derivation can be used. Examples of such a model in state-space form are given by Levi (1998); Rehaoulia et al. (2007).

A comparison between results of these two approaches using both Extended or Unscented KF will be a valuable contribution to the state-of-art.

6.3.2 Eliminate i_D, i_Q from State Space

As shown in sections 3.5 and 5.1, the ODW performance is greatly affected by noise and saturation, which directly reflects in the KF performance. Therefore it can be an advantage to substitute i_D, i_Q by other variables in the state-space, such as fluxes. Alternative representations of the synchronous machine without i_D, i_Q are explored by Levi (1998); Rehaoulia et al. (2007).

A comparison between results of this approach with the one given in this thesis will be a valuable contribution to the state-of-art, and can be combined with investigations for section 6.3.1.

6.3.3 Estimate Values of $L_0 + 3L_N, L_f, L_D, L_Q$

After proper handling saturation effects, the next natural step is estimating values of $L_0 + 3L_N, L_f, L_D, L_Q$. As mentioned earlier, this can be implemented with an Extended or Unscented KF by assuming these parameters as states with derivatives equal to zero. This approach was briefly investigated by this author estimating only the value of L_f with an EKF. Results were satisfactory without saturation, but errors of up to 15% were produced with the latter enabled. Therefore, this must be combined with investigations for section 6.3.1.

A different approach is revising the RLS algorithm to consider eq. (2.38) without simplifications, i.e. $\frac{d}{dt}\mathbf{i_{dq0fDQ}} \neq \mathbf{0}$. This would require an algorithm to calculate derivatives of the state values, which is the same approach used by Kyriakides et al. (2005).

Another option using this same approach is getting the derivative of the states from the Extended or Unscented KF algorithm, considering these blocks already calculate these values in each iteration step. However, this requires blocks from Control System Toolbox to be adapted, as they do not output the derivative of the states.

6.3.4 Validate Algorithm in a Real Power Plant

After solving the issues above, it is a good time to test the algorithm in a real power plant. The easiest way to perform that is merely recording several samples sets of required measurement $i_a, i_b, i_c, i_f, v_a, v_b, v_c, v_f$ with proper time stamping and sampling frequency ($f_s \geq$ 400Hz).

Later, these can be imported in Matlab, and the algorithm executed and fine-tuned. It would be a huge advantage to execute this procedure for a machine in which traditional methods from (IEEE, 2010; IEC, 2008) were recently applied for sake of comparison.

A more sophisticated approach is programming the algorithm using Matlab/Simulink Coder in an edge device, such as Raspberry Pi, and receiving measurements directly from equipment in a power plant, either by analog inputs or bus communication with time stamping such as OPC-UA or IEC 61850. This approach would allow the algorithm to run continuously and investigate issues of stability and robustness.

Acronyms

AVR Automatic Voltage Regulator 4, 32, 33, 42, 62

EKF Extended Kalman Filter 36, 60, 63

FEM Finite Element Method 2

ICT Information and Communication Technology 3, 62

IED Intelligent Electronic Device 36, 61, 62

KF Kalman Filter 27, 28, 31, 33, 34, 39, 41, 48, 49, 59, 60, 62, 63

NMSE Normalized Mean Square Error 34, 48, 59

ODW Observer for Damper Windings 31, 33, 34, 48, 60, 63

pu per-unit 12, 18, 20–22, 56–58

RLS Recursive Least Squares i, iv, 36, 37, 39–43, 46–48, 53, 54, 59, 63, 78–82, 92–96

RMS Root Mean Square 19, 32

SCADA Supervisory Control And Data Acquisition 61

SI International System of Units 32

SNR Signal-to-Noise Ratio 34, 59

SPS Simscape Power Systems 4, 26, 31, 33, 34, 43, 48, 59, 60, 69–76, 84–91

TSO Transmission System Operator 2, 61

Appendix A

Matlab Simulink model

This section presents an interactive report of the Matlab Simulink model developed for this thesis. It contains a detailed description of the model components and its parameters.

Instructions:

1. Unzip the file appendix-a.zip;
2. Open the folder sm_model_simplified;
3. Open the file webview.html with your preferred web browser;
4. Navigate the model and click over a element to see its properties on the right side.

Appendix B

Figures of the Model Validation

This section presents the figures generated for the validation described in section 3.5.

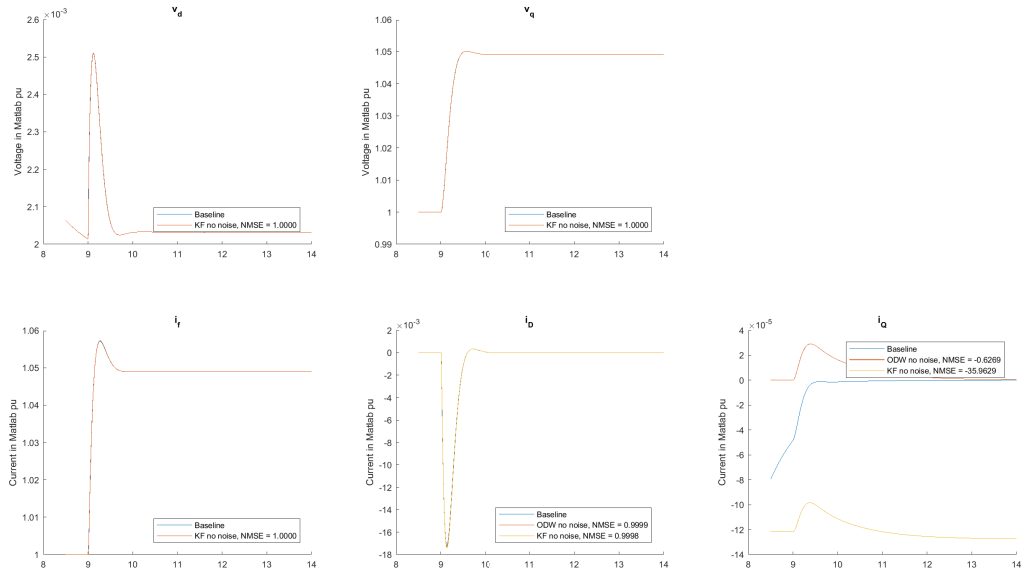

Figure B.1: Comparison of the Kalman filter versus SPS - Case 1, no noise

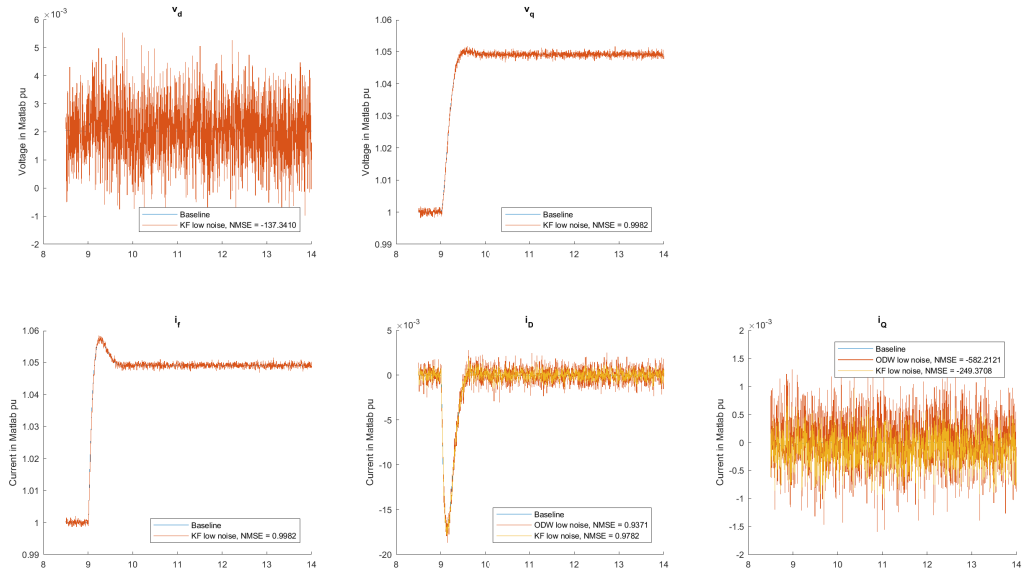

Figure B.2: Comparison of the Kalman filter versus SPS - Case 1, standard noise

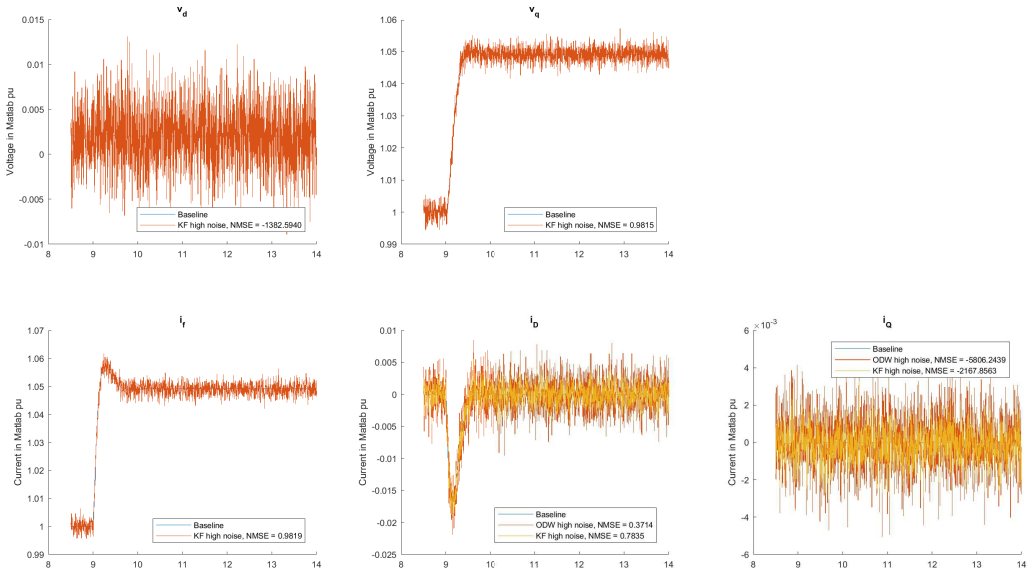

Figure B.3: Comparison of the Kalman filter versus SPS - Case 1, high noise

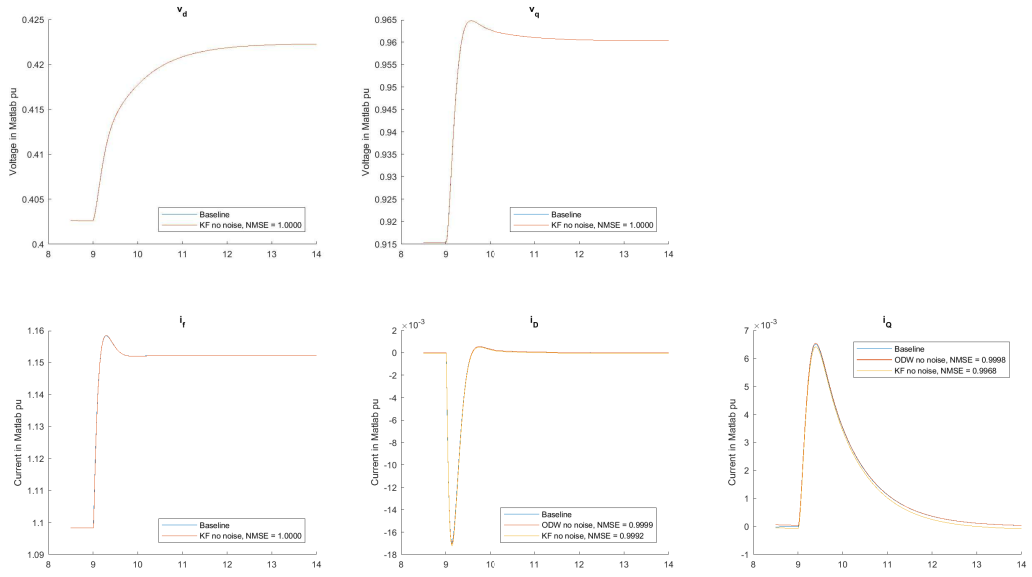

Figure B.4: Comparison of the Kalman filter versus SPS - Case 2, no noise

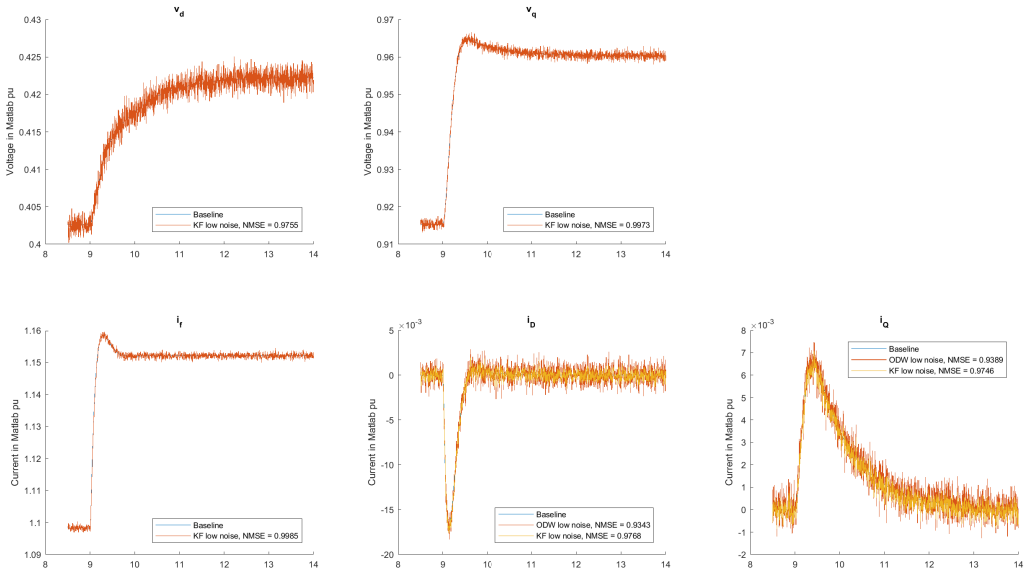

Figure B.5: Comparison of the Kalman filter versus SPS - Case 2, standard noise

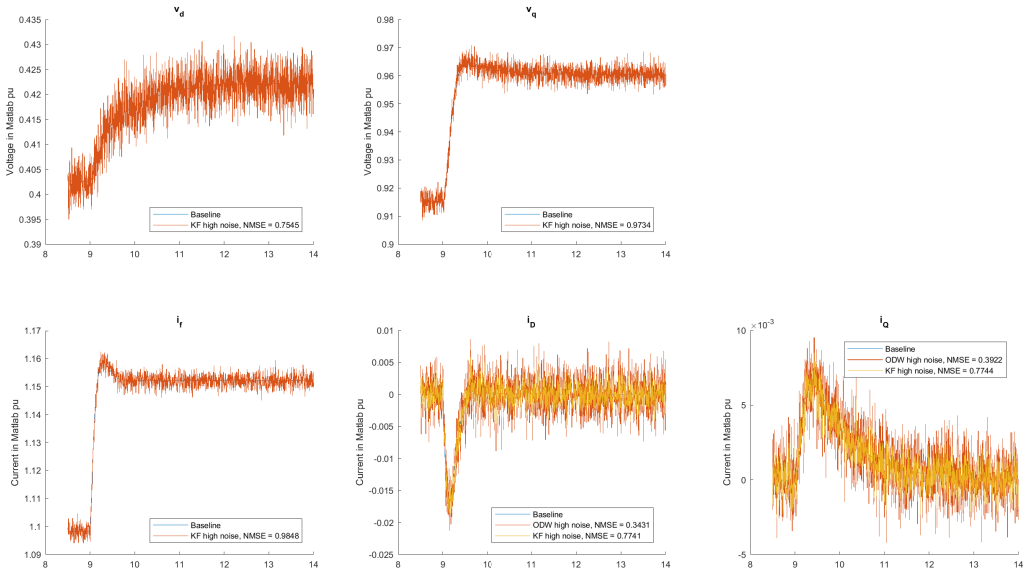

Figure B.6: Comparison of the Kalman filter versus SPS - Case 2, high noise

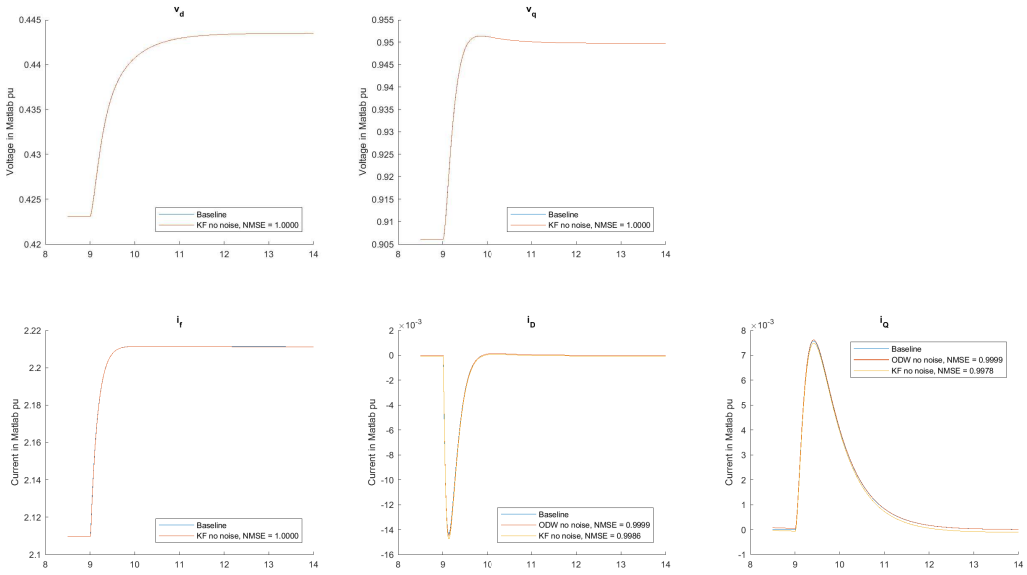

Figure B.7: Comparison of the Kalman filter versus SPS - Case 3, no noise

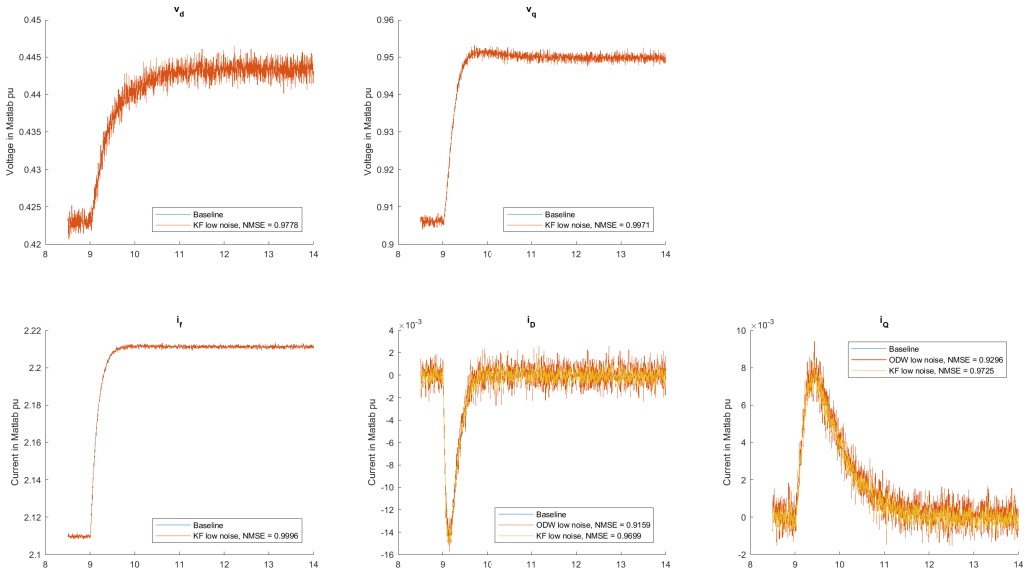

Figure B.8: Comparison of the Kalman filter versus SPS - Case 3, standard noise

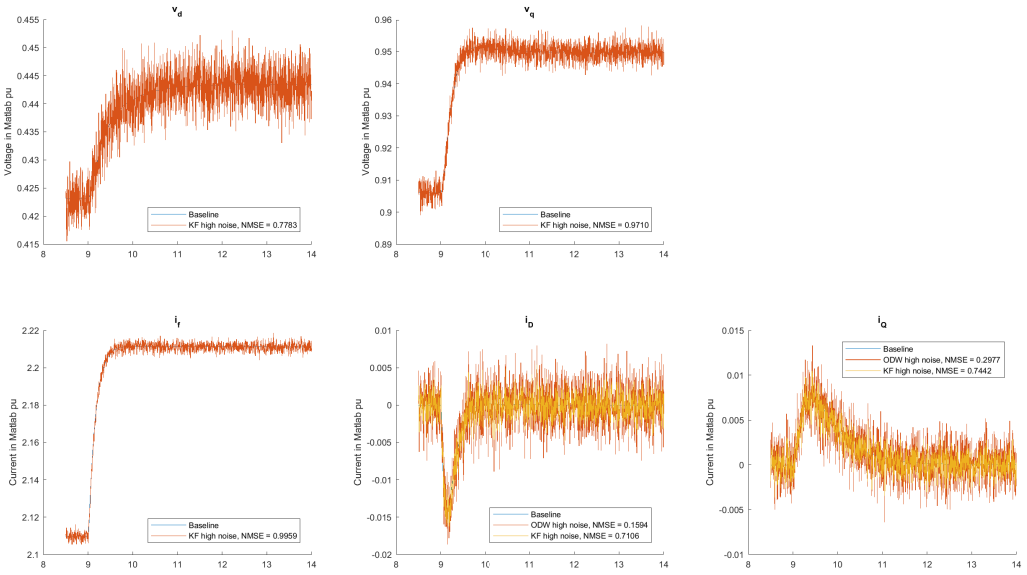

Figure B.9: Comparison of the Kalman filter versus SPS - Case 3, high noise

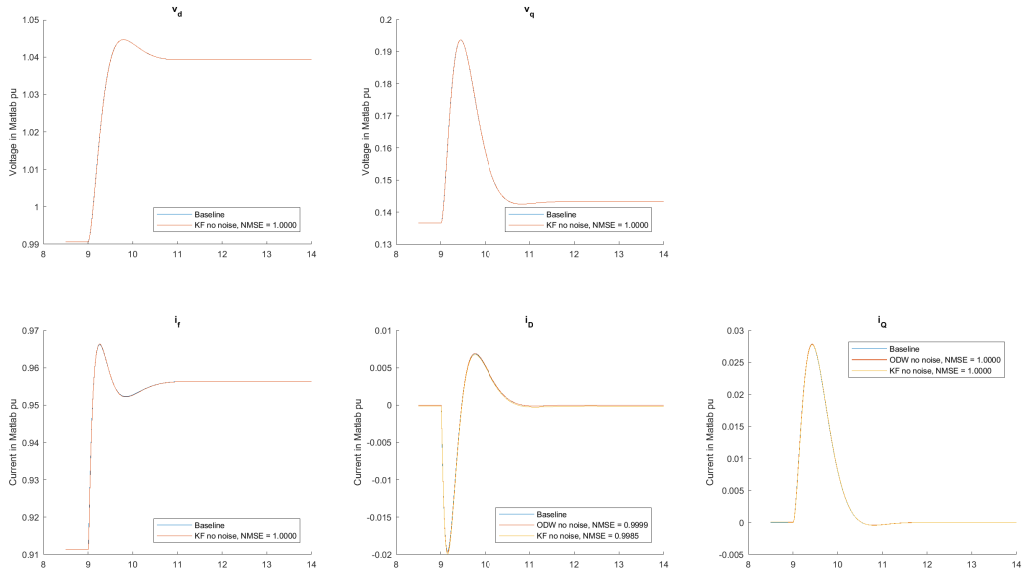

Figure B.10: Comparison of the Kalman filter versus SPS - Case 4, no noise

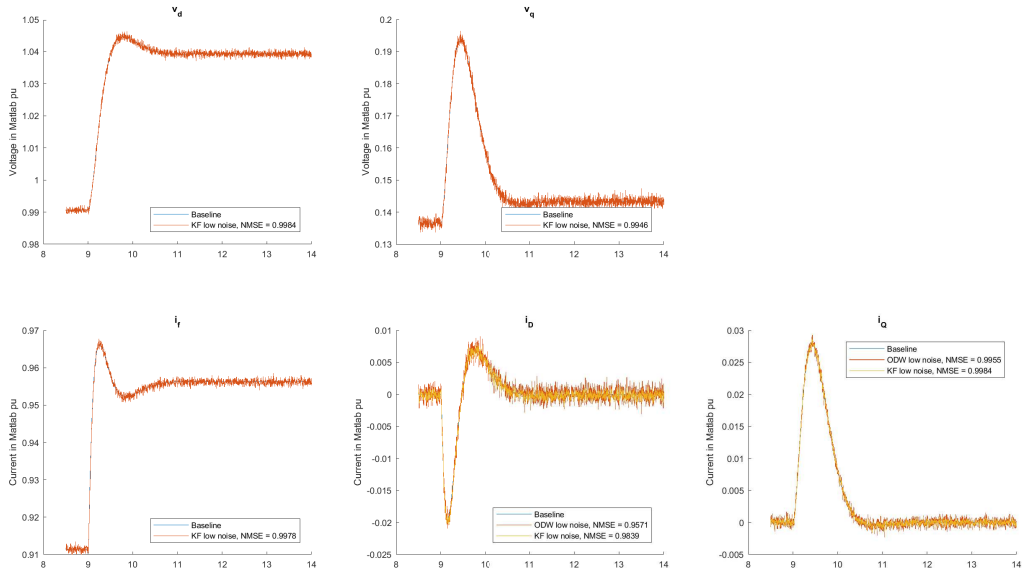

Figure B.11: Comparison of the Kalman filter versus SPS - Case 4, standard noise

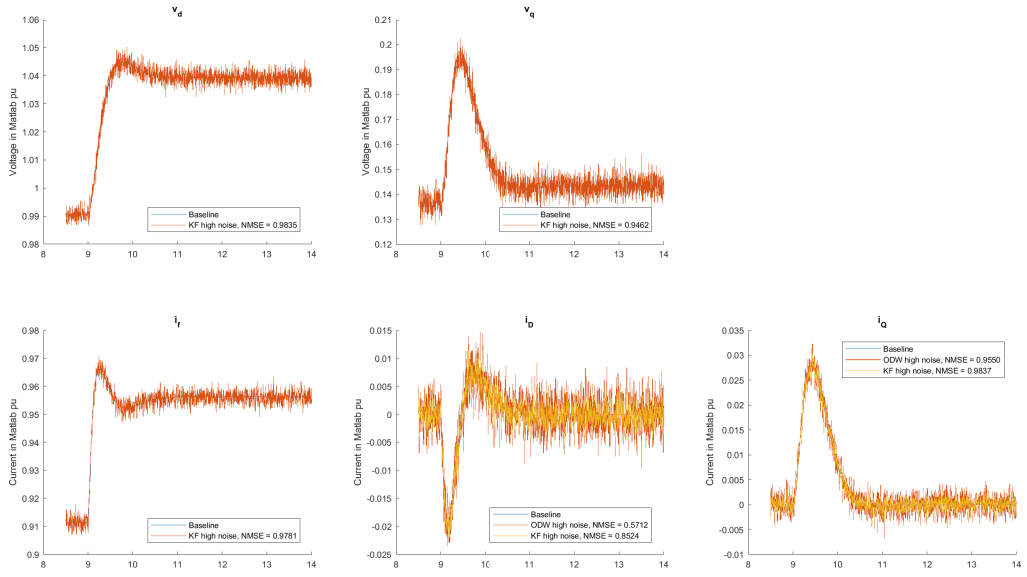

Figure B.12: Comparison of the Kalman filter versus SPS - Case 4, high noise

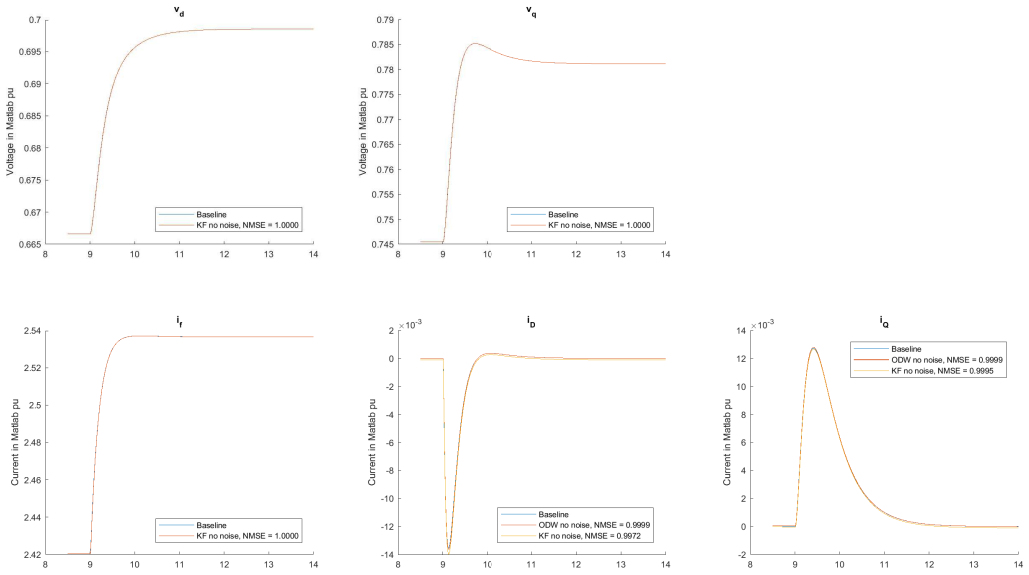

Figure B.13: Comparison of the Kalman filter versus SPS - Case 5, no noise

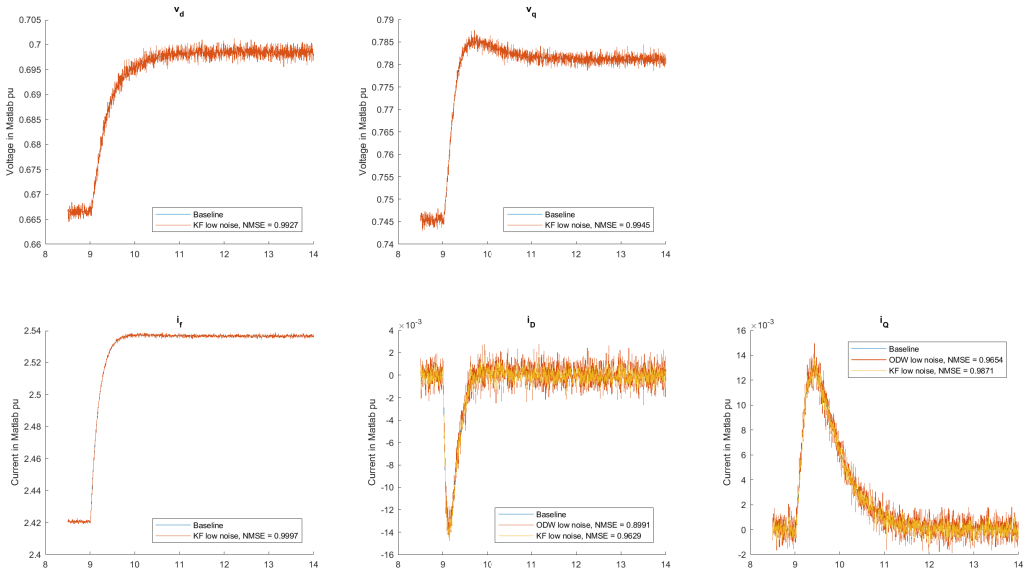

Figure B.14: Comparison of the Kalman filter versus SPS - Case 5, standard noise

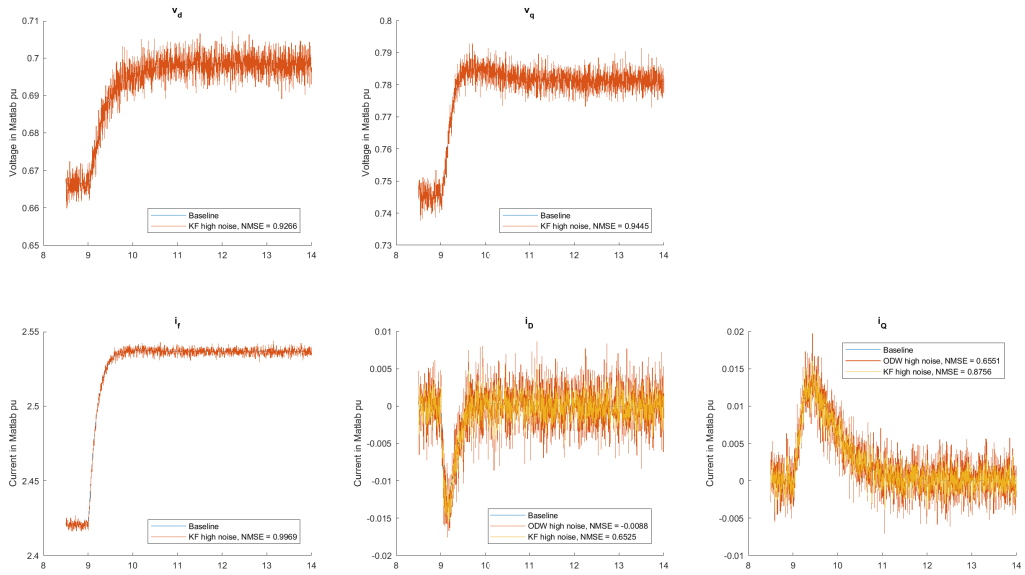

Figure B.15: Comparison of the Kalman filter versus SPS - Case 5, high noise

Appendix C

Figures of the Parameter Estimator Validation

This section presents the figures generated for the validation described in section 4.4.

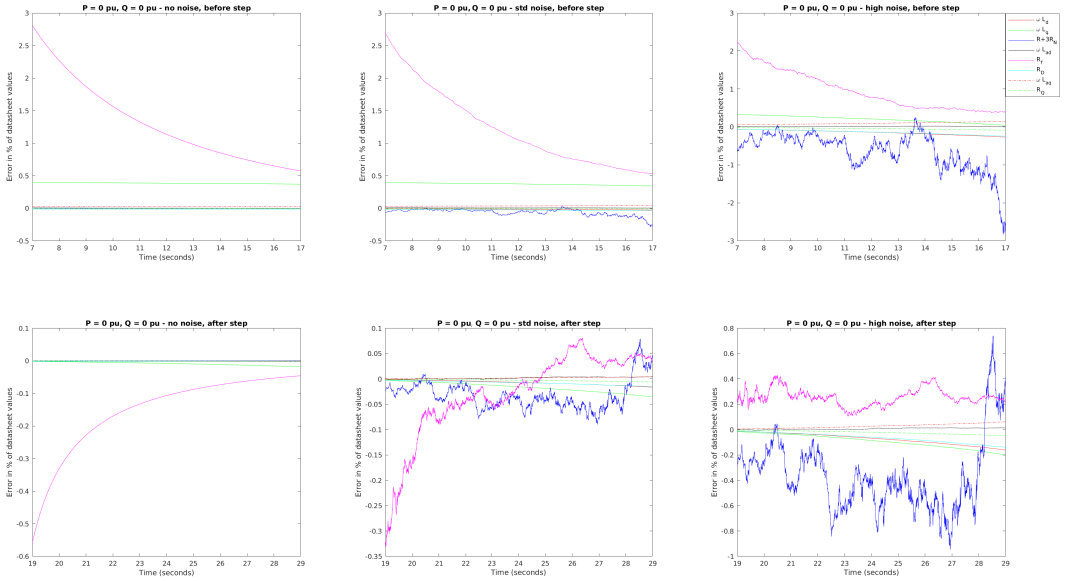

Figure C.1: Parameter estimation - Case 1

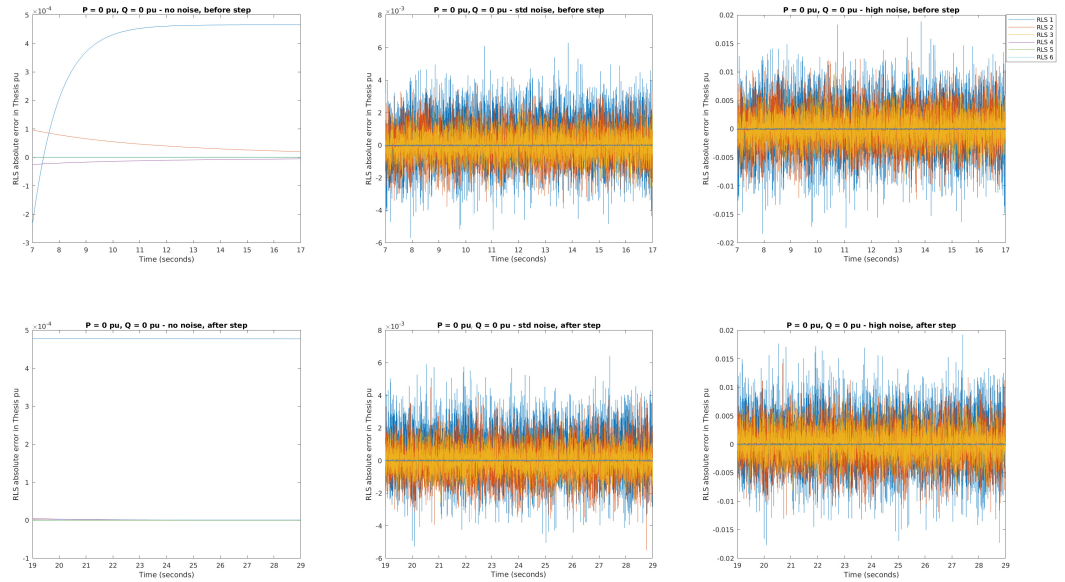

Figure C.2: RLS approximation error - Case 1

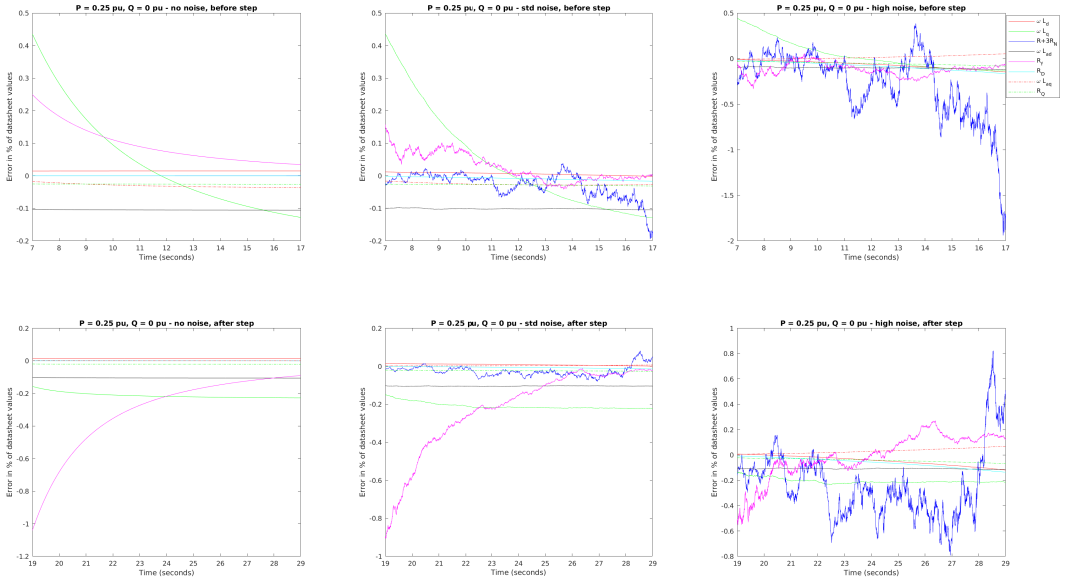

Figure C.3: Parameter estimation - Case 2

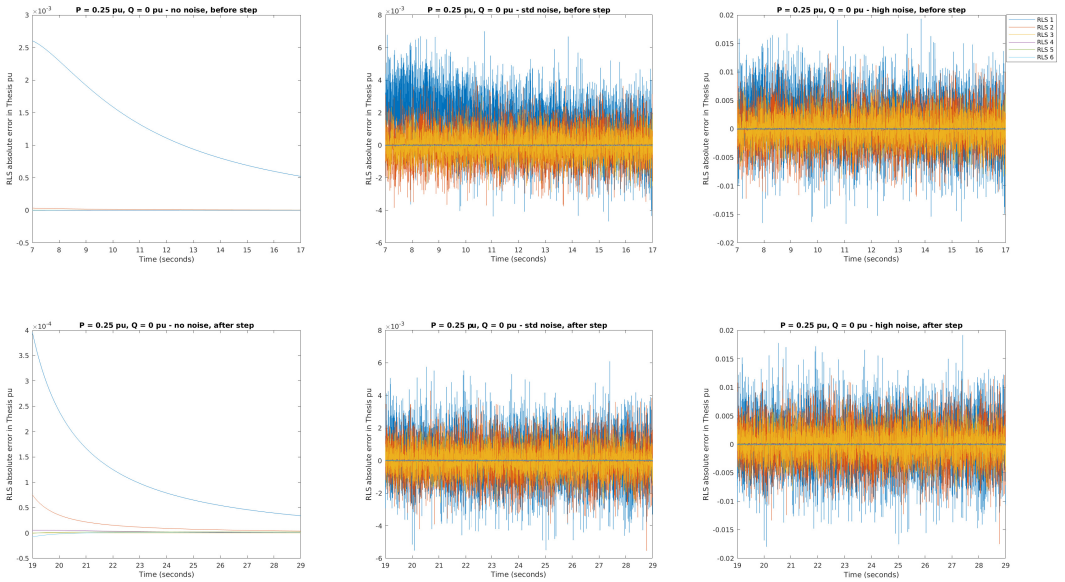

Figure C.4: RLS approximation error - Case 2

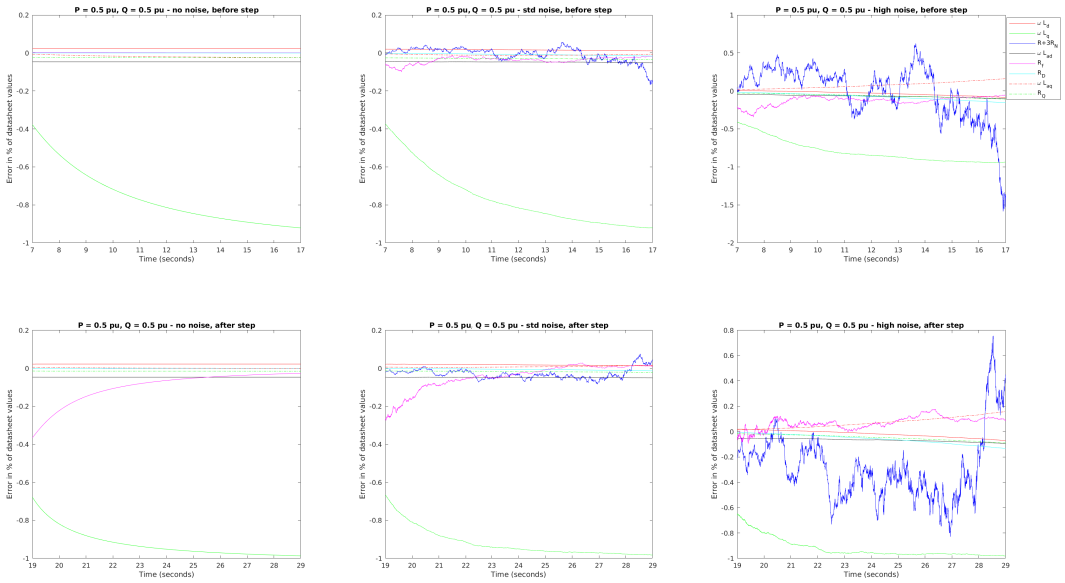

Figure C.5: Parameter estimation - Case 3

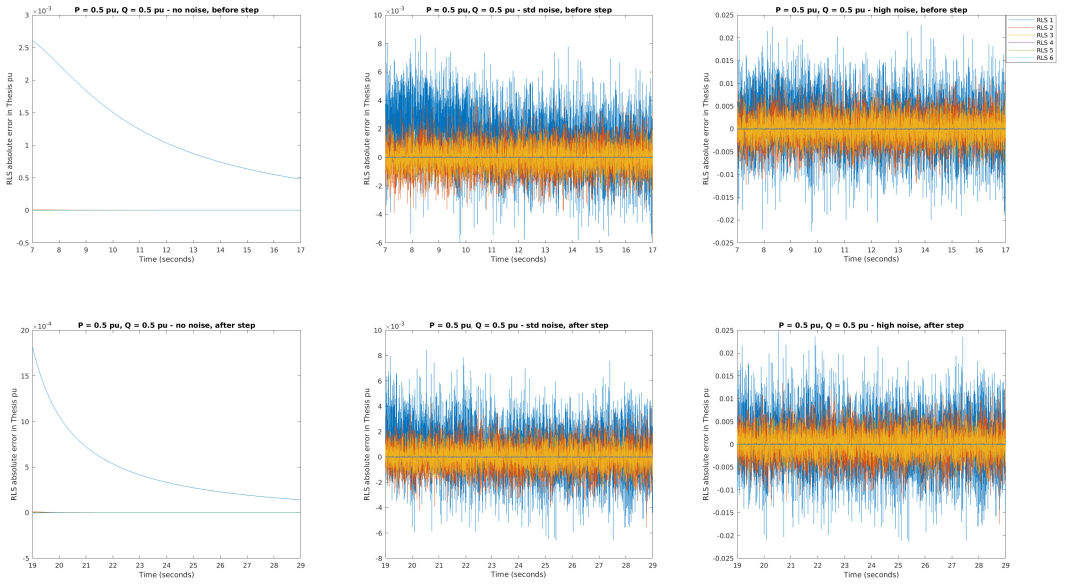

Figure C.6: RLS approximation error - Case 3

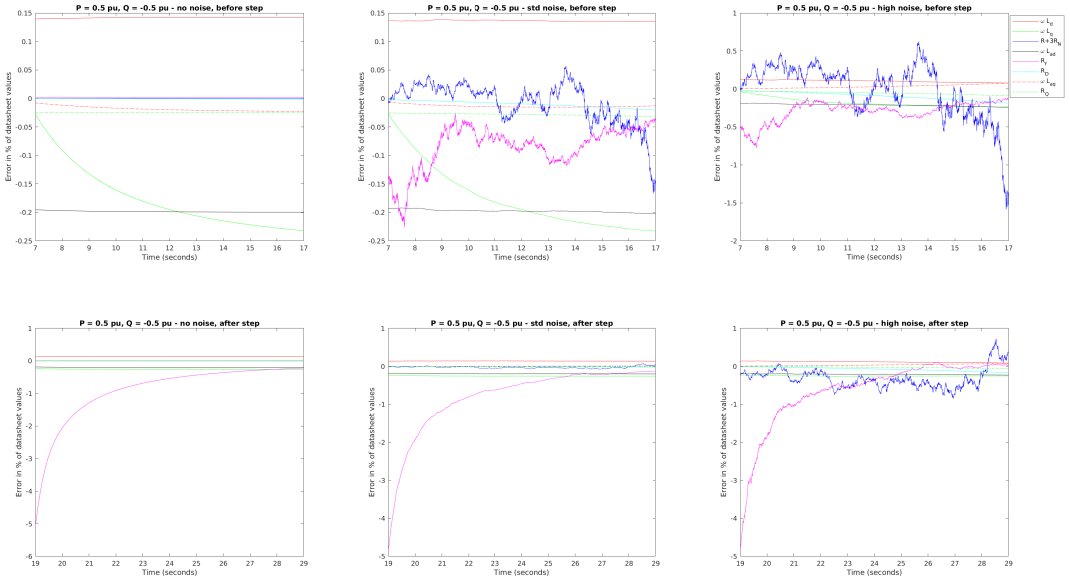

Figure C.7: Parameter estimation - Case 4

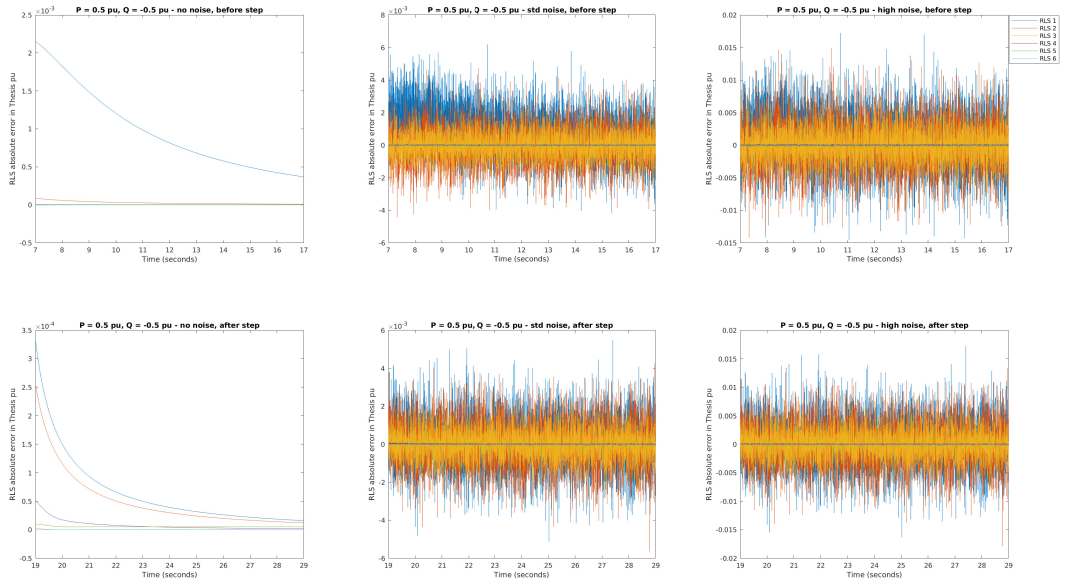

Figure C.8: RLS approximation error - Case 4

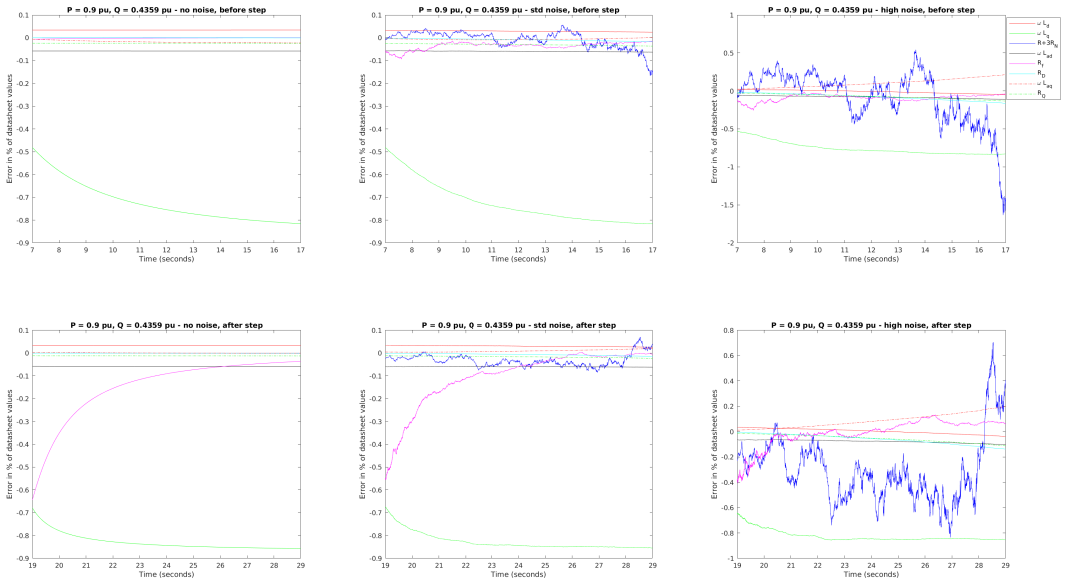

Figure C.9: Parameter estimation - Case 5

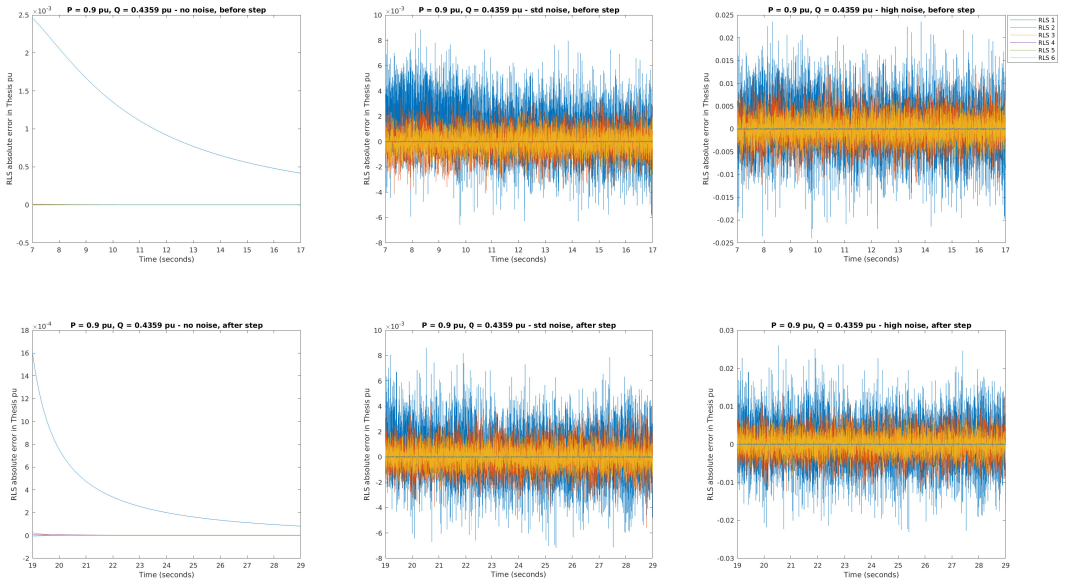

Figure C.10: RLS approximation error - Case 5

Appendix D

Figures of the Complete Validation with Saturation

This section presents the figures generated for the validation described in section 5.1.

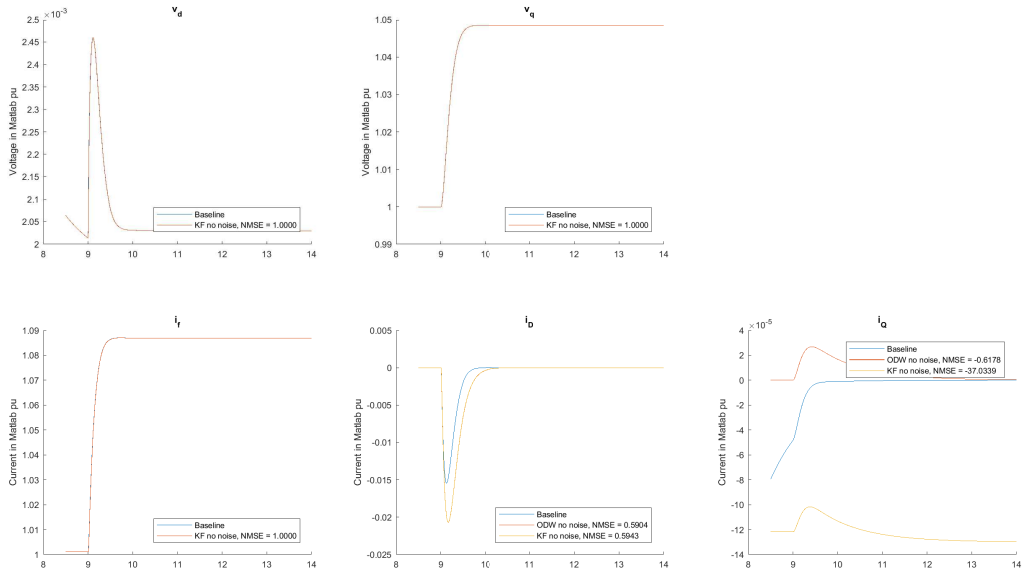

Figure D.1: Comparison of the Kalman filter versus SPS - Case 1, no noise

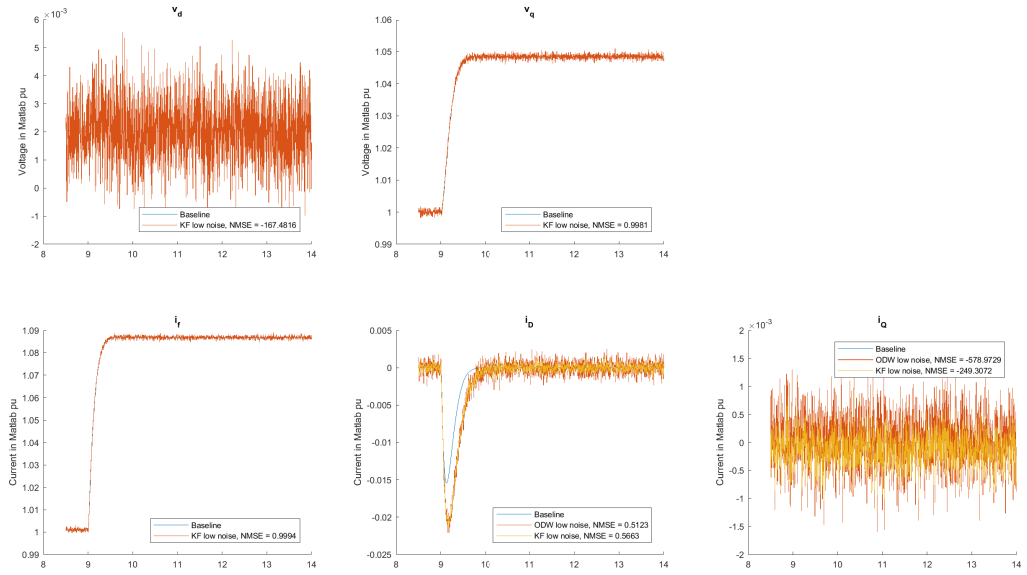

Figure D.2: Comparison of the Kalman filter versus SPS - Case 1, standard noise

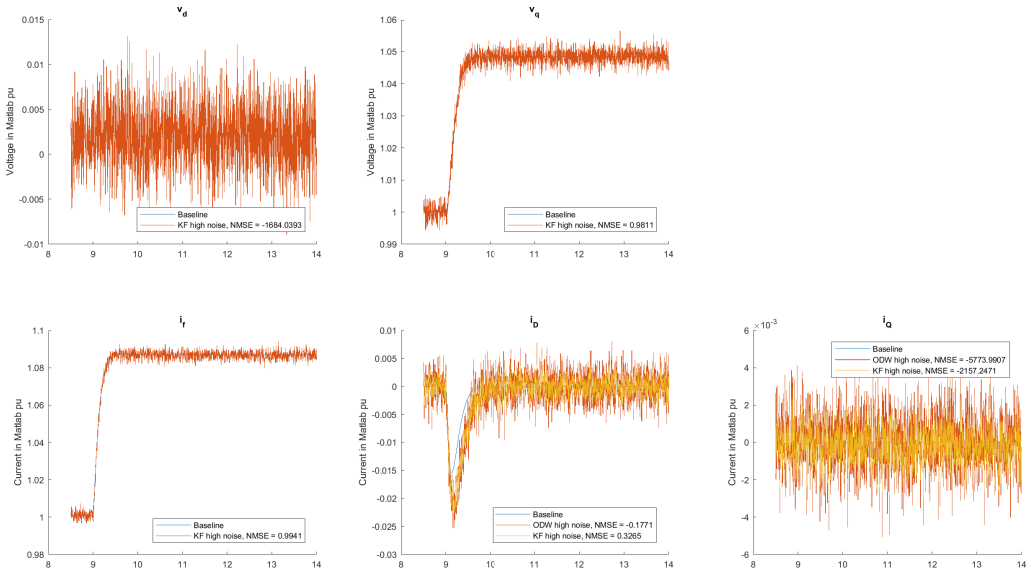

Figure D.3: Comparison of the Kalman filter versus SPS - Case 1, high noise

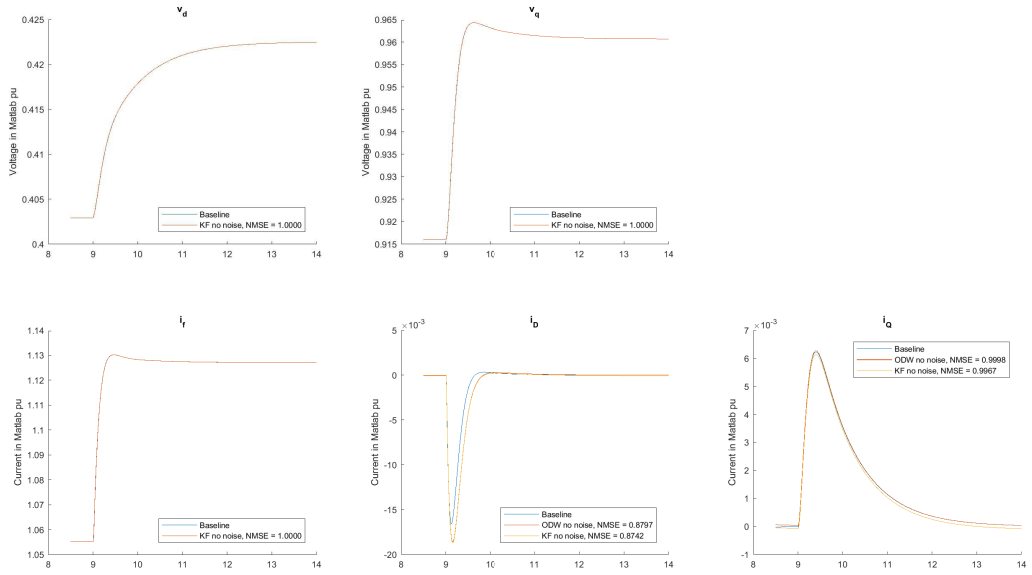

Figure D.4: Comparison of the Kalman filter versus SPS - Case 2, no noise

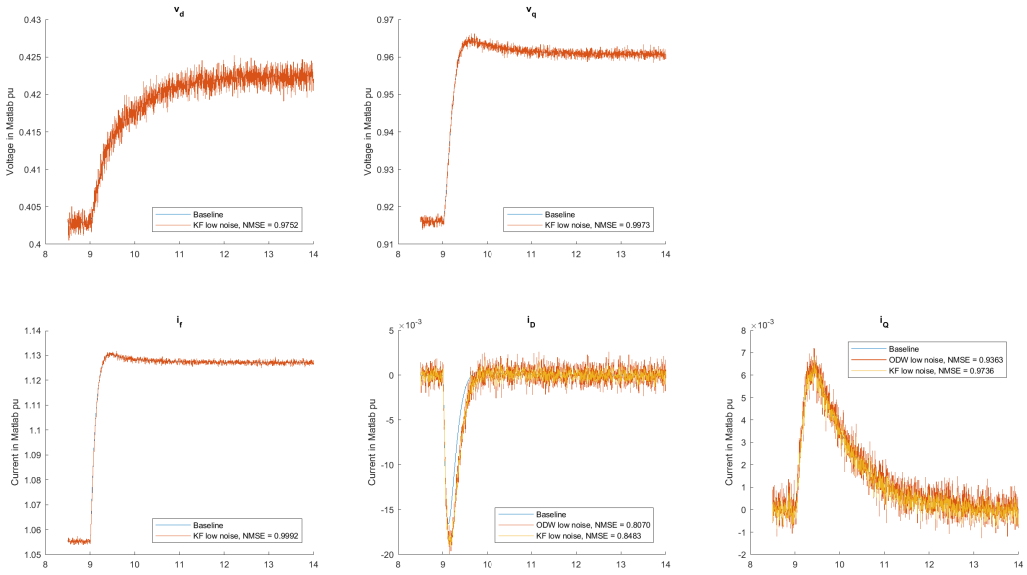

Figure D.5: Comparison of the Kalman filter versus SPS - Case 2, standard noise

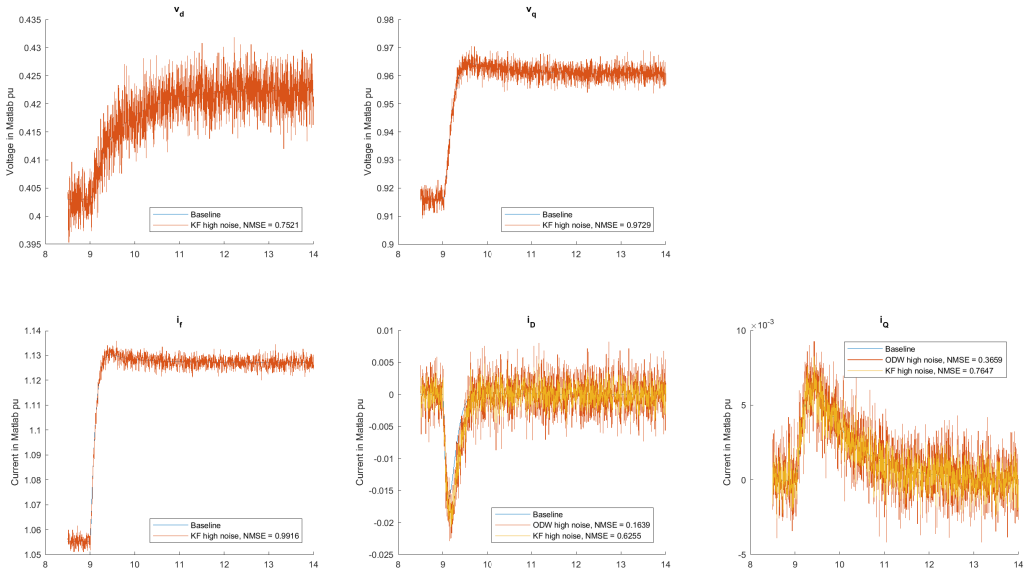

Figure D.6: Comparison of the Kalman filter versus SPS - Case 2, high noise

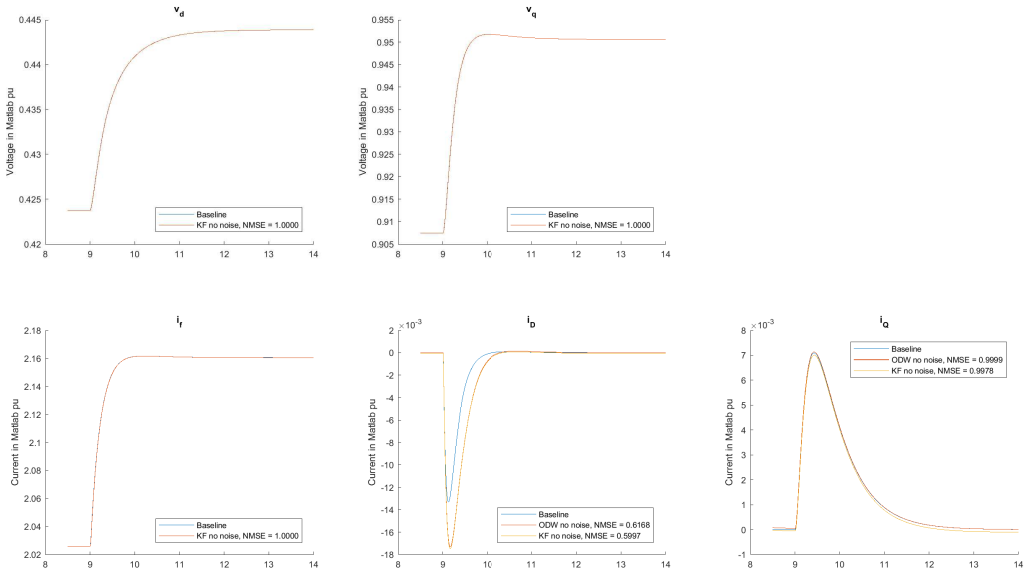

Figure D.7: Comparison of the Kalman filter versus SPS - Case 3, no noise

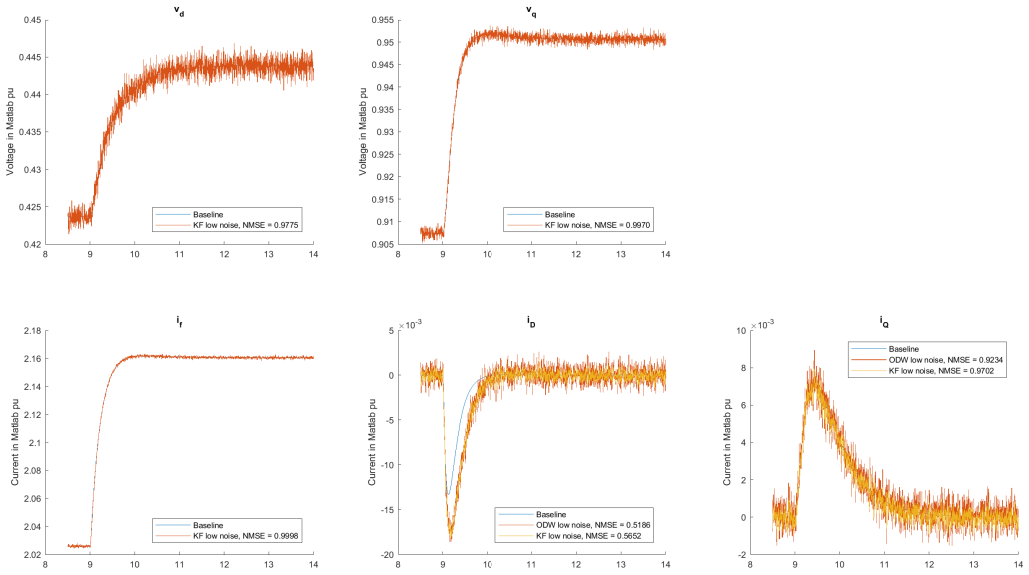

Figure D.8: Comparison of the Kalman filter versus SPS - Case 3, standard noise

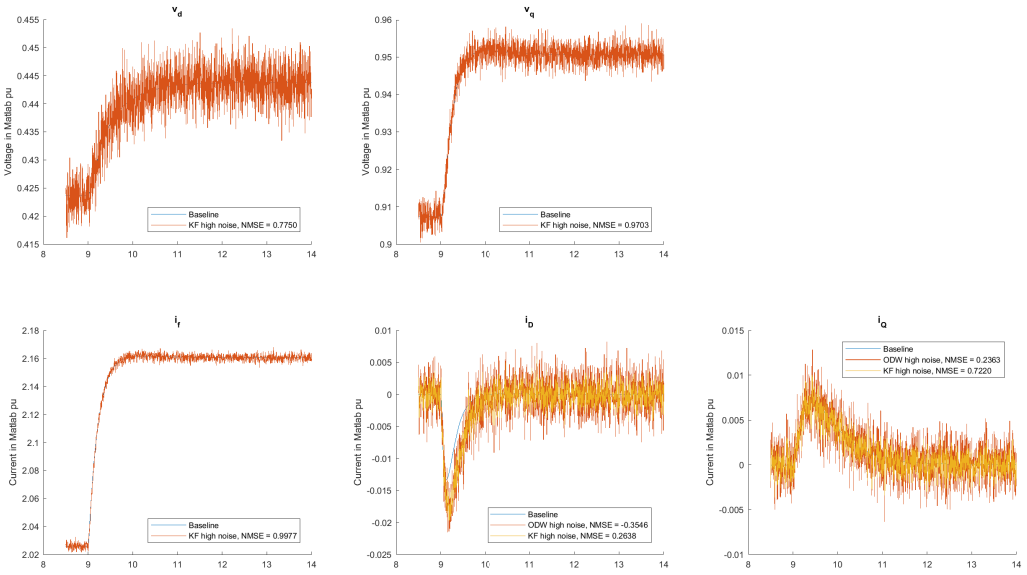

Figure D.9: Comparison of the Kalman filter versus SPS - Case 3, high noise

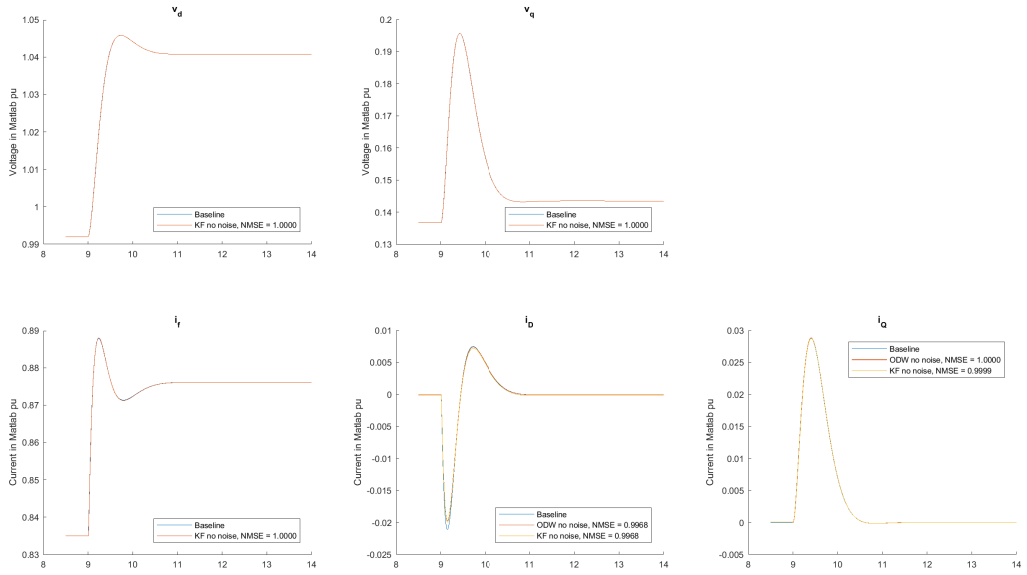

Figure D.10: Comparison of the Kalman filter versus SPS - Case 4, no noise

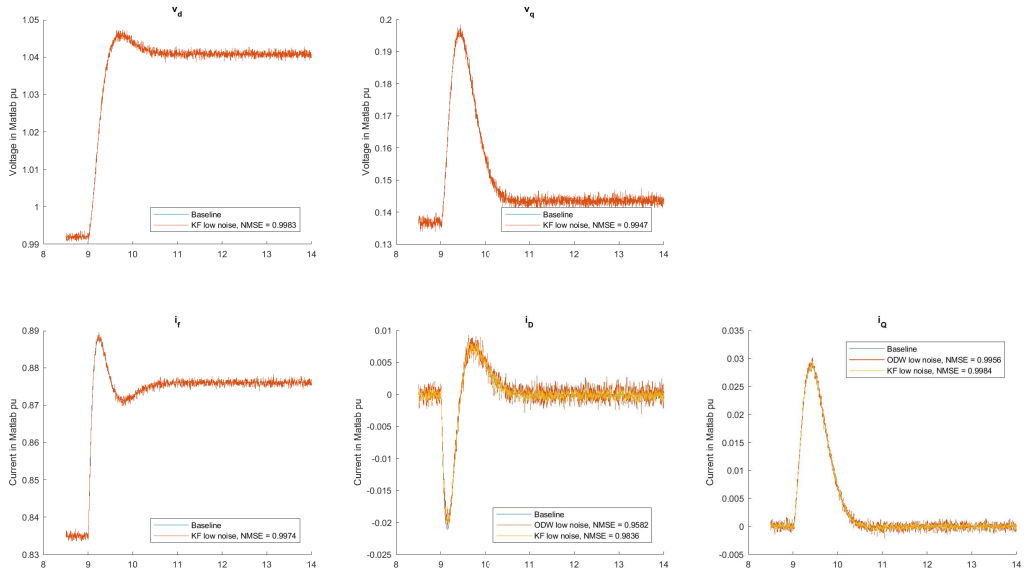

Figure D.11: Comparison of the Kalman filter versus SPS - Case 4, standard noise

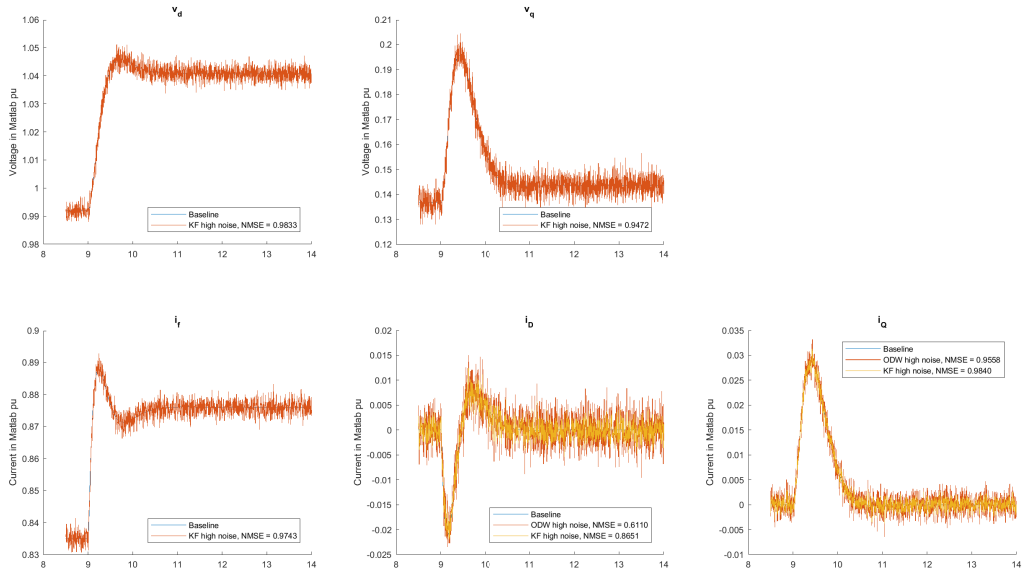

Figure D.12: Comparison of the Kalman filter versus SPS - Case 4, high noise

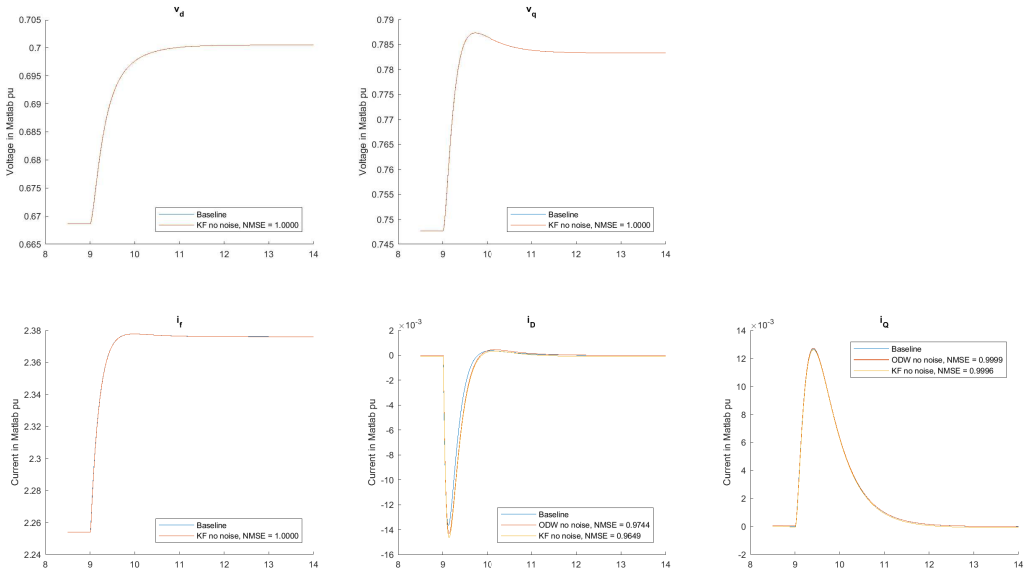

Figure D.13: Comparison of the Kalman filter versus SPS - Case 5, no noise

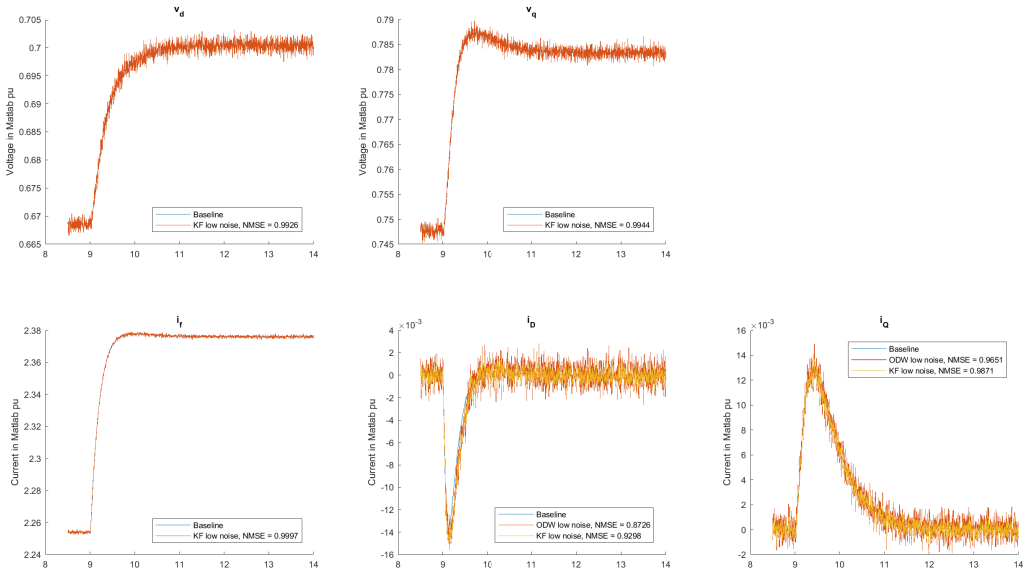

Figure D.14: Comparison of the Kalman filter versus SPS - Case 5, standard noise

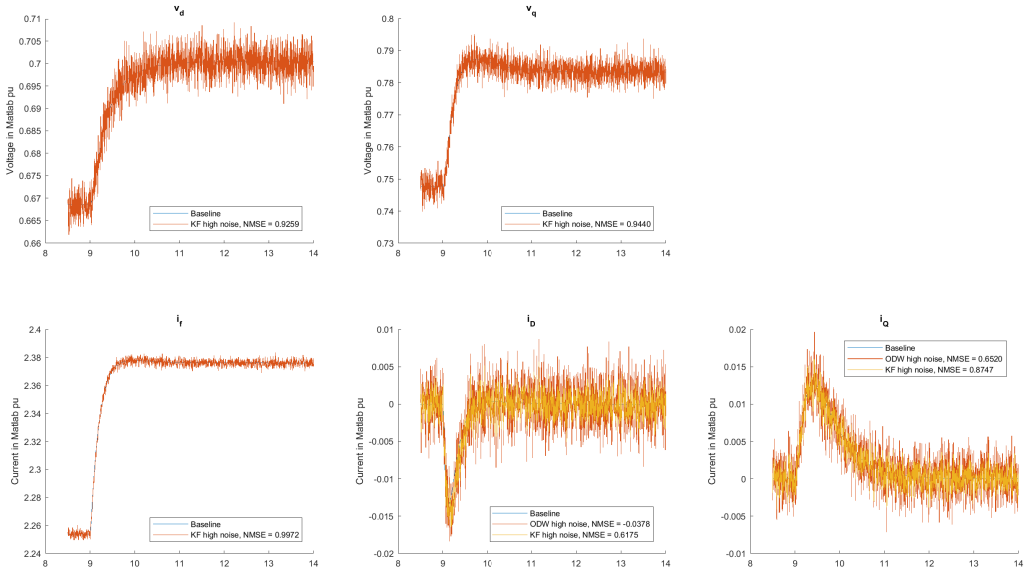

Figure D.15: Comparison of the Kalman filter versus SPS - Case 5, high noise

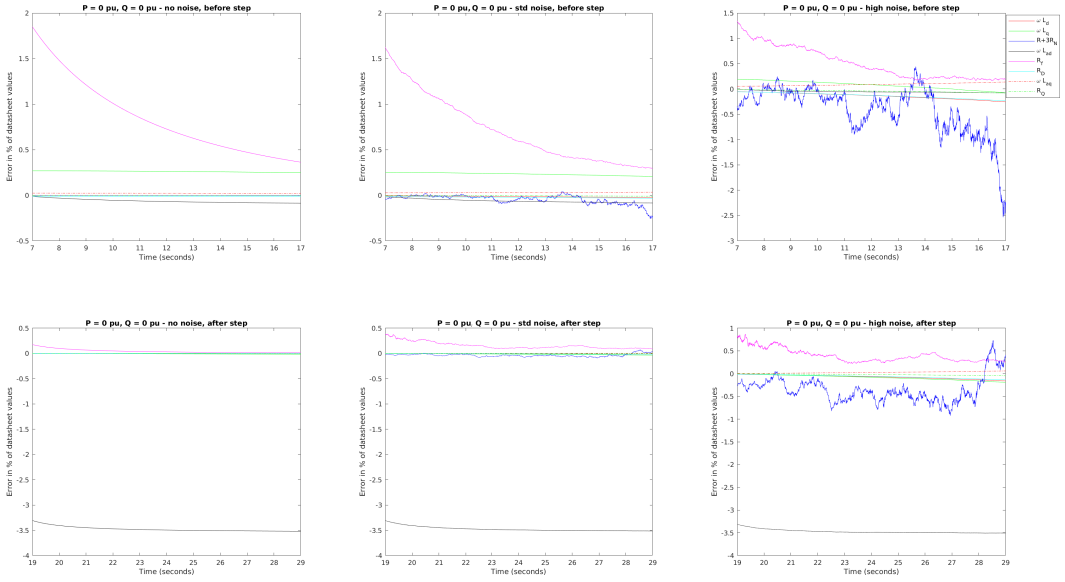

Figure D.16: Parameter estimation with saturation - Case 1

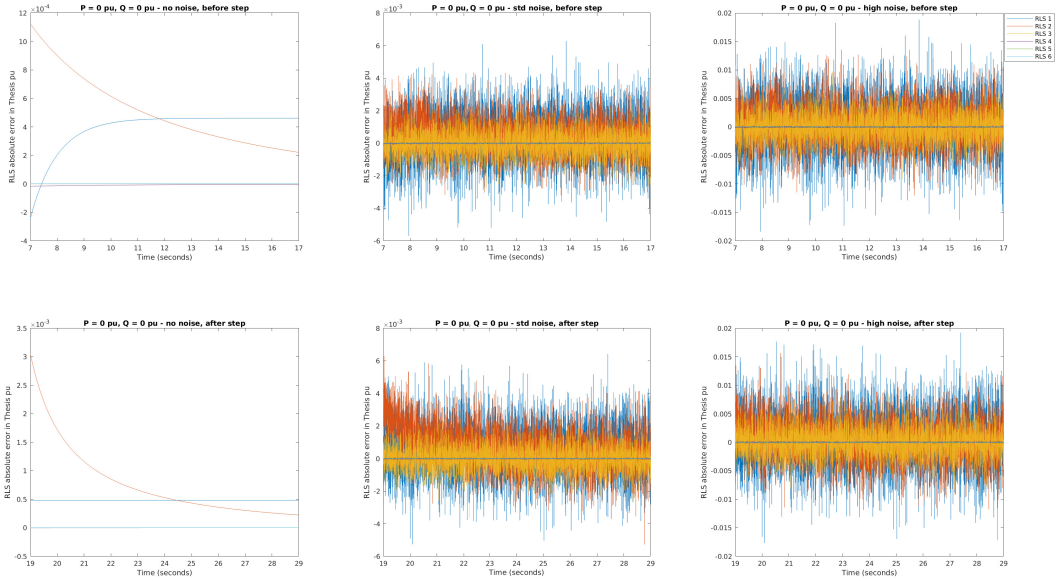

Figure D.17: RLS approximation error with saturation - Case 1

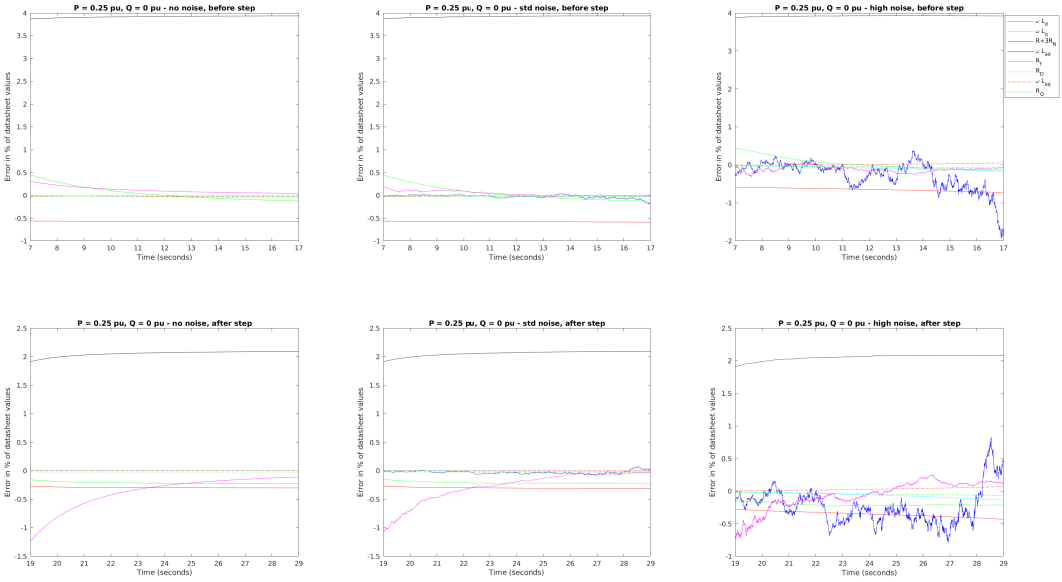

Figure D.18: Parameter estimation with saturation - Case 2

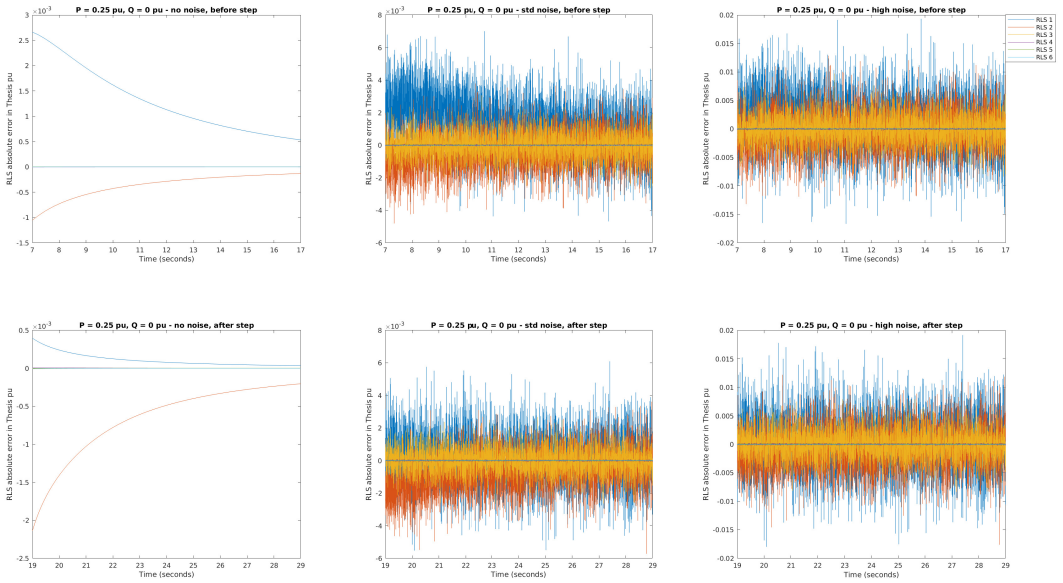

Figure D.19: RLS approximation error with saturation - Case 2

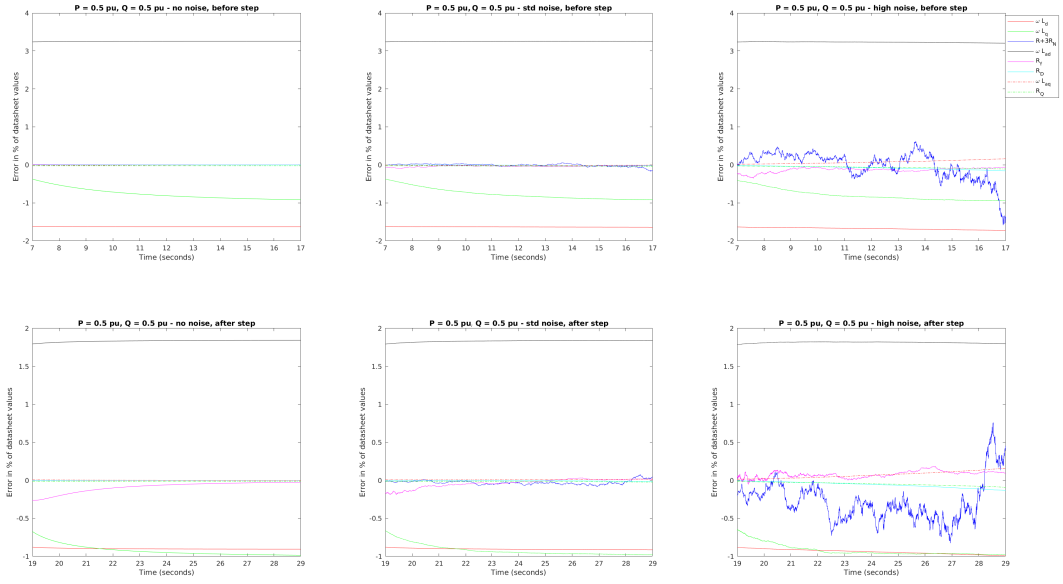

Figure D.20: Parameter estimation with saturation - Case 3

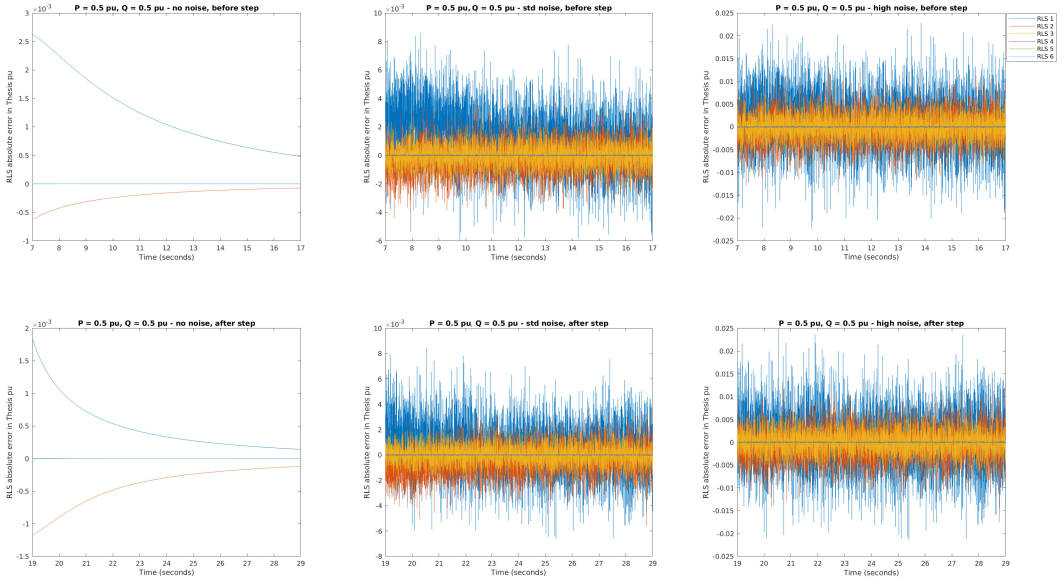

Figure D.21: RLS approximation error with saturation - Case 3

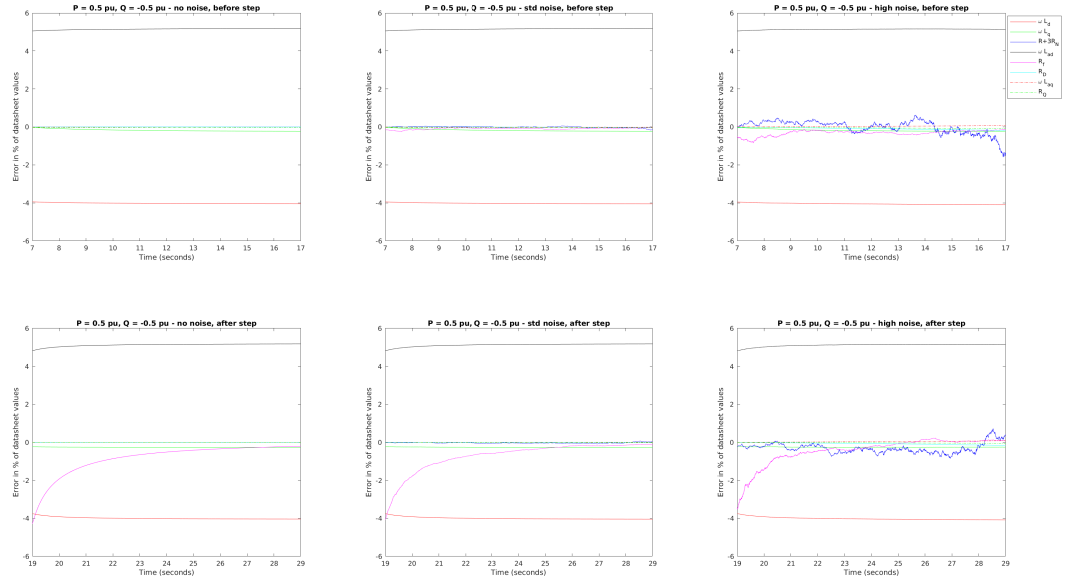

Figure D.22: Parameter estimation with saturation - Case 4

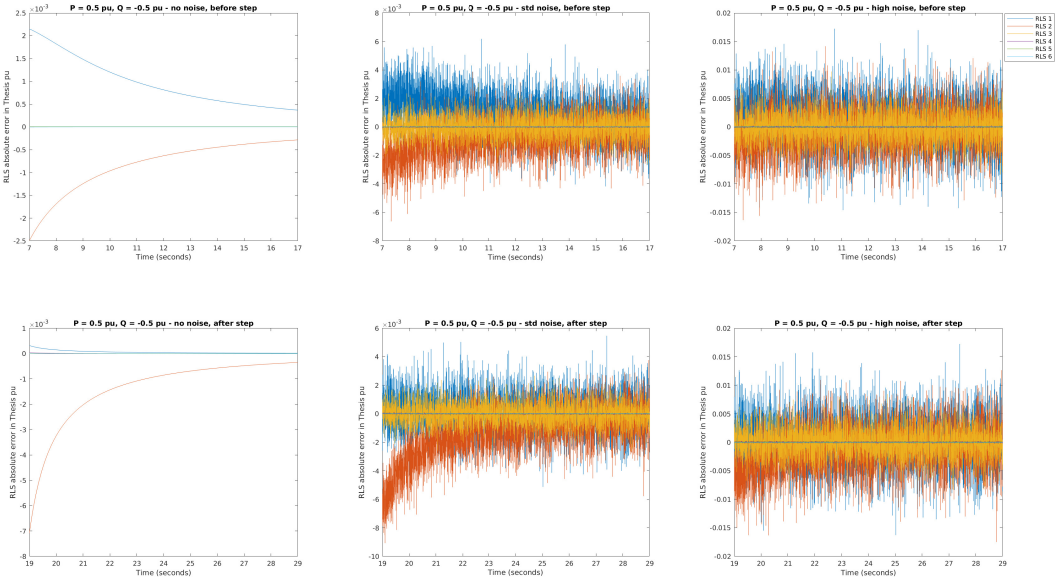

Figure D.23: RLS approximation error with saturation - Case 4

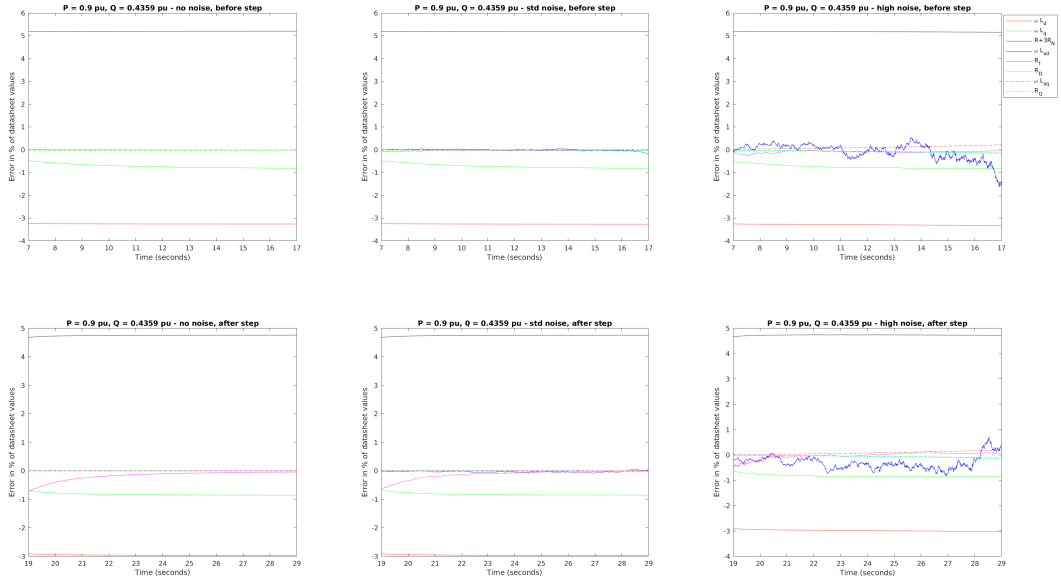

Figure D.24: Parameter estimation with saturation - Case 5

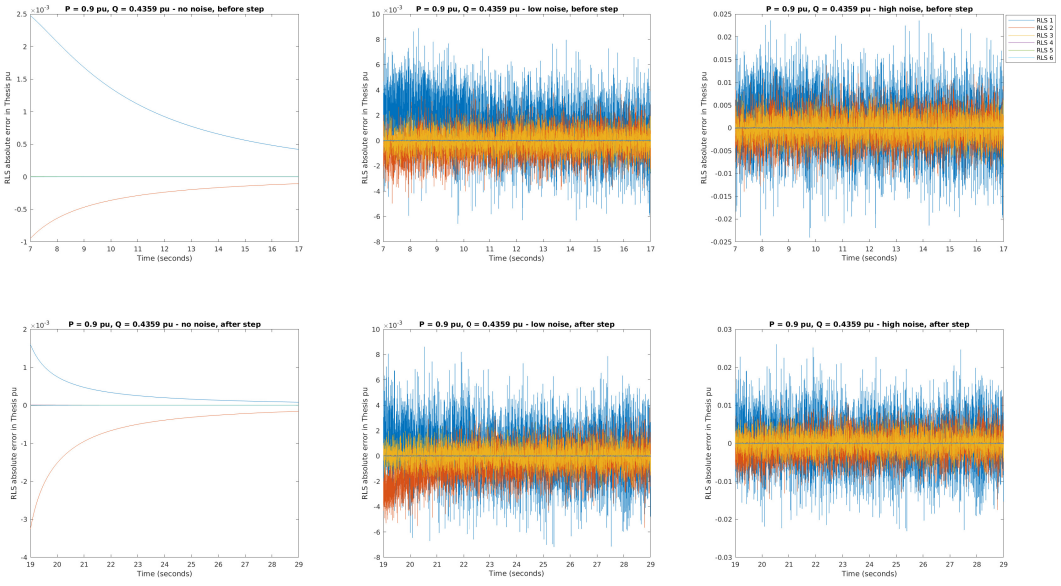

Figure D.25: RLS approximation error with saturation - Case 5

Bibliography

Adkins, B. and Harley, R. G. (1975). *The General Theory of Alternating Current Machines*. Springer US, Boston, MA.

Anderson, B. D. (1985). Adaptive systems, lack of persistency of excitation and bursting phenomena. *Automatica*, 21(3):247–258.

Anderson, B. D. (2005). Failures of Adaptive Control Theory and their Resolution. *Commun. Inf. Syst.*, 05(1):1–20.

Anderson, P. M. and Fouad, A. A. (2003). *Power System Control and Stability*. IEEE Press power engineering series. IEEE Press ; Wiley-Interscience, Piscataway, N.J, 2nd ed edition.

Barakat, A., Tnani, S., Champenois, G., and Mouni, E. (2010). Analysis of synchronous machine modeling for simulation and industrial applications. *Simulation Modelling Practice and Theory*, 18(9):1382–1396.

Bianchi, N. (2005). *Electrical Machine Analysis Using Finite Elements*. Power electronics and applications series. Talor & Francis, Boca Raton, FL. OCLC: ocm57694820.

Blondel, A. (1913). *Synchronous Motors and Converters: Theory and Methods of Calculation and Testing*. McGraw-Hill, New York.

Borodachev, S. M. (2016). Recursive least squares method of regression coefficients estimation as a special case of Kalman filter. page 110013.

Bortoni, E. and Jardini, J. (2002). Identification of synchronous machine parameters using load rejection test data. *IEEE Transactions on Energy Conversion*, 17(2):242–247.

Bush, S. F. (2014). *Smart Grid: Communication-Enabled Intelligence for the Electric Power Grid*. John Wiley & Sons, Ltd, Chichester, UK.

Canay, I. (1993a). Determination of the model parameters of machines from the reactance operators x/sub d/(p), x/sub q/(p) (evaluation of standstill frequency response test). *IEEE Transactions on Energy Conversion*, 8(2):272–279.

Canay, I. M. (1969). Causes of Discrepancies on Calculation of Rotor Quantities and Exact Equivalent Diagrams of the Synchronous Machine. *IEEE Transactions on Power Apparatus and Systems*, PAS-88(7):1114–1120.

Canay, I. M. (1993b). Modelling of alternating-current machines having multiple rotor circuits. *IEEE Transactions on Energy Conversion*, 8(2):280–296.

Capolino, G.-A. (May-Jun 2004). Andre Blondel (1863-1938) French scientist and engineer. *IEEE Industry Applications Magazine*, 10(3):12–15.

Clarke, E. (1943). *Circuit Analysis of A-C Power Systems; Symmetrical and Related Components.* General Electric series. Wiley, New York.

Concordia, C. (1937). Two-reaction theory of synchronous machines with any balanced terminal impedance. *Electrical Engineering*, 56(9):1124–1127.

Concordia, C. (1951). *Synchronous Machines, Theory and Performance.* Number viii, 224 p. in General Electric series. Wiley, New York.

Concordia, C. (1968). Considerations in planning for reliable electric service. *IEEE Spectrum*, 5(8):71–76.

Coultes, M. and Watson, W. (1981). Synchronous Machine Models by Standstill Frequency Response Tests. *IEEE Transactions on Power Apparatus and Systems*, PAS-100(4):1480–1489.

Crary, S. B. (1947). *Power System Stability.* Wiley, New York.

Dajaku, G. and Gerling, D. (2012). Air-Gap Flux Density Characteristics of Salient Pole Synchronous Permanent-Magnet Machines. *IEEE Transactions on Magnetics*, 48(7):2196–2204.

Dandeno, P., Hauth, R., and Schulz, R. (1973). Effects of Synchronous Machine Modeling in Large Scale System Studies. *IEEE Transactions on Power Apparatus and Systems*, PAS-92(2):574–582.

Dandeno, P., Kundur, P., Poray, A., and El-din, H. (1981). Adaptation and Validation of Turbogenerator Model Parameters Through On-Line Frequency Response Measurements. *IEEE Transactions on Power Apparatus and Systems*, PAS-100(4):1656–1664.

Dandeno, P., Kundur, P., and Schulz, R. (1974). Recent trends and progress in synchronous machine modeling in the electric utility industry. *Proceedings of the IEEE*, 62(7):941–950.

de Mello, F. and Ribeiro, J. (1977). Derivation of synchronous machine parameters from tests. *IEEE Transactions on Power Apparatus and Systems*, 96(4):1211–1218.

de Mello, F. P. and Hannett, L. N. (1986). Representation of Saturation in Synchronous Machines. *IEEE Transactions on Power Systems*, 1(4):8–14.

Dehghani, M. and Nikravesh, S. (2008). Nonlinear state space model identification of synchronous generators. *Electric Power Systems Research*, 78(5):926–940.

Dineley, J. and Morris, A. (1973). Synchronous Generator Transient Control: Part I -Theory and Evaluation of Alternative Mathematical Models. *IEEE Transactions on Power Apparatus and Systems*, PAS-92(2):417–422.

Doherty, R. E. and Nickle, C. A. (1926). Synchronous machines I - An extension of Blondel's two-reaction theory. *Transactions of the American Institute of Electrical Engineers*, XLV:912–947.

Doherty, R. E. and Nickle, C. A. (1927). Synchronous Machines III - Torque-Angle Characteristics Under Transient Conditions. *Transactions of the American Institute of Electrical Engineers*, XLVI:1–18.

Doherty, R. E. and Nickle, C. A. (1928). Synchronous Machines IV. *Transactions of the American Institute of Electrical Engineers*, 47(2):457–487.

Doherty, R. E. and Nickle, C. A. (1930). Three-phase short circuit synchronous machines-V. *Transactions of the American Institute of Electrical Engineers*, 49(2):700–714.

El-Serafi, A., Abdallah, A., El-Sherbiny, M., and Badawy, E. (Dec./1988). Experimental study of the saturation and the cross-magnetizing phenomenon in saturated synchronous machines. *IEEE Transactions on Energy Conversion*, 3(4):815–823.

Fairbairn, R. and Harley, R. (1990). On-line measurement of synchronous machine parameters. pages 134–139. IEEE.

Fuchs, E. F. and Erdelyi, E. A. (1973). Nonlinear Theory of Turboalternators Part II. Load Dependent Synchronous Reactances. *IEEE Transactions on Power Apparatus and Systems*, PAS-92(2):592–599.

Glad, T. and Ljung, L. (2000). *Control Theory: Multivariable and Nonlinear Methods*. Taylor & Francis, London. OCLC: 247761966.

Heydt, G. T., Kyriakides, E., Vittal, V., and Huang, G. (2005). Estimation of Synchronous Generator Parameters from On-line Measurements. Final Project Report S-15 05-36, Power Systems Engineering Research Center.

Huang, C.-T., Chen, Y.-T., Chang, C.-L., Huang, C.-Y., Chiang, H.-D., and Wang, J.-C. (1994). On-line measurement-based model parameter estimation for synchronous generators: Model development and identification schemes. *IEEE Transactions on Energy Conversion*, 9(2):330–336.

IEC (2008). *IEC 60034-4 Rotating Electrical Machines – Part 4: Methods for Determining Synchronous Machine Quantities from Tests*. IEC, 3.0 edition.

IEEE (1983). IEEE Guide: Test Procedures for Synchronous Machines. *IEEE Std 115-1983*.

IEEE (2010). *Std 115-2009 IEEE Guide for Test Procedures for Synchronous Machines*. IEEE, New York. OCLC: 958760789.

IEEE (2016). *421.5-2016 - IEEE Recommended Practice for Excitation System Models for Power System Stability Studies*. Number 5 in IEEE 421. IEEE, New York, 2016 edition.

IEEE, C. R. (1969). Recommended Phasor Diagram for Synchronous Machines. *IEEE Transactions on Power Apparatus and Systems*, PAS-88(11):1593–1610.

IEEE Power Engineering Society (1996). *IEEE Guide, Test Procedures for Synchronous Machines*. Institute of Electrical and Electronics Engineers, New York, NY. OCLC: 49704143.

International Electrotechnical Commission, International Electrotechnical Commission, and Technical Committee 57 (2011). *Communication networks and systems for power utility automation. Part 7-1, Part 7-1,*. International Electrotechnical Commission, Geneva. OCLC: 768449897.

Jackson, W. and Winchester, R. (1969). Direct- and Quadrature-Axis Equivalent Circuits for Solid-Rotor Turbine Generators. *IEEE Transactions on Power Apparatus and Systems*, PAS-88(7):1121–1136.

Kamwa, I., Viarouge, P., and Dickinson, E. (1990). Optimal estimation of the generalized operational impedances of synchronous machines from short-circuit tests. *IEEE Transactions on Energy Conversion*, 5(2):401–407.

Kamwa, I., Wamkeue, R., and Dai-Do, X. (1997). General approaches to efficient d-q simulation and model translation for synchronous machines: A recap. *Electric Power Systems Research*, 42(3):173–180.

Karayaka, H., Keyhani, A., Heydt, G., Agrawal, B., and Selin, D. (2003). Synchronous generator model identification and parameter estimation from operating data. *IEEE Transactions on Energy Conversion*, 18(1):121–126.

Kilgore, L. A. (1931). Calculation of Synchronous Machine Constants- Reactances and Time Constants Affecting Transient Characteristics. *Transactions of the American Institute of Electrical Engineers*, 50(4):1201–1213.

Kimbark, E. W. (1950). *Power System Stability*. Wiley, New York. OCLC: 314249047.

Kron, G. (1938). *The Application of Tensors to the Analysis of Rotating Electrical Machinery: Parts I-XVI, Elementary Engineering Treatment*. Number xii, 187 p. in Elementary engineering treatment. General Electric Review, Schenectady, N.Y.

Kron, G. (1967). *Equivalent Circuits of Electric Machinery*. Wiley, New York.

Kundur, P., Balu, N. J., and Lauby, M. G. (1994). *Power System Stability and Control*. The EPRI power system engineering series. McGraw-Hill, New York.

Kyriakides, E., Heydt, G., and Vittal, V. (2005). Online Parameter Estimation of Round Rotor Synchronous Generators Including Magnetic Saturation. *IEEE Transactions on Energy Conversion*, 20(3):529–537.

Lay, D. C., Lay, S. R., and McDonald, J. (2016). *Linear Algebra and Its Applications*. Pearson. OCLC: 934771561.

Lee, C. and Tan, O. (1977). A weighted-least-squares parameter estimator for synchronous machines. *IEEE Transactions on Power Apparatus and Systems*, 96(1):97–101.

Levi, E. (1998). State-space d–q axis models of saturated salient pole synchronous machines. *IEE Proceedings - Electric Power Applications*, 145(3):206.

Lipo, T. A. (1984). A Cartesian Vector Approach To Reference Theory of AC Machine. Reseach Report 84-2, Wiscosin Electric Machines and Power Electronics Consortium, Madison, Wisconsin.

Ljung, L. (1999). *System Identification: Theory for the User*. Prentice Hall information and system sciences series. Prentice Hall PTR, Upper Saddle River, NJ, 2nd ed edition.

Ljung, L. (2012). Lennart Ljung on System Identification Toolbox: History and Development - Video. https://www.mathworks.com/videos/lennart-ljung-on-system-identification-toolbox-history-and-development-96989.html.

Ljung, L. and Glad, T. (2016). *Modeling & Identification of Dynamic Systems*. Studentlitteratur AB, Lund, edition 1:1 edition. OCLC: 982167261.

Machowski, J., Bialek, J. W., and Bumby, J. R. (2008). *Power System Dynamics: Stability and Control*. Wiley, Chichester, U.K, 2nd ed edition. OCLC: ocn232130756.

Manchur, G., Lee, D., Coultes, M., A. Griffin, J., and Watson, W. (1972). Generator Models Established by Frequency Response Tests on a 555 MVA Machine. *IEEE Transactions on Power Apparatus and Systems*, PAS-91(5):2077–2084.

Marafioti, G., Bitmead, R. R., and Hovd, M. (2014). Persistently exciting model predictive control. *International Journal of Adaptive Control and Signal Processing*, 28(6):536–552.

Mohan, N. (2012). *Electric Machines and Drives: A First Course*. Wiley, Hoboken, NJ. OCLC: ocn712124934.

Mohan, N. (2014). *Advanced Electric Drives: Analysis, Control, and Modeling Using MATLAB/Simulink*. Wiley, Hoboken, New Jersey.

Moore, J. (1983). Persistence of excitation in extended least squares. *IEEE Transactions on Automatic Control*, 28(1):60–68.

Mukhopadhyay, S. (2004). Lec-24 Linear Regression-Recursive Least Squares.

Namba, M., Hosoda, J., Doi, S., and Udo, M. (1981a). Development for Measurement of Operating Parameters of Synchronous Generator and Control Systems. *IEEE Transactions on Power Apparatus and Systems*, PAS-100(2):618–628.

Namba, M., Nishiwaki, T., Yokokawa, S., Ohtsuka, K., and Ueki, Y. (1981b). Identification of Parameters for Power System Stability Analysis Using Kalman Filter. *IEEE Power Engineering Review*, PER-1(7):37–37.

NVE (2017). Vannkraftpotensialet. https://www.nve.no/energiforsyning-og-konsesjon/vannkraft/vannkraftpotensialet/.

Park, R. H. (1929). Two-reaction theory of synchronous machines generalized method of analysis-part I. *Transactions of the American Institute of Electrical Engineers*, 48(3):716–727.

Park, R. H. (1933). Two-reaction theory of synchronous machines-II. *Transactions of the American Institute of Electrical Engineers*, 52(2):352–354.

Pelckmans, K. (2013). Lecture Notes for a Course on System Identification, v2013.

Rankin, A. W. (1945). Per-unit impedances of synchronous machines. *Transactions of the American Institute of Electrical Engineers*, 64(8):569–573.

Rehaoulia, H., Henao, H., and Capolino, G. (2007). Modeling of synchronous machines with magnetic saturation. *Electric Power Systems Research*, 77(5-6):652–659.

Reimert, D. (2006). *Protective Relaying for Power Generation Systems*. CRC/Taylor & Francis, Boca Raton, FL. OCLC: ocm61463829.

Sauer, P. W., Pai, M. A., and Chow, J. H. (2017). *Power System Dynamics and Stability: With Synchrophasor Measurement and Power System Toolbox*. Wiley, Hoboken, NJ, USA, second edition edition.

Schulz, R., Jones, W., and Ewart, D. (1973). Dynamic Models of Turbine Generators Derived From Solid Rotor Equivalent Circuits. *IEEE Transactions on Power Apparatus and Systems*, PAS-92(3):926–933.

Shackshaft, G. (1974). New approach to the determination of synchronous-machine parameters from tests. *Proceedings of the Institution of Electrical Engineers*, 121(11):1385.

Shackshaft, G. and Henser, P. (1979). Model of generator saturation for use in power-system studies. *Proceedings of the Institution of Electrical Engineers*, 126(8):759.

Statnett (2012). Funksjonskrav i kraftsystemet.

Strang, G. (2005). *Introduction to Linear Algebra*. Wellesley-Cambridge Press, Wellesley, Mass, 3. ed., rev. internat. ed edition. OCLC: 255007465.

Tsai, H., Keyhani, A., Demcko, J., and Farmer, R. (1995). On-line synchronous machine parameter estimation from small disturbance operating data. *IEEE Transactions on Energy Conversion*, 10(1):25–36.

Ulusoy, M. (2018a). Understanding Kalman Filters. https://se.mathworks.com/videos/series/understanding-kalman-filters.html.

Ulusoy, M. (2018b). Understanding Kalman Filters, Part 4: An Optimal State Estimator Algorithm Video. https://se.mathworks.com/videos/understanding-kalman-filters-part-4-optimal-state-estimator-algorithm–1493129749201.html.

Verbeeck, J., Pintelon, R., and Lataire, P. (Sept./2000). Influence of saturation on estimated synchronous machine parameters in standstill frequency response tests. *IEEE Transactions on Energy Conversion*, 15(3):277–283.

Wang, J.-C. (1995). Identification of synchronous generator saturation models based on online digital measurements. *IEE Proceedings - Generation, Transmission and Distribution*, 142(3):225.

Wang, J.-C., Chiang, H.-D., Huang, C.-T., Chen, Y.-T., Chang, C.-L., and Chiou, C.-Y. (1994). On-line measurement-based model parameter estimation for synchronous generators: Solution algorithm and numerical studies. *IEEE Transactions on Energy Conversion*, 9(2):337–343.

Wright, S. H. (1931). Determination of Synchronous Machine Constants by Test Reactances, Resistances, and Time Constants. *Transactions of the American Institute of Electrical Engineers*, 50(4):1331–1350.

Yu, Y.-n. and Moussa, H. (1971). Experimental Determination of Exact Equivalent Circuit Parameters of Synchronous Machines. *IEEE Transactions on Power Apparatus and Systems*, PAS-90(6):2555–2560.

Zdanov, P. S. (1948). *Stability of electric power systems.* Gosudarstvennoe Energeticeskoe Izdatelstvo, Moscow.